UCID--20622-89-1

DE89 014303

Chemistry & Materials Science Research Report

Weapons-Supporting Research

and

Departmental Institutional Research & Development

June 1, 1989

FOREWORD

The research reported here in summary form was conducted under the auspices of Weapons-Supporting Research (WSR) and Institutional Research and Development (IR&D). The period covered is the first half of FY89.

WSR is the principal source of discretionary funds to support fundamental research in the Chemistry & Materials Science Department (C&MS). The purpose of WSR is to provide the scientific and technical base that is required in the longer term for success of the Weapons Program.

Administratively, WSR is organized into block-funded programs ("thrust areas") and a few smaller projects led by individual investigators. A thrust area is designed to provide a coordinated approach to a focused scientific or technological area and typically involves several senior scientists.

IR&D is intended to broaden the exploratory research base of C&MS. In FY89, IR&D funds have underwritten several single-investigator projects and (in part) relatively large programs such as Spin Polarization and High-Temperature Superconductivity.

In practice, research programs carried out under WSR auspices are similar in spirit and substance to those supported by IR&D. Indeed, some of the work is funded by both sources.

The results reported here are for work in progress; thus, they may be preliminary, fragmentary, or incomplete. Interested readers should consult one of the authors of a report before quoting it or otherwise referring to it.

T. T. Sugihara

CONTENTS

WEAPONS-SUPPORTING RESEARCH

DEPARTMENTAL INSTITUTIONAL RESEARCH & DEVELOPMENT

WEAPONS-SUPPORTING RESEARCH

Thrust Areas

HIGH-TEMPERATURE SUPERCONDUCTIVITY

M. J. Fluss *(Thrust Area Leader)*

Overview

The experimental tasks of the High-Temperature Superconductivity thrust area*—Electron Structure, Thin Films and Atomic Engineering, and Materials Synthesis and Properties—are guided and supported by a broad theoretical task in band structure, ligand field effects, and pairing mechanisms. The mission of the thrust area is to deduce the mechanism underlying the properties of the new high-T_c superconductors. These activities provide a flexible, focused program that is contributing to the solution of critical problems in understanding oxide superconductors. Additionally, the thrust is sensitive to opportunities for utilization of the new superconductors in future LLNL programs and has explored processing- and applications-oriented activities whenever appropriate.

Electron Momentum Densities

R. Howell, A. Wachs, G. Kaiser**, P. Turchi, P. Sterne, M. Fluss, R. West**

The angular correlations of the two gamma rays from the annihilation of positron-electron pairs (2D-ACAR) in a single crystal have been used to study the momentum distribution of electrons in single-crystal samples of the Mott-Hubbard insulators, NiO and La_2CuO_4, and the high-T_c superconductor, $YBa_2Cu_3O_7$. Experiments were performed using both "sandwiched" (source between two single crystals) and magnetically-guided positron ^{22}Na isotopic sources. The single crystals were verified as suitable for such experiments by positron-lifetime studies indicating either a single short lifetime (implying a delocalized positron state) or a short component from which the fraction of delocalized strength could be deduced as ≥50%. In all these studies, two common physical features were clearly evident: (1) most positron annihilations were taking place between the dominant deep-lying electron bands and the positron, accounting for ~85% of the data, and (2) the remaining data exhibited anisotropy attributable to valence electrons that are modeled in terms of localized bonding for a single CuO_6 cluster using an LCAO-MO formalism.

To accomplish these experiments, it was first necessary to calculate the positron wave function in the materials to be studied. The positron wave function was approximated by a variational wave function taking into account the strong ionic character of the host materials. The expected positron-electron momentum spectrum is deduced by reducing the many-body problem to a sum over all occupied electron states such that

* Supported also by Departmental IR&D.
** University of Texas, Arlington.

$$\rho^{2\gamma}(p_x,p_y) = \int_{-\infty}^{+\infty} dp_z\, \rho^{2\gamma}(\vec{p})$$

where $\rho^{2\gamma}(\vec{p})$ is the positron-electron momentum density, as given by

$$\rho^{2\gamma}(\vec{p}) \propto \sum_{j\ occ.} |\chi^j(\vec{p})|^2$$

where $\chi^j(\vec{p})$ is the probability amplitude for the emission of two photons with total momentum $\vec{p} = \bar{h}\cdot\vec{k}$. The approach to the electron structure is made very simple by considering only the last occupied valence states, the antibonding states that are formed with the 3d states of copper and the 2s and 2p states of the ligand oxygen sites. From this model, we directly obtain five states, three t_{2g} and two e_g, allowing us to express the $\rho^{2\gamma}(\vec{p})$ in terms of the five corresponding expectation values that represent the specific bonding contributions and their respective covalency strengths, given by

$$\rho^{2\gamma}(\vec{p}) = 2\{|\chi^{xy}(\vec{p})|^2 + |\chi^{yz}(\vec{p})|^2 + |\chi^{xz}(\vec{p})|^2\} + |\chi^{x^2-y^2}(\vec{p})|^2 + 2|\chi^{z^2}(\vec{p})|^2$$

There is a general belief that the observed carrier density of $\sim 8\times10^{22}$ electrons per cm^3 arises from electron (or hole) quasi-particles that exhibit the properties of a metal, including a definite Fermi-surface topology from which arises the hole-hole correlations leading to Cooper-like pairs. The search for and the description of this Fermi surface require high-quality, single-crystal samples that are free of defects and suitable for comparison to ideal models of the crystal lattice structure. In the present experiments, we have utilized the Lock-Crisp-West (LCW) theorem to test the electron structure data for evidence of a Fermi-surface topology. Extreme care was taken in the data analyses leading to the application of this theorem. Centers and symmetry operations were iteratively established in order to avoid the generation of artificial structures.

Simply stated, the LCW theorem folds all data into the first zone from which features related to the Fermi surface tend to be enhanced; the other features lead to a broad background without sharp changes in the derivative of the surface topology. It is possible to image the essential features of the Fermi surface by reading these results in terms of simple contour diagrams. Figure HT-1 shows the resulting LCW data, from which no evidence for an observable Fermi surface topology can be seen. To further test for evidence of a Fermi surface and to compare to recent calculations of Bansil et al. [1], we have taken various differential slices of the present data as shown in Fig. HT-2. Figure HT-2 shows the anisotropic representation of the electron momentum density in the basal plane. The peaks and valleys, respectively, represent regions in (p_x,p_y) that are rich and poor in electron density. The only topological features that are clearly evident arise from those features predicted by our LCAO-MO modeling of the present data. Cuts along several crystallographic directions are shown in Fig. HT-2, in which the two "bonding" or wave-function features are indicated by the arrows.

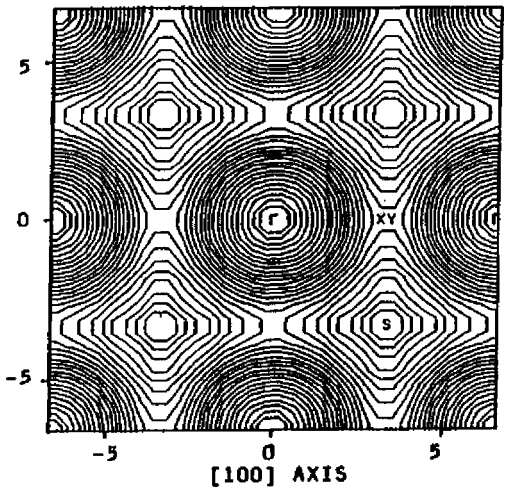

Fig. HT-1. LCW folded spectrum of the Y123 electron momentum density. The total amplitude of variation is 5% of the maximum (at center). Solid and dashed contours represent levels above and below the average density, respectively.

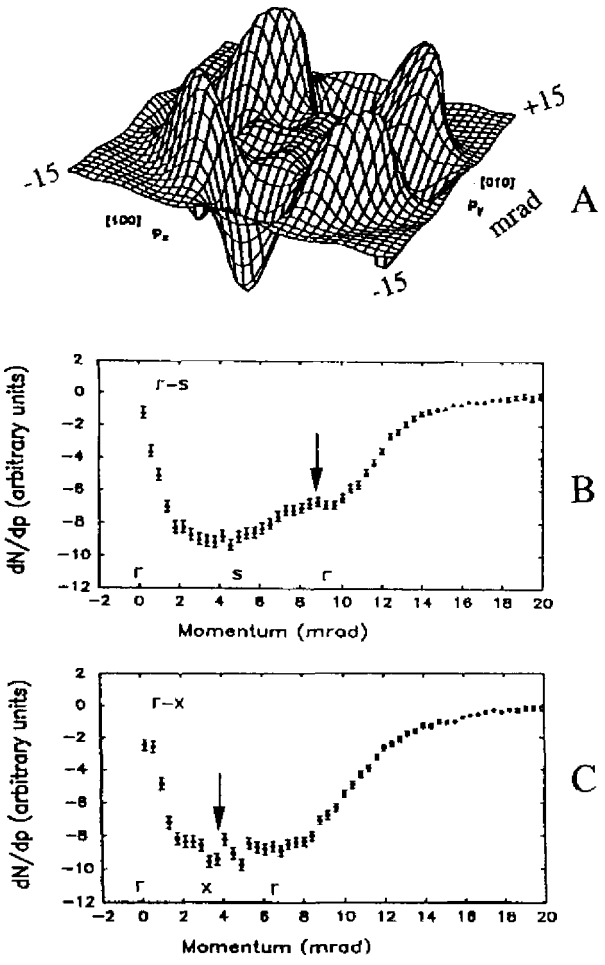

Fig. HT-2. Anisotropy (a) and differential slices (b and c) of the electron density show features (arrows) related to the local bonding nature of the Cu-O system. No evidence for Fermi "breaks" can be seen.

Experiments with one order of magnitude higher statistics are being started on a new set of high-quality single crystals. Our expectation is that a direct comparison of the electron structure of La_2CuO_4 with that of $La_{2-x}Sr_xCuO_4$ ($x = 0.12$) will elucidate the small but critical differences in the electronic structure of the parent and superconducting materials. The high-quality doped single crystals came from Kitazawa (Japan), the only group producing such crystals to date. In addition, large-area Y123 crystals have been prepared for a high statistics experiment. In all these studies, we will be using a modification of our existing (2D-ACAR) system with count rates ~25 times those obtained in previous studies. Cross-experiments with University of Texas, Arlington are planned to discover and avoid possible systematic errors. We also plan to obtain data at five or more orientations with sufficient statistics to accomplish 3-dimensional reconstructions of the electron momentum and, if present, Fermi-surface topology.

Lifetime studies, previously reported, have now been interpreted by Chakraborty [2]. The basis of the analysis is fully independent of particular models of superconductivity and simply invokes the existence of hole carriers. Such hole carriers, on condensation, can act as Coulomb shields for positron overlap with the more tightly bound electrons associated with deep-lying states when the correlation distance is <~2 nm. Such a model suggests a unique application of the positron data in determining pairing dynamics and studying pair-breaking phenomena.

Lifetime studies are now being completed on $Ba_{1-x}K_xBiO_3$ and $Nd_{2-x}Ce_xCuO_{4-\delta}$. In addition, modeling of the positron wave functions for these systems and the Bi systems is nearly complete. Preliminary results indicate that, in the electron or *n-type* materials [3], the lifetime-increase effect is not a consequence of strong electron pair-to-positron attraction. In the Bi compounds, we are discovering that the positron is repelled from the carrier regions and that the strong dependence of the lifetime on temperature should be missing or fully absent. Experiments performed on doped (Zn and Ga "123") compounds also point out that the variations in the details of the positron distribution (the expectation value) strongly affect the observed sensitivity to the superconducting transition.

Thin Films and Atomic Engineering

T. Barbee P. Sterne R. Russo*

This activity has been restructured to support our intent to produce critical materials configurations for specific physics experiments, gap studies, plasmon effects, and proximity studies that will enable us to understand the physical and materials basis and limitations for potential applications in LLNL programs. We have produced, by high-temperature isostatic pressing, $ErBa_2Cu_3O_7$ targets of such high quality that magnetron sputtering does not alter their composition and with erosion rates sufficiently low to allow very uniform depositions at or near the desired composition. This work was done in collaboration with TRW and Stanford University, but it has also provided us with a distinct

* Lawrence Berkeley Laboratory.

new capability to manufacture thin-film materials. Oxygen pressures have been introduced into the laser ablation system and Y123 material has been produced that is directly superconducting without post-oxygenation treatment. The goal of reducing substrate temperatures below 500 °C is being investigated. The single-target magnetron-sputtering system is operational and samples are being produced. The multi-target system is being prepared for a series of experiments leading to our first attempts at producing samples suitable for physics studies of the proximity effect (Josephson junctions) and artificial layered structures that might lead to new superconducting materials.

Important components of this task are predicting, modeling, and interpreting results from studying thin-film materials at the level of the coherence length of the superconducting pairs. Electronic structure calculations on high-temperature superconductors using the LMTO method [4] are now under way. We expect (and have demonstrated for several cases) that such calculations will indicate which electron states should be considered when constructing a model for high-temperature superconductivity. Such an approach is particularly important in the study of these layered-like materials, since it is generally held that true two-dimensional superconductivity cannot exist as a consequence of fluctuations destroying the boson state. Thus, the nature of the exchange among or between layers must be considered in detail. The development of suitable models requires insight into the nature of the spatially- and chemically-resolved DOS (density-of-state) and the underlying full-band structure interpretation of the properties of high-T_c materials.

The recent discovery of new *n-type* materials only serves to emphasize the importance of this approach because similarities and differences between the two classes of high-T_c materials may reveal fundamental information about the actual pairing mechanism and the nature of the quasi-particle. An example of the resolution of the partial DOS for the constituents of the $Bi_2Sr_2CaCu_2O_8$ superconductor is shown in Fig. HT-3. In these results, we see that the states below the Fermi energy are mostly associated with Cu-O_2 states whereas those ~2 eV above it are Bi-O states. From these results, we have been able to deduce a strong oxygen overlap with the Bi states, but the states crossing the Fermi energy are true Bi states. This nature of the Bi materials had been observed previously in our positron lifetime studies and is now being confirmed by expanded modeling.

Of particular concern in much of our work is the remaining possibility of mixed-phase systems at the level of 10 nm or smaller. These phase-stability questions affect almost all studies now under way. We have successfully modeled the phase stabilities of six compositions of the Y123 material for various oxygen concentrations using the Connolly-Williams method. We have found that these results are in good agreement with experimental data and confirm the validity of earlier Ising-like models of de Fontaine et al. The implications of these results will be further explored with regards to atomic engineering and electronic structure studies.

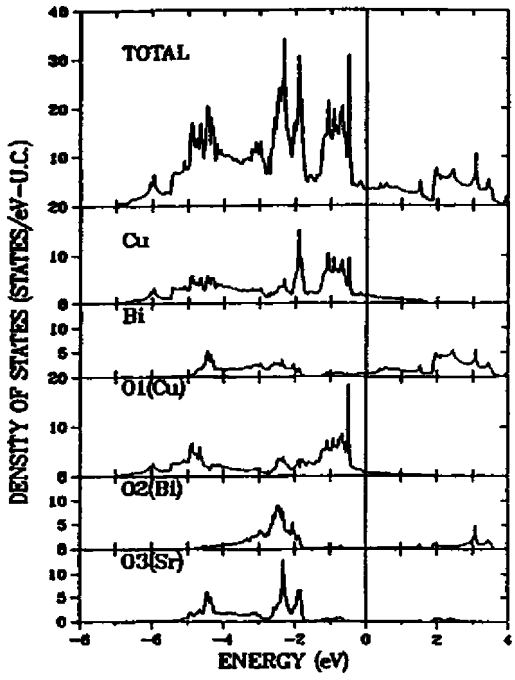

Fig. HT-3. Density of states and partial densities of states for $Bi_2Sr_2CaCu_2O_8$.

Materials Synthesis and Properties

H. Radousky
R. Howell
R. Shelton**
P. Hahn
E. Larson
M. Fluss
K. McCarty*

We have completed an extensive investigation of the system $Y_{1-x}Pr_xBa_2Cu_3O_{7-\delta}$ to clarify the role of increasing Pr concentration in the "quenching" of the superconducting transition. The motivation for this study was the large number of studies [5] that had not successfully explained this quenching. Among the various techniques employed earlier were magnetization, heat capacity, thermal power, Hall effect, neutron diffraction, pressure effects, x-ray absorption, and Raman spectroscopy. A major problem in studying this system was the phase separation, which increased in tendency as a function of increasing Pr concentration. This was resolved by development of sintering and grinding techniques. High temperature and high-oxygen-pressure soaks unique to LLNL facilities provided the ability to control oxygen stoichiometry at or near the 7(δ=0) level. The samples used in this study have less than 1% separation as determined by field-cooled magnetization as shown in Fig. HT-4. As indicated in Fig. HT-4, the samples at x=0.2 and 0.35 Pr show small amounts of a second phase; however, compared to earlier studies, the sharpness of the transitions are extraordinary. In Fig. HT-5, we show the Pr concentration dependence of the critical temperature, which is observed to follow the classical Abrikosov-Gorkov pair-breaking theory. This suggests a pair-breaking mechanism that we searched for by

* Sandia National Laboratories–Livermore.
** University of California, Davis.

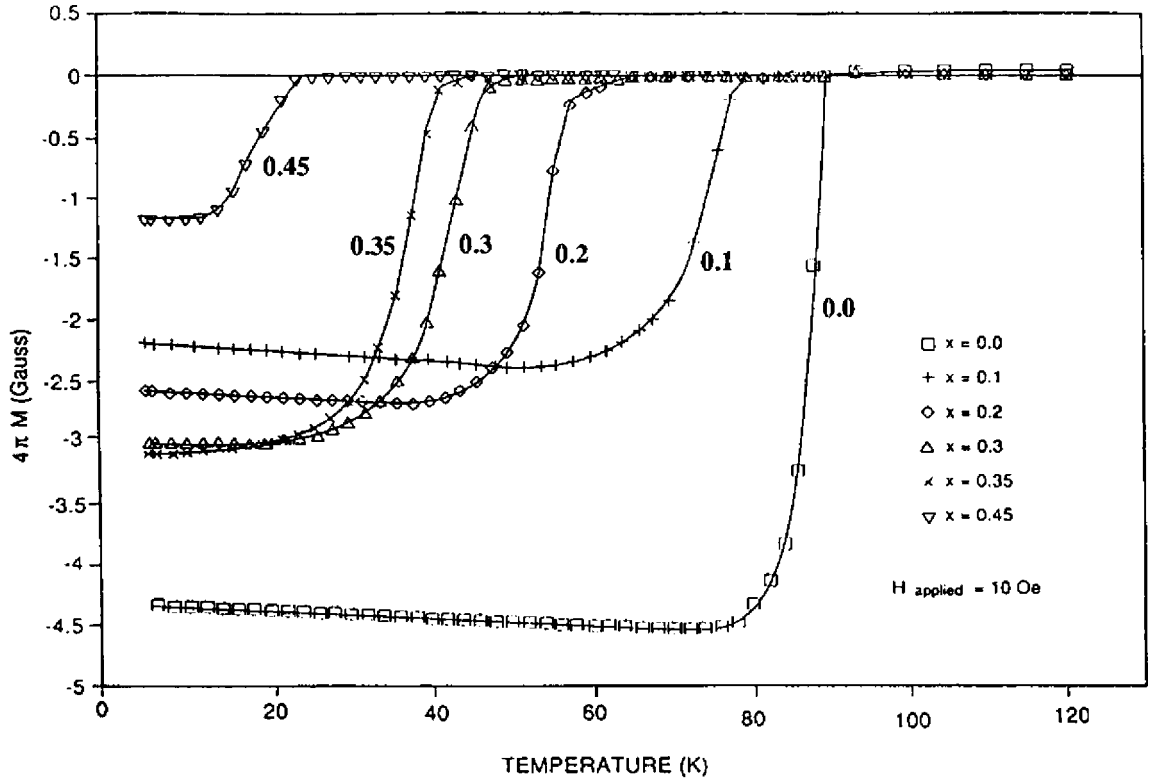

Fig. HT-4. Field-cooled magnetization ($4\pi M$) *vs.* temperature as measured with a SQUID magnetometer in a field of 20 Oe.

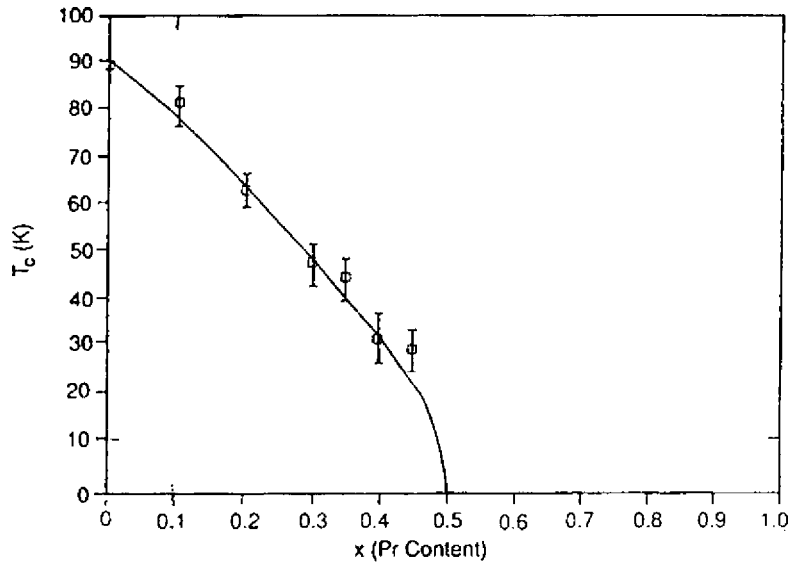

Fig. HT-5. The transition temperature (T_c) determined by the midpoints of the resistivity data as a function of Pr content. The vertical bars indicate the 10–90% resistivity transition widths (ΔT_c). The solid line is a fit of T_c *vs.* Pr concentration by the Abrikosov and Gorkov theory.

carrying out measurements of the critical field, H_{c2}, as a function of Pr concentration. The appearance of a "bell-shaped" temperature response (Fig. HT-6) is interpreted as consistent with the presence of magnetic pair breaking. By means of the slope of the T_c dependence, the critical Ginzburg-Landau parameters can be derived from the BCS Gorkov equations near T_c in the dirty limit.

After *n-type* superconductivity [3] at high T_c had been discovered, it was imperative to begin comparative studies on these materials. By annealing in a reducing atmosphere, we have successfully synthesized $Nd_{1.85}Ce_{0.15}CuO_{4-\delta}$. We have developed a new vacuum method for preparing high-purity, single-phase material that is suitable for

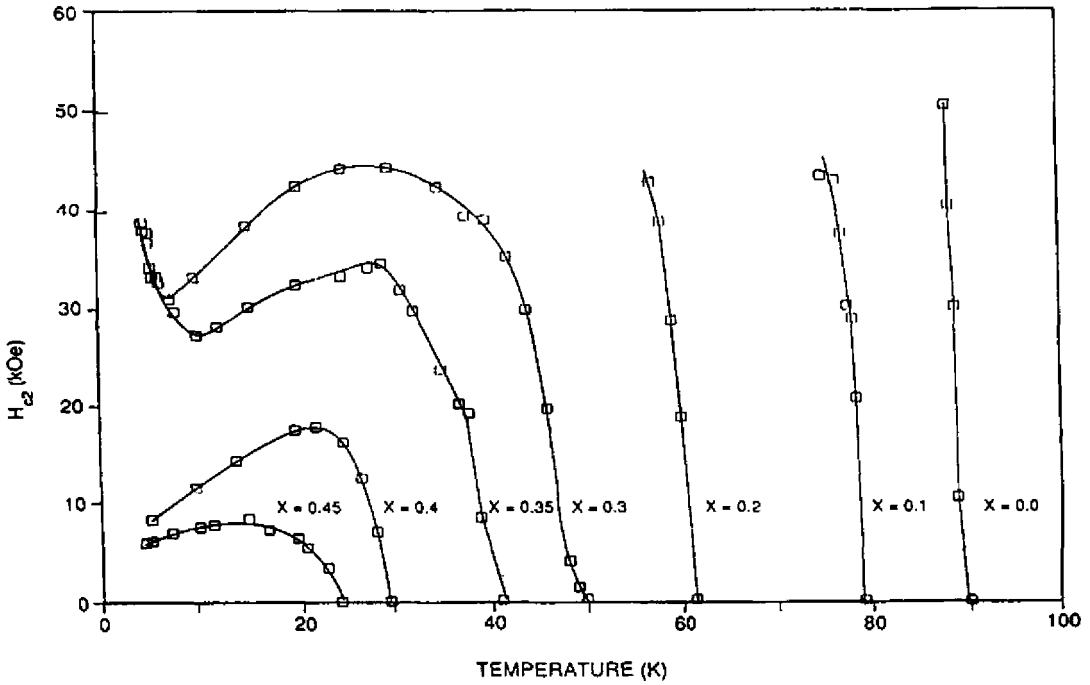

Fig. HT-6. H_{c2} as a function of temperature for Pr = 0.0, 0.1, 0.2, 0.3, 0.35, 0.4, and 0.45 atoms per unit cell.

extensive physical-properties measurements. It was observed that the temperature dependence of the normal state resistivity of this material is logarithmic and a universal feature in electron-cuprate superconductors. The observed logarithmic term is reminiscent of materials displaying Kondo effects. Additional Raman studies indicate the absence of significant phonon scattering by the lattice but suggest that the dominant contribution to the normal state resistivity in these *n-type* materials comes from magnetic scattering. Future work will pursue the lack of such scattering in the metallic phases of the parent material.

Additional work, still under way, includes studying, in collaboration with SNLL, electron-phonon coupling in $Ba_{0.6}K_{0.4}BiO_3$ using Raman spectroscopy. A specific vibrational mode has been discovered that is clearly coupled to the electrons in $Ba_{0.6}K_{0.4}BiO_3$ and $YBa_2Cu_3O_7$ at 348 cm^{-1} and 340 cm^{-1}, respectively. A new project, stimulated by reports of partial success from the Russians, to study the replacement of

halogens for oxygen in the Y123 material appears to indicate that this chemistry may enable the low-temperature processing of high-T_c materials that would allow integration into the electronics industry. At present, we continue to explore the nature of this halogen doping, since preliminary results appear to indicate that most of the halogen (Br in this case) is distributed in an intercalated manner, most likely along open chain positions.

Other Experiments

Part of our resources have been used to carry out studies of an exploratory or enabling nature. Two of these activities have led to important new results: one in the area of cluster modeling of the oxide superconductors, the second in shock processing.

Cluster Modeling of Oxide Superconductors

Nick Winter (H-Division, Physics) has been modeling the electronic properties of high-T_c materials using a fully self-consistent Hartree-Fock calculation for large representative clusters, an area that is somewhat of a speciality at LLNL. C. Stevens, C. Violet, R. Ward, and C. Merzbacher have performed a series of Mössbauer and NMR studies to provide local-site chemistry information that could be used to benchmark these calculations.

The result of this comparison between experiment and theory was surprising indeed. There are two different Cu sites and four O sites in the Y123 material. Comparisons of predictions for the ^{17}O and ^{63}Cu sites (chemical shifts and nuclear quadrapole coupling constants) made it possible to establish a unique picture of the oxidation states of these two constituents. It was found that the Cu(1) site must be a $Cu^{+2}(3d^9)$ and that the Cu(2) site was a $Cu^{+2}(3d^9)$ with a small amount of $Cu^{+1}(3d^{10})$ character. Photoemission studies should confirm this in the near future. More interestingly, the consequence of this is that the O^{2-} must be decorated with 2p holes. The mixed-valence character at the Cu(2) does not lead to the desired mobile holes, but it is a requirement of the fit between experiment and theory. These results make strong implications regarding hole coupling and spin pairing.

Shock Processing

W. Nellis B. Maples* R. Feigelson**

We have continued to support studies of shock compaction of powders and filaments in an attempt to produce composite high-critical-current materials. The bulk of this activity is carried by reimbursable funds going through the physics department, although transport and characterization studies are being performed using some thrust area resources.

The compaction studies are conducted using the compressive energy from a two-stage light-gas gun at LLNL. Because compaction occurs from application of 10 GPa pressures

* University of California at San Diego.
** Stanford University.

on μs time scales, compressive energy and heating are localized on powder-grain boundaries allowing for heterogeneous processing. Initial studies have focused on shock-induced defects in the bulk of the materials, which could either destroy or improve superconducting properties. Present data indicate that bulk properties are indeed maintained, and the possibility that extrinsic defects are being introduced as pinning centers remains an open but important technological question under study. Recent successes have included the shock compaction of a variety of crystalline superconducting materials into a Ag-composite matrix. The present microscale techniques can be scaled to produce usable macroscopic materials for special cables, wires, and large ceramic parts such as levitating "bearings."

Work is continuing with the expectation of breakthroughs that will warrant program, agency, or industrial participation.

Theory

A. McMahan P. Turchi P. Sterne
B. Grant J. Mikalopas

The theory task of the High-Temperature Superconductivity thrust area provides both interpretation and modeling capabilities to the experimental tasks and is leading in the development of new formalisms. The activities associated with cluster-model approaches and the modeling of positron annihilation and hyperfine studies have been described above as have the calculations being developed to study the nature of 3D exchange between insulating and metallic layers in the metal-oxide systems in support of the atomic engineering effort and the electron structure and Raman experiments.

In order to isolate the material characteristics crucial to high-T_c superconductivity, we are also considering four K_2NiF_4-structure materials that appear to have very similar electronic and magnetic properties but only one of which, La_2CuO_4, can be doped to superconductivity. The approach is to use local-density functional theory to calculate parameters defining extended Hubbard models for these materials, then to solve the models in various approximations. Previous work for La_2CuO_4 has shown such an approach to be reliable, and we anticipate even better results for the quantitative differences between these materials.

To date, the local-density parameter calculations for La_2CuO_4 and La_2NiO_4 have been completed, as well as the many-body solutions of the extended Hubbard model in M_1O_6 and M_2O_8 clusters. As shown in Table HT-1, the doped holes in these two materials are very similar in regard to their spatial symmetry, O(2p) makeup, and strong antiferromagnetic interaction with the preexisting spin lattice. The major difference between the two appears to be the spin 1/2 *vs.* spin 1 lattices through which the holes move. This would tie in with an idea of G. Sawatzky that it may be crucial to the superconductivity for the spin lattice to be on the verge of melting, due to zero-point fluctuations, which may be the case for the spin 1/2 Cu but not for the more classical spin 1 Ni lattice.

Table HT-1. Comparisons of the Stoichiometric and Doped M_1O_6 Clusters

Stoichiometric M_1O_6 Cluster

AF Mott Insulator	La_2CuO_4	La_2NiO_4	Comments
N (holes/formula unit)	1	2	Additional hole per unit in Ni material
ground state (spin)	$^2B_1$ (b_1) (1/2)	$^3B_1$ (a_1b_1) (1)	Spin 1/2 versus spin 1 lattice
E_{gap}	1.85	3.38	Ni 1.5 eV larger
J_{dd}	0.40 0.28		M_2O_8 cluster t_{pd} reduced 20%

Doped M_1O_6 Cluster

Hole properties	La_2CuO_4	La_2NiO_4	Comments
1st ionization (spin)	$^1A_1$ (b_1^2) (0)	$^2A_1$ ($a_1b_1^2$) (1/2)	
Symmetry of doped hole	b_1	b_1	$x^2 - y^2$ symmetry
Oxygen fraction of doped hole	0.87	0.76	mostly O(2p)
J_{pd}	0.44	0.54	Strong AF inter. w/ preexisting hole

Conclusions: Nature of doped holes in La_2NiO_4 appears to be very similar to La_2CuO_4. One significant difference is the spin 1 (Ni) *vs.* spin 1/2 (Cu) lattice in which the holes move.

These calculations will now be repeated for K_2CuF_4 and K_2NiF_4 to complete this investigation. Additionally, it is planned to calculate the full anisotropy of the superexchange frequencies, which should provide a stringent test of our techniques given the neutron-scattering data. Other work that is nearing completion involves determination of the level separation (epsilon) between O(2p) and Cu(3d) holes, which is crucial for obtaining accurate exchange frequencies. Previously observed difficulties have been overcome by new calculations with truly extended O(2p) Wannier functions.

References

1 A. Bansil, R. Pankaluoto, R. S. Rao, P. E. Mijnarends, W. Dlugosz, R. Prasad, and L. C. Smedskjaer, *Phys. Lett.* **61**, 2480 (1988).
2. B. Chakraborty, *Phys. Rev. B* **39**, 215 (1989).
3. Y. Tokura, H. Takagi, and S. Uchida, *Nature* **337**, 345 (1989).
4. P. A. Sterne and C. S. Wang, *J. Phys. F* **17**, L319 (1987); *J. Phys. C* **21**, L949 (1988).
5. J. L. Peng, P. Klavins, R. N. Shelton, H. B. Radousky, P. A. Hahn, and L. Bernardez, Lawrence Livermore National Laboratory, Livermore, Calif., UCRL-100698 (1989); in press *Phys. Rev. B.*

Publications and Presentations

Refereed Journals

K. C. Ott, R. M. Aikin, L. Bernardez, A. Connor, Z. Fisk, M. J. Fluss, E. Garcia, M. Goldblatt, W. B. Hutchinson, G. H. Kwei, C. J. Maggiore, J. A. Martin, R. Meisenheimer, M. Nastasi, E. J. Peterson, E. J. Tesmer, J. D. Thompson, T. E. Walker, J. O. Willis, and P. J. Yvon, "Oxygen Isotope Effects in Yttrium Barium Copper Oxides," *Phys. Rev. B* **39**, 4283 (1989).

J. L. Peng, P. Klavins, R. N. Shelton, H. B Radousky, P. A. Hahn, and L. Bernardez, "Upper Critical Field and Normal State Properties of Single Phase $Y_{1-x}Pr_xBa_2Cu_3O_{7-\delta}$ Compounds," *Phys. Rev. B*, in press; UCRL-100698.

K. F. McCarty, H. B. Radousky, D. G. Hinks, Y. Zheng, A. W. Mitchell, T. J. Folkerts, and R. N. Shelton, "Electron-Phonon Coupling in Superconducting $Ba_{0.6}K_{0.4}BiO_3$: A Raman-Scattering Study," submitted to *Phys. Rev. B*; UCRL-100740.

J. L. Peng, R. N. Shelton, and H. B. Radousky, "Preparation and Magnetic Scattering in $Nd_{2-x}Ce_xCuO_{4-\delta}$," submitted to *Sol. St. Commun.*; UCRL-100148.

J. F. Annett, R. M. Martin, A. K. McMahan, and S. Satpathy, "The Electronic Hamiltonian and Antiferro Magnetic Interactions in La_2CuO_4," *Phys. Rev. Lett.*, in press.

J. L. Peng, P. Klavins, R. N. Shelton, H. B. Radousky, P. A. Hahn, L. Bernardez, and M. Costantino, "Preparation, Characterization and Superconducting Properties of Tetragonal $LaBaCaCu_3O_7$," *Phys. Rev. B* **39**, 9074 (1989).

H. B. Radousky, K. F. McCarty, J. L. Peng, and R. N. Shelton, "Preparation and Raman Analysis of Single Phase $Y_{1-x}Pr_xBa_2Cu_3O_7$," accepted by *Phys. Rev. B*; UCRL-100164.

A. L. Wachs, P. E. A. Turchi, R. H. Howell, Y. C. Jean, M. J. Fluss, J. H. Kaiser, R. N. West, K. L. Merkle, A. Revcolevschi, "Positron Annihilation Studies of the Electronic Structure of NiO," *Phys. Rev. B*, in press; UCRL-100154.

C. E. Violet, P. A. Hahn, T. Datta, C. Almasan, and J. Estrada, "Magnetic Behavior of $Ho_1Ba_2(Cu_{1-x}Fe_x)_3O_{7-y}$," *J. Appl. Phys.* **64**, 5911 (1988).

Y. C. Jean, H. Nakanishi, M. J. Fluss, A. L. Wachs, P. E. A. Turchi, R. H. Howell, Z. Z. Wang, R. L. Meng, P. H. Hor, Z. J. Huang, and C. W. Chu, "A Comparison of the Temperature Dependence of Electron-Positron Momentum Density Characteristics in T1(2223), Y(123) and La(214) Superconductors," *J. Phys. C*, in press; UCRL-99081.

Y. C. Jean, J. Kyle, H. Nakanishi, P. E. A. Turchi, R. H. Howell, A. L. Wachs, M. J. Fluss, R. L. Meng, H. P. Hor, J. Z. Huang, and C. W. Chu. "Evidence for a Common High Temperature Superconducting Mechanism in $La_{1.85}Sr_{0.15}Cu0_4$ and $YBa_2Cu_30_7$," *Phys. Rev. Lett.* **60**, 1069 (1988); UCRL-97909.

E. Garcia, R. R. Ryan, N. N. Suer, M. J. Fluss, L. Bernardez, Z. Fisk, and B. Pierce, "Synthesis and Superconducting Critical Temperature of $YBa_2Cu_3{}^{18}O_{7-\delta}$," *Phys. Rev. Lett.* **60** (1988).

A. L. Wachs, P. E. A. Turchi, Y. C. Jean, K. H. Wetzler, R. H. Howell, M. J. Fluss, D. R. Harshman, J. P. Remeika, A. S. Cooper, and R. M. Fleming. "Electronic Structure Studies of La_2CuO_4," *Phys. Rev. B* **38**, 913 (1988); UCRL-98219.

K. C. Ott, J. L. Smith, J. 0. Willis, R. M. Aikin, E. Garcia, M. Goldblatt, W. B. Hutchinson. G. H. Kwei, C. B. Pierce, J. F. Smith, J. D. Thompson, T. E. Walker, M. J. Fluss, R. G. Meisenheimer, and L. Bernardez. "A Large Oxygen Isotope Shift in $YBa_2Cu_3O_{7-x}$," Los Alamos National Laboratory, Los Alamos, N.M., LA-UR 88-533.

D. R. Harshman, L. F. Schnemeyer, J. V. Waszczak, Y. C. Jean, M. J. Fluss, R. H. Howell, and A. L. Wachs, "Temperature Dependence of the Positron Annihilation Lifetime in Single-Crystal $YBa_2Cu_3O_7$," *Phys. Rev. B* **38**, 848 (1988); UCRL-97969.

R. B. Laughlin, "Why I Think High-Temperature Superconductivity and the Fractional Quantum Hall Effect are Related," *Science* **242**, 525 (1988).

A. K. McMahan, R. M. Martin, and S. Satpathy, "Calculated Effective Hamiltonian For La_2CuO_4 and Solution in the Impurity Anderson Approximation," *Phys. Rev. B* **38**, 6650 (1988); UCRL-98744.

H. M. Ledbetter, M. W. Austin, S. A. Kim, T. Datta, and C. E. Violet, "Shear-Modulus Change Below T_c in $YBa_2Cu_30_{7-x}$," *J. Mater. Res.* **2**, 790 (1987).

P. E. A. Turchi, A. L. Wachs, K. H. Wetzler, R. H. Howell, M. J. Fluss, J. H. Kaiser, and R. N. West, "Electron Momentum Density Studies in High T_c Materials by Positron Annihilation Spectroscopy: Theory and Experiment," submitted to *Phys. Rev. B* (1989).

Conference Proceedings

H. B.Radousky and P. Hahn, "Magnetic Pair Breaking in the $Y_{1-x}Pr_xBa_2Cu_3O_{6.95}$ System," submitted for the Proceedings of the International Conference Materials and Mechanisms of Superconductivity High-Temperature Superconductors, Stanford, Calif., Jul. 23–28, 1989; UCRL-100538.

M. Sluiter and P. E. A. Turchi, "Electronic Theory of Phase Stability in Substitutional Alloys: A Comparison Between the Connolly-Williams Scheme and the Generalized Perturbation Method," submitted for the Proceedings of the 1987 NATO Advanced Study Institute on Alloy Phase Stability, Maleme, Crete, Greece, Jun. 14–27, 1989; UCRL-100606.

P.A. Sterne, "Electronic Structure of High Temperature Superconductors," submitted for the Proceedings of the Fourth International Conference on Superconducting, Santa Clara, Calif., Apr. 30–May 5, 1989; UCRL-100604.

W. J. Nellis, C. L. Seaman, M. B. Maple, E. A. Early, J. B. Holt, M. Kamegai, G. S. Smith, D. G. Hinks, and D. Dabrowski, "Shock Compaction of $YBa_2Cu_3O_{7-x}$ and $HoBa_2Cu_3O_{7-x}$ Powders in a Metal Matrix," submitted for the 1989 TMS Symposium on High Temperature Superconducting Oxides: Processing and Properties, Las Vegas, Nev., Feb. 1989; UCRL-100472.

Y. C. Jean, H. Nakanishi, P. E. A. Turchi, R. H. Howell, A. L. Wachs, M. J. Fluss, R. L. Meng, P. H. Hor, Z. J. Huang, and C. W. Chu, "Defect Properties of High Temperature Superconductors Probed by Positrons," submitted for the Proceedings of the Materials Research Society meeting, Boston, Mass., Nov. 28–Dec. 3, 1988; UCRL-98899.

A. L. Wachs, J. H. Kaiser, R. N. West, P. E. A. Turchi, et al. "Electronic Structure Studies of High-T_c Perovskites and Related Materials," submitted for the Proceedings of the International Conference on Positron Annihilation, Gent, Belgium, Aug. 29–Sep. 3, 1988; UCRL-98696.

W. J. Nellis, M. B. Maple, and T. H. Geballe, "Synthesis of Metastable Superconductors by High Dynamic Pressure," submitted for the Proceedings of the meeting of the Optical Engineering and SPIE—The International Society for Optical Engineering, Los Angeles, Calif., Jan. 11, 1988; UCRL-98108.

C. E. Violet, T. Datta, H. M. Ledbetter, C. Almasan, and J. Estrada, "Reentrant Softening in Copper-Oxide Superconductors," *Mater. Res. Soc. Symp. Proc.* **99**, 376 (1988).

Abstracts

J. L. Peng, R. N. Shelton, H. B. Radousky, and P. Hahn, "Preparation and Properties of $Nd_{1-x}Ce_xCuO_{4-\delta}$ Superconductor," submitted for the International Conference on Materials and Mechanisms of Superconductivity—High-Temperature Superconductors, Stanford, Calif., Jul. 23–28, 1989; UCRL-100695-Abstr.

P. E. A Turchi and A. Finel, "Possible Ordered States Based on the A15 Crystalline Structure," Lawrence Livermore National Laboratory, Livermore, Calif., UCRL-100495-Abstr. (1989).

R. H. Howell, H. B. Radousky, A. L. Wachs, M. J. Fluss, P.E.A. Turchi, Y. C. Jean, C. S. Sundar, C. W. Chu, R. N. Shelton, and D. G. Hinks, "Systematics in

Positron Annihilation Lifetime Analysis of High-T_c Superconducting Transitions," submitted for the International Conference on Materials and Mechanisms of Superconductivity—High-Temperature Superconductors, Stanford, Calif., Jul. 23–28, 1989;.UCRL-100480-Abstr.

A. L. Wachs, R. N. West, J. H. Kaiser, P. E. A. Turchi, S. Rayner, H. Haghighi, R. H. Howell, Y. C. Jean, M. J. Fluss, K. L. Merkle, A. Revcolevschi, and Z. Z. Wang, "Electron-Positron Momentum Distribution Measurements of High-Tc Superconductors and Related Systems," submitted for the International Conference on Materials and Mechanisms of Superconductivity—High-Temperature Superconductors, Stanford, Calif., Jul. 23–28, 1989; UCRL-100596-Abstr.

P. E. A. Turchi, R. H. Howell, A. L. Wachs, and M. J. Fluss, "Electronic Structure Studies of High T_C Materials: Theory and Experiment," submitted for the International Conference on Materials and Mechanisms of Superconductivity—High-Temperature Superconductors, Stanford, Calif., Jul. 23–28, 1989; UCRL-100595-Abstr.

J. B. Grant and A. K. McMahan, "Electronic Structure of La_2NiO_4," submitted for the Materials Research Society meeting, San Diego, Calif., Apr. 24–28, 1989; UCRL-100269-Abstr.

C. I. Merzbacher, B. P. Bonner, R. G. Bedford, P. A. Hahn, and C. E. Violet, "Diffuse Reflectance Infrared Spectroscopy as an Indicator of Oxygen Content and Annealing History of $YBa_2Cu_3O_{7-x}$," submitted for Symposium M—High Temperature Superconductors: Relations Between Properties, Structure and Solid-State Chemistry, San Diego, Calif., Apr. 9–14 1989; UCRL-99807-Abstr.

A. L. Wachs, P. E. A. Turchi, R. H. Howell, M. J. Fluss, J. H. Kaiser, R. N. West, Y. C. Jean, J. Z. Liu, and K. L. Merkle, "Comparative Electronic Structure Studies of $La_2CuO_{4-\delta}$, $YBa_2Cu_3O_7$, and NiO by Positron Annihilation Spectroscopy," submitted for the Materials Research Society meeting, San Diego, Calif., Apr. 24–28, 1989; UCRL-100146-Abstr.

H. B. Radousky, M. Costantino, J. L. Peng, and R. N. Shelton, "Superoxygenation Studies of $Y_{1-x}Pr_xBa_2Cu_3O_{7-\delta}$," submitted for the Materials Research Society meeting, San Diego, Calif., Apr. 24–28, 1989; UCRL-100210-Abstr.

N. W. Winter and C. E. Violet, "Quantum Chemistry Calculation of the Electric Field Gradients in $YBa_2Cu_3O_{7-x}$," submitted for the Materials Research Society meeting, San Diego, Calif., Apr. 24–28, 1989; UCRL-100750-Abstr.

J. L. Peng, R. N. Shelton, H. B. Radousky, and M. S. Costantino, "Synthesis and Superconducting Properties of the Tetragonal Superconductor $LaBaCaCu_3O_{7+\delta}$," *Bull. Am. Phys. Soc.* **34**, 929 (1989); UCRL-100093-Abstr.

M. S. Costantino, H. B. Radousky, J. L. Peng, and R. Shelton, "Superoxygenation of $Pr_xY_{(1-x)}Ba_2Cu_3O_{(7+y)}$," *Bull. Am. Phys. Soc.* **34**, 971 (1989); UCRL-100698-Abstr.

H. B. Radousky, R. Howell, P. Hahn, L. Bernardez, M. Costantino, J. L. Peng, R. N. Shelton, P. Klavins, and K. McCarty, "Superconducting and Normal State Properties of $Y_{1-x}Pr_xBa_2Cu_3O_7$," *Bull. Am. Phys. Soc.* **34**, 742 (1989); UCRL-100698-Abstr.

T. J. Folkerts, R. N. Shelton, H. R. Radousky, and E. M. Larson, "Physical Properties Measurements of $Ba_{1-x}K_xBiO_3$," *Bull. Am. Phys. Soc.* **34**, 845 (1989); UCRL-100094-Abstr.

A. K. McMahan, R. M. Martin, J. F. Annett, and S. Satpath, "Nature of the Hole Carriers in the 2-1-4 Superconductor," *Bull. Am. Phys. Soc.* **34**, 425 (1989).

A. L. Wachs, P. E. A Turchi, R. H. Howell, Y. C. Jean,. M. J. Fluss, K. L. Merkle, and A. Revcolevschi, "Electronic Structure Studies of NiO," *Bull. Am. Phys. Soc.* **34**, 1008 (1989).

J. L. Peng, R. N. Shelton, and H. B. Radousky, "Preparation of Single Phase $Y_{1-x}Pr_xBa_2Cu_3O_7$," submitted for Symposium F—High T_c Superconductivity, San Diego, Calif., Apr. 24–28 1988; UCRL-99864-Abstr.

R. M. Martin, J. F. Annett, and A. K. McMahan, "*Ab Initio* Calculations of Electronic Interactions in CuO Materials," submitted for the Materials Research Society meeting, Boston, Mass., Nov. 1988.

Presentations

N. W. Winter, "Theoretical Calculation of the Optical and Hyperfine Spectra of Cu in $YBa_2Cu_3O_{7-x}$," prepared for the 44th Symposium on Molecular Spectroscopy, Columbus, Oh., Jun. 12–16, 1989; UCRL-100751.

M. J. Fluss, P. E. A. Turchi, A. L. Wachs, R. H. Howell, J. H. Kaiser, R. N. West, Y. C. Jean, Z. Z. Wang, and C. W. Chu, "Electron Structure Studies with Positron Annihilation Spectroscopy," presented at International Superconductor Applications Convention, San Francisco, Calif., Jan. 11–13, 1989; UCRL-100077.

R. H. Howell, "Search for the Fermi Surface of High-T_c Materials," presented at DOE Teleconference, LBL, Berkeley, Calif., Jan. 27, 1989.

H. Radousky, "Rare Earth Substitution in Y123," presented at DOE Teleconference, LBL, Berkeley, Calif., Jan. 27, 1989.

TRITIUM

P. C. Souers, J. L. Maienschein *(Thrust Area Leaders)*

Introduction

The specialty of the LLNL Tritium Facility lies in two areas: cryogenics and lithium-beryllium hydrides. We believe these special low-Z fuels have bright futures in pure fusion. We also sample other tritium areas looking for a long-lasting project of interest.

Our goal in the next year will be the synthesis of ultrapure liquid and solid molecular DT. This should have a 100- to 1000-second triton relaxation time, which one hopes will be long enough for a try at nuclear polarization. Also of importance is learning ultrafast cooldown procedures for the cryostats, so that a DT sample can be solidified within minutes. Although the 0.5 K, 2 mW magnet/cryostat has been ordered for the eventual actual polarization, construction of this system is not expected to begin for a year.

Nuclear Spin Polarization*

Nuclear Magnetic Resonance

Pure tritium (T_2) and deuterium-tritium (D-T, actually D_2-DT-T_2) were adsorbed in thin layers on amorphous silica aerogel of a 600 m^2/g surface area. The longitudinal nuclear relaxation time, T_1, was found to be longer for tritons in thin layers than for those in the bulk solid. In the temperature range 4.2–6.5 K, we have

$$T_1 = AT^{-7}$$

where A is a constant and T is temperature. The T^{-7} function is characteristic of nuclear relaxation by phonons. The longest T_1 seen was 16 s (compared to 0.1 s in the bulk) for 0.5 monolayer (ML) at 4.2 K. We believe that the electric fields on the silica aerogel surface destroy the nuclear-rotational coupling that dominates nuclear relaxation in the bulk solid. Nuclear-phonon relaxation is a much longer process. This surface effect offers the long nuclear memory time needed for spin polarization. Unfortunately, the effect seen so far extends for only a few molecular MLs away from the wall. This effect could be enhanced in pure molecular DT at lower temperatures.

Electron Spin Resonance

Heat spikes have been seen in tritiated solid hydrogens cooled below ~3 K. Figure T-1 shows the hydrogen atom density as seen in solid D-T at 1.8 K. When spikes occur, the atoms disappear, then start to grow back in again. The spikes appear to involve a sudden and large-scale recombination of hydrogen atoms. Spikes are caused by fast temperature changes (e.g., from 3 K to 5 K) or magnetic field shifts (>30 G/s). Some spikes appear to

* Also a Director's Initiative IR&D Program.

be spontaneous at constant temperature. These can be halted in many cases by submersing the sample in liquid helium. The heat spikes are caused by the presence of tritium and are not seen in solid hydrogen deuteride.

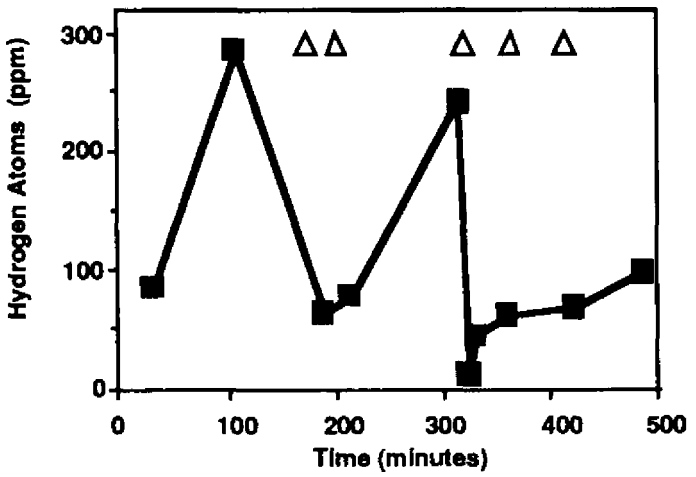

Fig. T-1. Effect of heat spikes (Δ) on the atom density in solid D-T at 1.8 K. Where spikes occur, the atoms disappear.

We have noted that the temperature sensed by a germanium sensor (seated in sapphire 13 mm from the D-T) increases from 4 K to ~8 K during a heat spike. A simple model of the flow of heat from an instantaneous source confirms that this temperature is consistent with the recombination of 300 ppm hydrogen atoms. The sapphire, because of its high thermal conductivity, acts as a thermal amplifier for this effect.

Almost two years ago, we observed an unexpected increase in the thermal conductivity of solid D-T when temperature suddenly increased. This result is shown in Fig. T-2. We believe now that this unusual effect is a result of the thermal spiking. Our current theory is

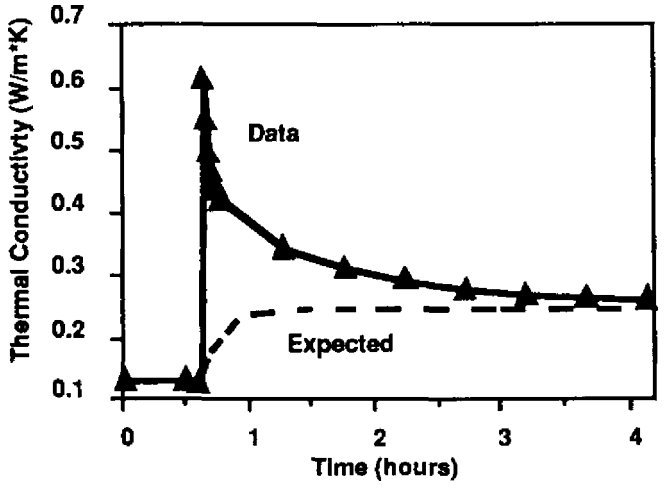

Fig. T-2. Unexpected increase in the thermal conductivity of solid D-T with a sudden temperature increase from 2.7 to 3.2 K. This effect is surely related to the thermal spike phenomenon.

that ~5–10 ppm of ions and electrons recombine with the atoms. This produces atoms having 5 eV energy each. These atoms may run in a conduction band and provide heat-carrying capacity. So much energy is released that the Air Force has given a small grant to J. Gaines, one of our collaborators at the University of Hawaii, to study this field further.

The heat spikes have been triggered in sapphire cells and a flash of light observed. The light has proved to be the red Cr_2O_3 line in the alumina, somehow stimulated by the atom recombination.

DT Purification System

In order to increase the triton nuclear relaxation times to 100 to 1000 seconds, we intend to purify our present 95 mol% molecular DT to 99.99%. We plan to use an absorption column, which will separate the hydrogen isotopes by mass. A literature survey indicates best separation with zeolite 4A or 5A or with activated alumina at 20 K and pressures up to 46 kPa. A mass-transfer model has been developed and is being moved to a Cray. A small test column has been built in a flow cryostat. The column is 250 mm long with a 1-mm inner diameter; therefore, packing in zeolite is very difficult. Acceptable flow rates have been obtained using zeolite 5A of 70 μm mean diameter.

The purity of the molecular DT will be checked in the liquid phase using a Raman spectrometer. The argon ion laser runs with 10 W at 488 nm. The reflected signal passes through an 1800-groove/mm monochromator and into a detector with a multichannel intensifier plate and photoresistive anode. This state-of-the-art system has been completed, and the pure rotational spectrum of hydrogen deuteride has been observed. The molecular DT will be measured at 20 K in a completed flow cryostat cell that has been tested to 10 K. Besides pure DT, the Raman system will also be used to analyze all routine Tritium Building samples.

Lithium-Beryllium Hydride Program

Reaction of lithium hydride and beryllium hydride to form new compounds has been observed. It is our hope that these compounds may have a higher proton density and be useful for inertial-confinement fusion (ICF). These compounds were made by heating the mixed reactants at 3.3 GPa for 50 to 100 hours at the low indicated temperatures. The products were determined by x-ray diffractometry by J. Cantrell of Miami Univ. (Ohio). The determinations as to "Li_2BeH_4" or "Li_3BeH_5" are taken from Ashby and Prasad [1], and the exact identity of the new compounds must be taken as tentative. Their densities and structures are unknown. Table T-1 shows the best results with there being considerable room to maximize future product yields. The sum of the percents do not add to 100% because LiH and BeH_2 are usually left over. We do not know what details of synthesis lead to one compound instead of the other.

Table T-1. Current Best Results: Lithium Hydride and Beryllium Hydride Reactions

Best Li_2BeH_4 Syntheses

$LiH-BeH_2$ mol% mix	Type of BeH_2	Temperature (K)	Mol% Composition Li_2BeH_4	Mol% Composition Li_3BeH_5
67-33	crystalline	403	73	27
67-33	crystalline	423	55	19
50-50	crystalline	503	47	25
50-50	amorphous	363	39	15
50-50	crystalline	383	37	37

Best Li_3BeH_5 Syntheses

$LiH-BeH_2$ mol% mix	Type of BeH_2	Temperature (K)	Mol% Composition Li_2BeH_4	Mol% Composition Li_3BeH_5
50-50	crystalline	363	77	23
50-50	crystalline	363	50	15
50-50	crystalline	383	47	33
50-50	crystalline	403	40	28
50-50	crystalline	383	37	37

References

1. C. Ashby and H. S. Prasad, *Inorg. Chem.* **14**, 2869 (1975).

Publications

J. R. Gaines, P. C. Souers, E. M. Fearon, J. D. Sater, and E. R. Mapoles, "The Effects of High Atom Densities on the NMR Relaxation Times in Solid T_2 and DT," *Phys. Rev. B* **39**, 3943 (1989).

J. S. Cantrell, T. A. Beiter, P. C. Souers, and P. E. Barry, "Thermal Stability and Phase Studies of the LiH + BeH_2 System," accepted by *Z. Phys. Chem. Neue Folge.*

P. C. Souers, P. A. Fedders, and T. O. Niinikoski, "Simple Models of Thermal Mixing (Dynamic Cooling)," submitted to *J. Magn. Res.*

W. G. Wolfer, C. L. Bisson, P. C. Souers, and R. T. Tsugawa, "The DC Electrical Conductivity of D-T Gas," submitted to *Phys. Rev. A.*

P. C. Souers, R. T. Tsugawa, C. L. Bisson, and W. G. Wolfer, "Thomson Space Charge in D-T Gas," submitted to *J. Vac. Sci. Technol. A.*

P. C. Souers and P. A. Fedders, "Considerations in the Deuteron Polarization of Solid DT," submitted to *Phys. Rev. B.*

P. C. Souers, E. M. Fearon, J. D. Sater, E. R. Mapoles, J. R. Gaines, and P. A. Fedders, "NMR of D-T Adsorbed onto Silica Aerogel at 4.2–23 K," submitted to *J. Chem. Phys.*

Presentations

P. C. Souers, E. M. Fearon, E. R. Mapoles, J. R. Gaines, and P. A. Fedders, "Nuclear Relaxation Time of Tritiated Solid Hydrogen Adsorbed onto Silica Aerogel," *Bull. Am. Phys. Soc.* **34**, 476 (1989).

G. W. Collins, P. C. Souers, E. R. Mapoles, and J. R. Gaines, "Properties of H and D Atoms in Solid Molecular HD," *Bull. Am. Phys. Soc.* **34**, 476 (1989).

INTERFACES, ADHESION, AND BONDING

W. E. King *(Thrust Area Leader)*

Overview

This report describes the technical activities and progress of the Interfaces, Adhesion, and Bonding thrust area. Research concentrated on investigation of the bond strength of metal/ceramic interfaces and the structure and properties of metal grain boundaries. Areas highlighted in this report are:

- Measurement of bond strength at metal/ceramic interfaces
- Trace impurity analysis of bulk single crystals
- Electronic structure calculations at metal grain boundaries.

In addition to these, substantial progress has been made in simulation of high-resolution electron microscope images and production of precisely-oriented, flat single crystals.

Measurement of Bond Strength at Metal/Ceramic Interfaces

G. L. Nutt W. Lai K. E. Froeschner
W. E. King

We have constructed an apparatus for measuring the bond strength of metal/ceramic interfaces. It has been successfully used to measure the strength of the Ni-sapphire bond. The method consists of rapidly breaking the bond by spalling the metal film from the ceramic substrate. The stress history of the interface during the disbonding process is recorded using a laser interferometer. The mechanical stress at the bond interface is generated by a magnetic hammer, which projects a thin metal flyer into the substrate [1,2]. A shock wave is generated on impact that propagates through the substrate and film. At the free surface, the compressive wave is reflected as a tensile wave that is subsequently incident on the bonded interface as indicated in Fig. IA-1. If the tensile stress at the bond surface, σ_z, exceeds the strength of the bond, σ_s, the interface will spall.

The spall stress is related to the velocity measurements through the relation [2]:

$$\sigma = \frac{\rho_0 C}{2}(u_0 - u_k) \qquad \text{(Eq. IA-1)}$$

where σ is the stress on the surface at the instant of rupture, ρ_0 is the density of the film, and C is the velocity of propagation of the stress wave. The free surface velocity gives the initial jump off velocity, u_0, and the velocity at the first pullback, u_k.

This interpretation of the measured velocity history in terms of bond strength is valid if the amplitude of the stress wave is not great enough to cause the material to deform plastically, i.e., the axial stress does not exceed the Hugoniot elastic limit (HEL) of the material. In this case, C is the elastic sound speed of the metal film. Thus, Eq. IA-1

applies to interfacial bonds between strong materials. If the stress wave is great enough to introduce some plasticity into the film, the appropriate value of C is the harmonic mean of the elastic and plastic sound speeds [3].

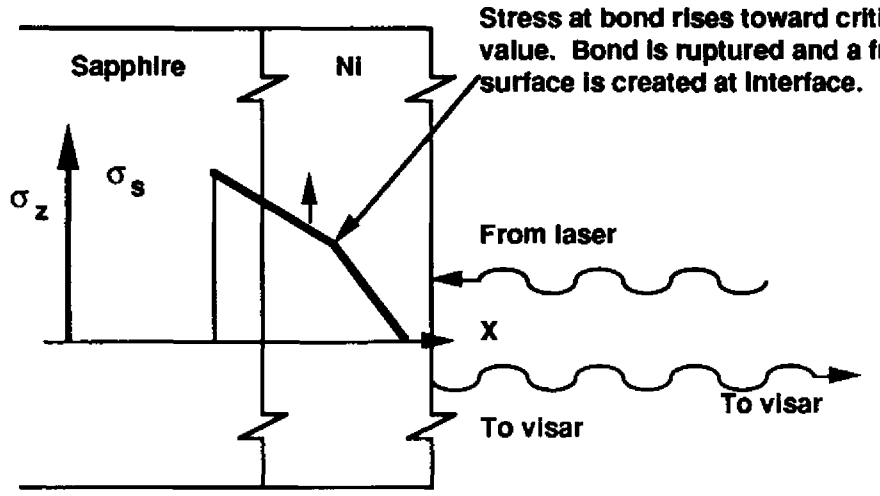

Fig. IA-1. Schematic diagram of stress history at bonded interface.

Two of the most important features of this method of bond testing are (1) that no fixtures are attached to the specimen and (2) that rapid rise times are possible in the application of the tensile stress. Attachments to the specimen can affect the bond by inducing residual stresses. It is also important in bond-strength measurements that the bond is ruptured rapidly enough that separation through crack growth cannot occur. Crack growth as a method of bond breaking allows stress concentrations at the edge of the disbond. Therefore, the critical stress for separation by crack growth is not simply related to the atomic forces of attachment across the interface.

The time required for disbonding by crack growth can be estimated. Roberts and Wells [4] derived the velocity of growth of a two-dimensional crack of length l under an applied stress σ:

$$\dot{l} = \frac{2\pi E}{k\rho}\left(1 - \frac{l_0}{l}\right)\left(1 + \frac{l_0}{l} - \frac{4TE}{\pi\sigma^2 l}\right) \qquad \text{(Eq. IA-2)}$$

where E is Young's modulus, T is the surface tension, and k is a dimensionless parameter. For typical numbers (T = 2 J/m^2 and $E = 7\times10^4$ J/cm^3) and a stress of 0.1 GPa, the cracks that propagate are greater than 1 μm in size. Integrating the equation of motion for l, we find that, at slightly above the threshold stress, a 1-μm crack doubles in size in 100 ns whereas the free surface velocity measurements show the rise time to be <1 ns. Hence, with sufficient care in sample preparation, atomic bond rupture should be the mechanism of separation in this experiment rather than propagation and merging of cracks.

The Experiment

For bond-strength experiments, special conditions are desired:

- The magnitude of the incident shock should not exceed the HEL of either material, to avoid plastic deformation of the substrate or overlayer.
- The wave should be sharply peaked.
- The interface must be the weakest part of the system.

These constraints require rather weak shocks generated by thin flyers. The magnetic hammer produces such precisely controlled shock conditions in the required stress range. The details of operation are discussed elsewhere [6].

The velocities u_0 and u_k of Eq. (IA-1) are measured using a visar (velocity interferometer system for any reflector) laser interferometer [6]. The light reflected from the surface of the film is split into two parts, one of which is sent through a delay; the two are then mixed. The interference fringes are recorded using four photomultiplier tubes.

The photomultiplier data are recorded digitally. A five-point running average is made of the raw data to smooth the photon noise. The velocity history of the film free surface is calculated using the length of the delay section, the index of refraction of the etalon block, and the laser light frequency.

Samples were prepared by sputter deposition of 20 μm of nominally pure Ni on a sapphire substrate at room temperature. The Ni was deposited on a 1.27-cm-diameter piece of sapphire 0.32 cm thick. The substrate was impacted with a Cu flyer 0.0064 cm thick with velocities in the range 0.02–0.029 cm/μs, producing a peak axial stress in the Ni film in the range 2.4–3.6 GPa near the interface with a pulse 32 ns long. The yield strength of Ni is nominally 1.2 GPa, and the HEL of sapphire is 14 GPa.

Results

A typical measured free-surface velocity is shown in Fig. IA-2. The rise time of the incident shock is too short to record, even with our 3-ns resolution, indicating that crack propagation was not the mechanism of bond separation. With an assumed elastic sound speed of 0.587 cm/μs for Ni, the ringing period of the metal film is estimated to be ~6.8 ns and is clearly evident. On recovering the test specimens, we found the Ni film attached around the edge but the foil detached in the center, with an occasional "dog-ear" standing as evidence of film separation. Thus, after initial separation, the foil near the center would return to contact with the substrate. It is our conjecture that this is the source of the other periods appearing in the velocity data. For example, the 21.0-ns ringing period of the Cu flyer appears for at least two cycles. Any two-dimensional effects, in the form of relief waves from the lateral surfaces, are estimated to appear ~0.24 μs after jumpoff.

Four determinations were made of the bond strength of the sapphire-Ni bond. Estimating the HEL of Ni as 2.1 GPa, we see that the experiments are in a region where the transition of the metal film from elastic to plastic behavior occurs. Limiting the stress to

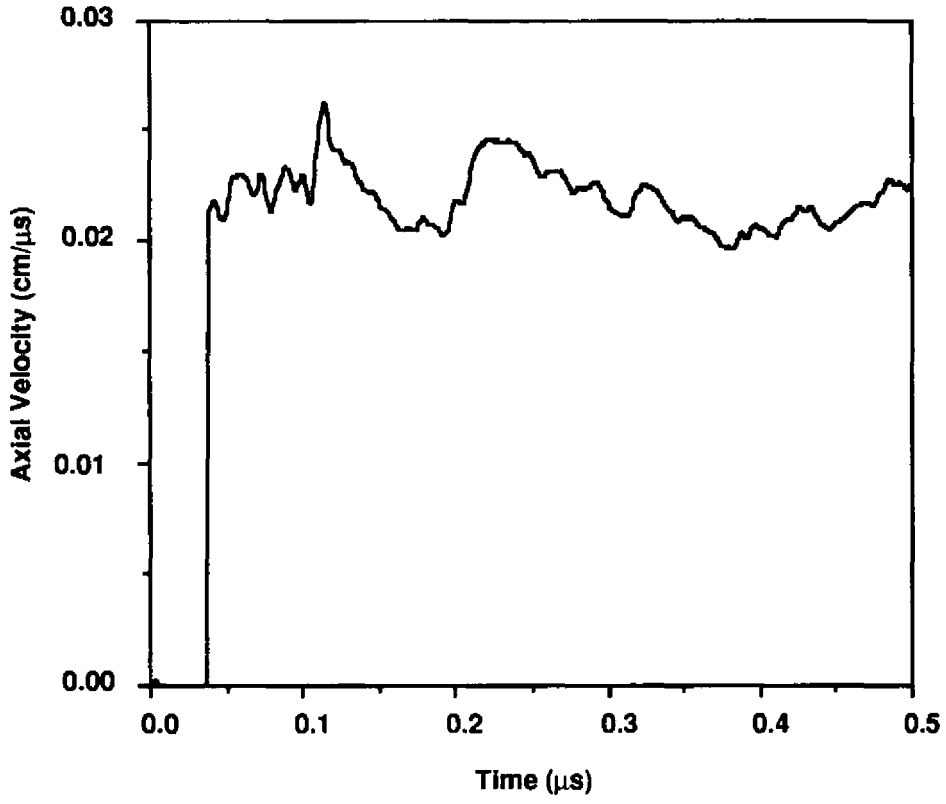

Fig. IA-2. Measured axial velocity as a function of time for spall of Ni from sapphire.

less than 1.0 GPa would have ensured that the Ni remained in the elastic region. However, our main concern in these exploratory measurements was to demonstrate spall. The data give the mean value of 0.177±0.024 GPa for the spall strength of the bond.

Trace-Impurity Analysis of Bulk Single Crystals

S. Fadeff W. E. King

High-purity Nb samples were sent to Ames National Laboratory, LLNL, and Leco Corporation to be analyzed by various analytical techniques.

The Experiment

There are two standard techniques for H, N, and O analysis: (1) vacuum fusion and (2) ignition in a gas stream (usually done in Leco gas analyzers). Carbon in metals was determined by combustion methods. Silicon and iron were analyzed by scanning laser mass spectrometry (SLMS) at Ames. SLMS is semiquantitative with wide element application and few interferences. Another well-established method, which is useful for analyzing a large number of elements, is inductively-coupled plasma mass spectrometry (ICPMS). ICPMS provides quantitative results with a relative standard deviation of ~10% at trace impurity levels of ~10 ppmw (parts per million by weight). Because ICPMS is so

sensitive, sample solutions can be greatly diluted so that matrix matching to standard solutions is relatively easy. Therefore, this instrument provides the most accurate method of analysis for trace-level metals.

Results and Discussion

The results of the tests of various methods for determining trace impurity are presented in Table IA-1. Ten impurity elements were positively identified, with oxygen and tantalum being the most abundant. Agreement between methods for elements of atomic number higher than 42 was good. For the other elements, either a comparison was not made or agreement was poor.

Table IA-1. Comparison Study of Nb Analytical Results*

Element	Ames Vac. Fus.	Ames SLMS	Ames Combust.	Leco Ignit.	LLNL Comb./Ignit.	LLNL ICPMS
H	22				3.9±0.3	
C		80	11		16±1	
O	18	127		43,39	61±16;9±7	
N	20	39		2	0.8±0.2; 0.2±0.2	
S		<2			6±2	
Si		0.6				
Fe		3.6				
Cr		1.7				<0.2
Mo		6.7				3
Ta		66				89
W		17				10.6
Others		not detected				not detected**

* Results are in parts per million by weight.
** Au, Zr, Tm may be present at or below the detection limit.

The results of H determination were 22 and 4 ppmw by vacuum fusion and ignition, respectively. Even with the estimated error taken into account, these values do not compare well. Because it is extremely difficult to accurately measure H at these low levels in metals, this discrepancy may require extensive studies to resolve. Further analyses are being carried out at the Univ. of Illinois.

Nitrogen analysis by the ignition method showed the impact of sample-handling techniques on analysis results:

- Initially, after a routine acid bath for surface cleaning, N content measured 40 ppmw with excellent precision by ignition. In two trials of surface machining under Ar atmosphere, N values measured by the same technique were 0.8±0.2 and 0.2±0.2 ppmw (4 determinations in each case).
- Sample preparation by Leco was simple surface abrasion and gave N values of 1 and 2 ppmw.

- Sample preparation at Ames entailed electropolishing the sample in chilled phosphoric acid/methanol solution and produced relatively high results of 20 ppmw. Furthermore, it was the opinion of the Ames chemists that the nitrogen number obtained by the vacuum fusion technique tends to be low by as much as 10% relative.

It is interesting to note that SLMS came up with a value of 39 ppmw for N content, similar to the initial N values obtained by ignition. The surface preparation constituted laser ablation in the 1–10 μm range. Thus, a subsurface analysis technique shows relatively high N concentration. It therefore seems evident that the N is concentrated at the sample surface and that acid etching/electropolishing techniques do not remove the surface contamination adequately.

Oxygen analysis results were similar to N results in indicating a surface concentration effect. A first-pass analysis at LLNL gave 200 ppmw O for a sample that had been simply acid cleaned/etched in HNO_3. (SLMS analysis gave a comparable result of 127 ppmw.) Two trials of surface machining under Ar atmosphere gave 61±16 ppmw and 9±7 ppmw, with 4 analyses in each set. The sample file-abrasion method by Leco on two samples gave O results of 43 ppmw and 39 ppmw. The electropolishing done at Ames followed by vacuum fusion analysis gave 18 ppmw O. It is unclear why this should be low relative to the other analysis results. The bulk O content appears to approach 40±20 ppmw.

Further analysis methods will be investigated for H, N, and O determinations. Also, a study will be conducted to determine the best sample preparation procedure prior to bulk analysis as it seems this causes the widest variation among repeat analyses. When the appropriate sample preparation procedures have been defined and the resultant discrepancies have been resolved, we intend to take full advantage of the vacuum fusion method of analysis.

The carbon analysis results from LLNL and Ames compare well with values of 16 and 11 ppmw, respectively. The SLMS method gave a C result of 80 ppmw, but not much weight can be placed on it without a standard.

Sulfur analysis at LLNL, in conjunction with analysis for C, showed 6 ppmw present in the sample; the SLMS sample showed <2 ppmw, which may make these numbers comparable when the associated error associated is taken into account. Because the SLMS value is so low, surface concentration of S may be insignificant.

The SLMS analysis for Si and Fe showed very low levels of contamination, 0.6 and 3.6 ppmw, respectively. We will confirm these values by an alternative analysis method.

Trace impurities of Mo, Ta, and W were found by SLMS and ICPMS, and agreement within the expected standard deviation was obtained. Chromium was found by SLMS at a level of 1.7 ppmw. A Cr peak was evident in the ICPMS sample scan but was just a little higher than the blank; therefore, according to the ICPMS detection limit for Cr, it would be present at less than 0.2 ppmw.

ICPMS also indicated that Au and Zr are present at less than 2 ppmw, and Tm may be present at less than 0.1 ppmw. These were reported as not-detected by SLMS. The two methods do essentially agree with each other in the identification and quantification of the heavier elements >3 ppmw.

Conclusions

Further study needs to be done on sample-preparation techniques for the interstitial gas analysis. Also, the surface concentration of some of these interstitial gases may need to be differentiated from the bulk concentration to be properly applied to the UHV bonding studies. All elements of interest can be analyzed with current techniques. In most cases, the detection limits should be adequate. Where improved detection limits are needed, some methods development would be required. A summary of the ideal choices of analysis methods (assuming the preparation problems for interstitial gas analysis can be solved), precision, detection limits, and estimated costs are presented in Table IA-2. A total of ~1.7 grams would be required for the complete analysis including duplicates for the interstitial gases at an estimated cost of $1030/analysis.

Table IA-2. Recommended Methods of Analysis

Element	Lab/ Method	Detection Limit (ppm)	Precision	Number	Total Weight	Estimated Cost
H	Ames/ Vac. Fus.	1	10%	2	0.4 g	$630*
C	LLNL/ Leco	2	30%	2	1.0 g	$200
N	Ames/ Vac. Fus	1	10%	2	same for H**	*
O	Ames/ Vac.Fus.	4	10%	2	same for H**	*
Si	Ames/ SLMS	0.01	300%	na***	≤0.1 g	*
Fe	Ames/ SLMS	0.03	300%	na***	≤0.1 g	*
General impurities	Ames/ SLMS	≤3	300%	na***	same for Si	*
General impurities	LLNL/ ICPMS	≤2	10%	1	0.2 g	$200
TOTALS					1.7 g	$1,030

* The cost for analysis at Ames Laboratory is $630 which includes C, N, O, H, and SLMS analyses.
** One sample is used for the H, N, and O analyses.
*** One sample is rastered many times to obtain an average value; the total quantity used is on the order of micrograms

Electronic-Structure Calculations at Metal Grain Boundaries*

E. C. Sowa A. Gonis

Electronic-structure calculations with the real-space multiple-scattering theory (RSMST) have been performed at $\Sigma 5$ (100) 36.9° twist and $\Sigma 5$ (310) tilt grain boundaries in Cu. The effects of boundary relaxations predicted by the embedded-atom method (EAM) on the local electronic DOSs were investigated. This report summarizes the RSMST solution to the problem of calculating the electronic structure of systems of reduced symmetry such as interfaces; it also describes the first results on interfaces obtained in this manner.

The Electronic Structure Problem at Interfaces

The performance of electronic-structure calculations requires two distinct, although interrelated ingredients: (1) the knowledge of atomic positions (the atomic structure of the material) and (2) the existence of methods capable of providing a proper treatment of the one-electron Schrödinger equation under the boundary conditions imposed by a particular structure. For materials with full translational periodicity (e.g., bulk single crystals), the atomic structure can be determined experimentally by standard techniques. In systems with reduced symmetry (surfaces or internal interfaces), the determination of both the atomic and electronic structure becomes much more problematic. However, the experimental determination of surface atomic structure can be accomplished with satisfactory accuracy through, for example, low-energy electron diffraction (LEED) and, more recently, scanning tunneling microscopy (STM) techniques. For interfaces, one must almost always rely on computer simulation studies such as those afforded by EAM.

Now, unlike materials based on regular-lattice structures, knowledge of the atomic coordinates for defective systems does not necessarily allow the calculation of electronic structure with conventional methods. This is because nearly all existing first-principles formalisms for performing such calculations are based on the properties of translational invariance and Bloch's theorem. Consequently, it has often been found necessary to invoke rather severe approximations with respect to the structure of the system under study, such as the use of slabs of finite thickness to treat surfaces or of repeating slabs or supercells to study internal interfaces.

Recently, we have developed a first-principles multiple-scattering formalism which allows the exact treatment of the one-particle Schrödinger equation for a broad spectrum of systems. In this formalism, full translational invariance and Bloch's theorem are replaced by semi-infinite periodicity and removal invariance. The range of applicability includes (but is not limited to) pure elemental solids, compounds, ordered alloys, substitutionally disordered alloys, surfaces, and interfaces in either ordered or substitutionally disordered materials. Initial results obtained using this method on Cu grain boundaries with relaxed atomic structures predicted by the EAM are discussed below.

---

* See also "Electronic Structure of Systems with Reduced Symmetry" in Departmental IR&D, p. 95.

Results and Discussion

The first interfaces studied with RSMST were unrelaxed and relaxed Σ5 (100) 36.9° twist and Σ5 (310) tilt grain boundaries in Cu. These boundaries were chosen because of the availability of relaxed atomic configurations, obtained by S. M. Foiles with the EAM. In each of these systems, the effect of boundary relaxation on the local electronic DOS of an atom at the interface was investigated. Tilt boundary results are shown in Fig. IA-3. It is clear that the DOS of the unrelaxed boundary (Fig. IA-3a) loses some of the structure seen in bulk Cu; this is associated with the expected destruction of the Van Hove singularities in an aperiodic structure. Relaxations predicted by the EAM are dominated by an increased intergranular separation; they yield DOSs that display a reemergence of some of the bulk structure (Fig. IA-3b), as well as a narrowing of the band similar to that produced by a decrease in the coordination number. The results for the twist boundaries are qualitatively similar.

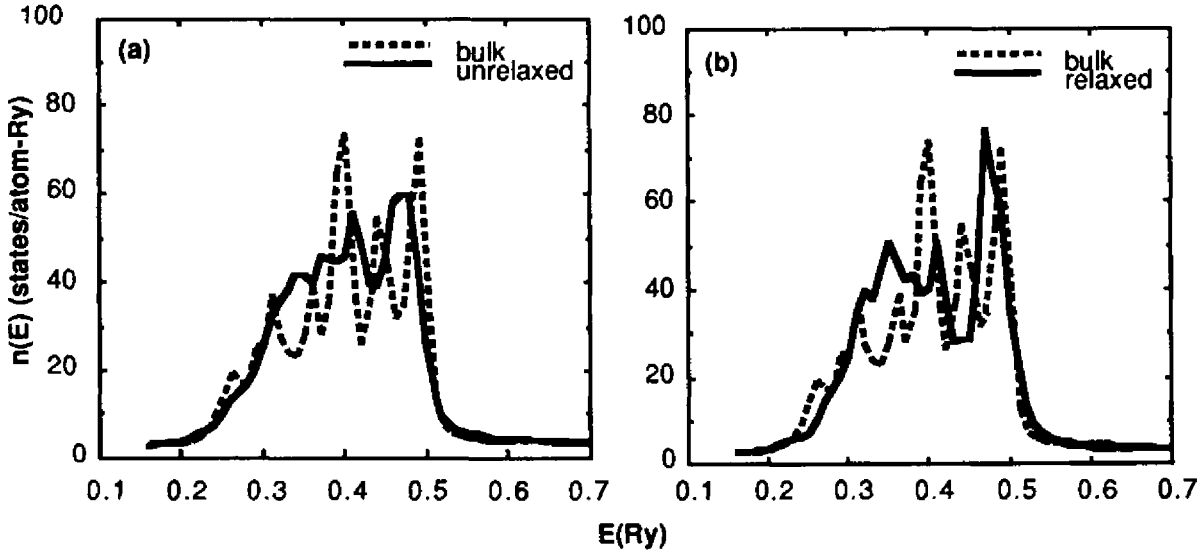

Fig. IA-3. Density of states for Σ5 unrelaxed (a) and relaxed tilt grain boundary (b) in Cu. Bulk DOS shown as dashed line.

Conclusions

In future, the RSMST codes will be used to perform electronic structure calculations of tilt grain boundaries in Cu and Nb (both unrelaxed and relaxed configurations) and to compare the energetics of the two types of systems within a bond-energy (non-self-consistent) mode. In turn, these will be compared with the predictions of EAM calculations that yield the atomic positions of the relaxed configurations. In the next series of calculations, the electronic structure of unrelaxed and relaxed grain boundary configurations in Cu and Nb will be calculated within a charge self-consistent mode. Band energies (kinetic energy terms) of various configurations will be computed; predictions based on them will be compared to those of EAM calculations. Our goal is to be able to calculate total energies of unrelaxed and relaxed grain boundaries in Cu and Nb within a

fully self-consistent total-energy approach. The results will then be compared to those of non-self-consistent studies of the EAM.

References

1. W. E. Snowden and I. A. Aksay, *Mater. Sci Res.* **14**, 651 (1981).
2. S. A. Novikov and A. V. Chernov, *J. Appl. Mech. Tech. Phys.* **5**, 703 (1982).
3. V. I. Romanchenko, D. Maiden, and H. Chou, *J. Appl. Mech. Tech. Phys.* **21**, 555 (1980).
4. D. K. Roberts and A. A. Wells, *Eng.* **178**, 820 (1954).
5. G. L. Nutt, W. Lai, K. E. Froeschner, and W. E. King, *Acta Metall.* (1989), in press.
6. D. R. Goosman and N. L. Parker, Lawrence Livermore National Laboratory, Livermore, Calif., UCRL-52792 (1979).

Publications

X. -G. Zhang and A. Gonis, "A New, Real Space, Multiple Scattering Theory Method for the Determination of Electronic Structure," *Phys. Rev. Lett.* **62**, 1161 (1989).

X. -G. Zhang, E. C. Sowa and A. Gonis, "A First-Principles Method for the Determination of the Electronic Structure of Grain Boundaries," *Scripta Metall.* (1989), in press.

J. Pelz, J. Clarke and W. E. King, "Flicker (1/*f*) Noise in Copper Films due to Radiation-Induced Defects," *Phys. Rev. B* **38**, 386 (1988).

G. L. Nutt, W. Lai, K. E. Froeschner and W. E. King, "Direct Measurement of Interface Bond Strength," *Scripta Metall.* (1989), in press.

W. E. King, K. S. Grabowski, D. F. Mitchell and P. M. Baldo, "Rutherford Backscattering Study of High Temperature Oxidation of Y Implanted Fe-24Cr," *Oxid. Met.* **3331**, 181 (1989).

W. E. King and J. H. Park, "Anion Grain Boundary Diffusion in Cr_2O_3 and Cr_2O_3-0.09 Weight Percent Y_2O_3," *Mater. Res. Soc. Symp. Proc.* **122**, 193 (1989).

Presentations

X. –G. Zhang, A. Gonis and J. MacLaren, "A New Method for the Determination of Electronic Structure," *Bull. Am. Phys. Soc.* **34**, 640 (1989).

E. C. Sowa, A. Gonis, X. –G. Zhang and S. M. Foiles, "The Electronic Structure of Unrelaxed and Relaxed Grain Boundaries in Cu," *Bull. Am. Phys. Soc.* **34**, 825 (1989).

E. C. Sowa, A. Gonis and X. –G. Zhang, "First-Principles Calculations of the Electronic Structure of Grain Boundaries," to be presented at Session 1: INTERFACIAL AND ATOMIC STRUCTURE of the International Congress on Intergranular and Interphase Boundaries in Materials: IIB89, Ecole des Mines des Paris, France, Sep. 4–8, 1989,

G. L. Nutt, W. Lai, K. E. Froeschner and Wayne E. King, "Direct measurement of interface bond strength," invited paper presented at The Acta Metallurgica/Scripta Conference on Bonding, Structure, and Mechanical Properties of Metal Ceramic Interfaces, Santa Barbara, Calif., Jan. 15–18, 1989

G. L. Nutt, W. Lai, K. E. Froeschner and W. E. King, "Direct Measurement of the bond strength of metal/ceramic interfaces," abstract to be presented at Session 3: HETEROPHASE INTERFACES of the International Congress on Intergranular and Interphase Boundaries in Materials: IIB89, Ecole des Mines des Paris, France, Sep. 4–8, 1989.

W. E. King, "Anion and Cation Diffusion in Cr_2O_3 and Cr_2O_3 doped with Y_2O_3," presented at University of Pennsylvania, Philadelphia, Pa., Oct. 1988.

PLUTONIUM AND ACTINIDES

G. F. Gallegos *(Thrust Area Leader)*

For FY89, a new project on liquid-metal/solid interactions has been added to the Plutonium and Actinides thrust area. The remaining four projects have continued with some redirection and definition of goals in order to meet longer-term research objectives.

Examination of the Pu-Ce and Pu-Sc Alloy Systems by Triode-Sputtering

H. Rizzo *(Principal Investigator)* A. W. Echeverria T. B. Massalski*
E. C. McClanahan** Mike Stevens† T. Zocco†

The objective of this project is evaluation of the binary systems Pu-Ce and Pu-Sc in order to gain insight into the alloying behavior of plutonium, which may lead to the development of dense, stable alloys. These two binary systems were chosen because they both possess large regions of δ-phase stability over a wide range of temperatures and pressures (at the Pu-rich end) similar to the more-studied Pu-Ga and Pu-Al systems. The Pu-Sc and Pu-Ce binary systems differ from the other two in that Pu-Sc only forms one intermetallic compound and Pu-Ce forms none.

Triode-sputtering is an excellent choice of technique to study these systems. By use of a split-target technique, a wide region of compositions can be fabricated in one or two runs. In addition, varying the sputtering parameters enables production of sputtered materials ranging from "equilibrium" conditions to high-quench-rate, non-equilibrium structures. Finally, the cleanliness of the sputtering process produces fewer inclusions and macro-defects in the materials fabricated, which is important in TEM (transmission electron microscopy) studies.

Progress during the period includes sputtering of compositions between 2 and 62 at.% Sc at substrate temperatures of 22 and 200 °C. X-ray diffraction (XRD) analysis indicated that coatings prepared at the lower temperature resulted in extending the fcc Pu(Sc) solid-solution range to ~50 at.% Sc, compared to the equilibrium value of ~20 at.% Sc [1]. In addition, the ζ double-hexagonal phase was not observed, and only the hexagonal α-Sc solid-solution phase was observed at the Sc-rich compositions (52 and 57 at.% Sc). This result is not surprising since the rapid quenching and high deposition rates at the low substrate temperature would tend to suppress formation of this double-hexagonal crystal structure compared to the fcc phase. The phases observed in coatings sputtered at 200 °C correspond to those observed in the equilibrium phase diagram.

* Carnegie-Mellon University.
** Battelle Pacific Northwest Laboratory.
† Los Alamos National Laboratory.

Microhardness measurements of the sputtered deposits made at the 20 °C substrate temperature (shown in Fig. PA-1) illustrate a two-phase mixture of (α+δ)-Pu between 2 and 13 at.% Sc followed by a linear increase in hardness up to 50 at.% Sc. This could be attributed to solid-solution strengthening of the δ-Pu lattice by the Sc. A comparison to our earlier work on Pu-Ce (shown in Fig. PA-2) does not show the hardening effect. This difference in behavior will be evaluated further.

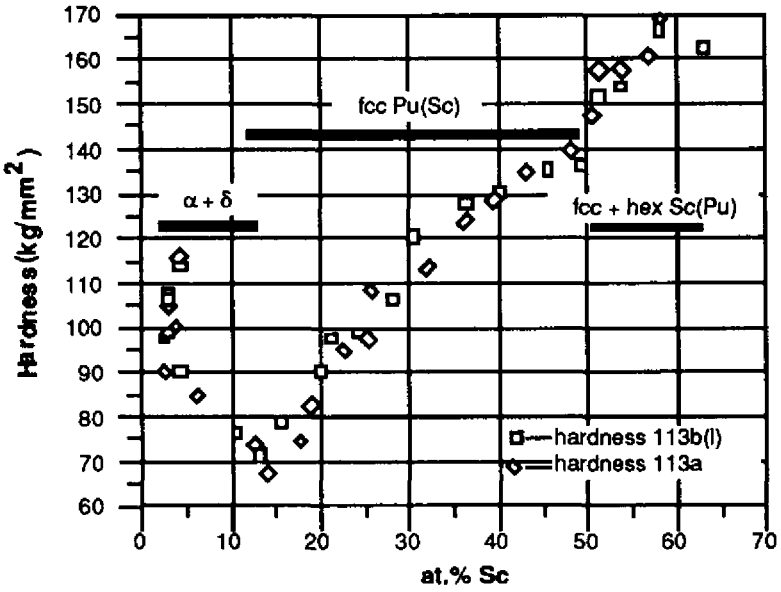

Fig. PA-1. Microhardness of PuSc coatings sputtered at 20 °C.

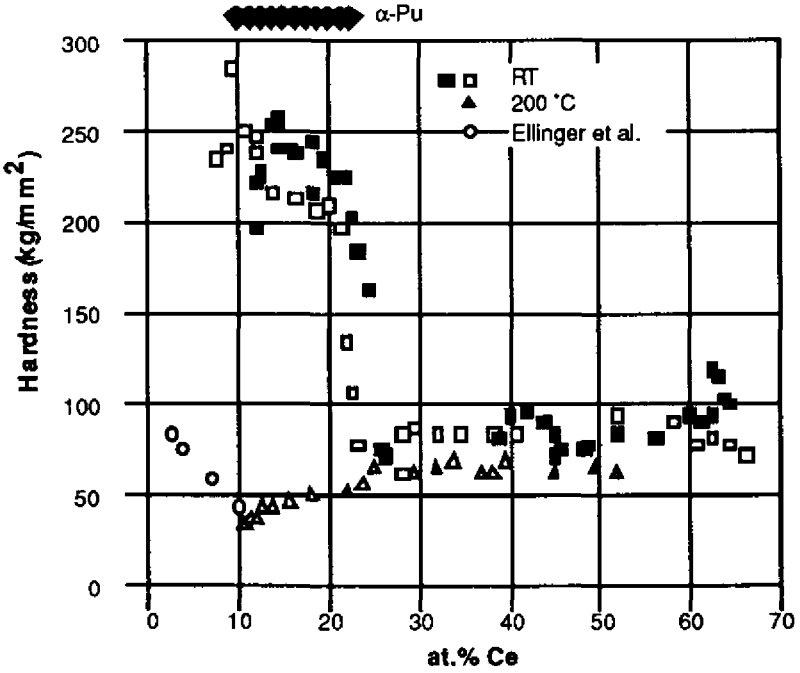

Fig. PA-2. Microhardness of Pu-Ce alloys sputtered at 20 °C and 200 °C.

Above 50 at.% Sc, the hexagonal (a-Sc) phase was observed. Lattice-parameter measurements of the solid-solution phases indicate a volume expansion of ~3 at.% for the sputtered sample (compared to annealed samples from [1]), which indicates a volume expansion of ~5 at.%) and is in agreement with Vegard's Law. Microhardness measurements of annealed phases from [1] were reported as 44–52 for δ-phase; 77–106 for ζ; and 84–97 for the α-Sc phase. The greater hardness values observed for the sputtered deposits may be due to the higher densities observed from the lattice-parameter measurements.

Sputtered samples of Pu-Sc and Pu-Ce are being sent to LANL for TEM analyses. These results, coupled with differential scanning calorimetry (DSC) measurements, should further establish the projected metastable phase diagrams, which are currently based on only XRD, metallography, and microhardness measurements.

We have continued our analysis of results from sputtered compositions done last fiscal year. One set of comparisons between Pu-Ce and Pu-Yb shows a wide difference in alloying behavior. Pu and Yb are reported as being completely immiscible whereas Pu-Ce alloys are not. In order to complete this study, heats of mixing calculations are being computed for Pu-Ce. Specimens of both alloy systems are being sent to LANL for TEM characterization.

Studies involving several systems with positive heats of mixing (including Ag-Fe, Mo-Cu, W-Cu) are being concluded. It appears that these calculations, coupled with a series of sputtering experiments using a Cu-50 at.% W composite target, illustrates our ability to sputter amorphous phase compositions in most of these systems due to kinetic freezing of the amorphous phases that is achieved by the high deposition rates in our triode-sputtering system.

Electronic Structure Calculations

A. Gonis

Electronic-structure calculations from first principles are of interest for several reasons. For some alloys, it is possible to calculate physical properties and compare them with experimental measurements. In addition, certain observations made on Pu-alloy systems formed by sputtering can only be explained by changes in the electronic structures of Pu. Similar arguments have been made to explain certain phase-transformation phenomena. In future, it may be possible to calculate phase boundaries for alloy systems; however, this is recognized as a longer-term objective. Because of unique features of actinides and (in particular) Pu, significant needed code development is being supported by this thrust area.

As the first step in these efforts, the electronic structure of dilute fcc Pu-Ce alloys (5 at.% and 10 at.% Ce in Pu) was calculated by P. Weinberger using a fully relativistic, but non-self-consistent, Green's-function method. A paper is in preparation on these results, and charge self-consistency is currently being incorporated into Weinberger's code.

Note that the Weinberger codes can only accommodate cubic structures and are incapable of handling the monoclinic (α-phase) Pu.

Our goals for this fiscal year are to make the new RSMST code [1] self-consistent and fully relativistic. For Pu, the RSMST code is preferred because it can handle nonsymmetric systems (e.g., monoclinic α-Pu), surfaces, and interfaces. A relativistic form is necessary to accommodate the 5f electrons in actinides. Achieving charge self-consistency is also needed for correct handling of surface effects and for the ability to handle a bulk material, advantageous over a slab configuration currently calculated by other investigators.

This fiscal year, F. Pinski (Univ. of Cincinnati) has been hired to help develop this code with initial emphasis on incorporating charge self-consistency into the RSMST code. Incorporation of relativistic effects will be addressed later in the year.

Pu-Si Thermodynamics

O. Krikorian D. Hagerty

Objective and Discussion

The overall objective of this research is to measure free energies and enthalpies of formation for Pu compounds, especially compounds that are of current or future interest to LLNL programs and that are lacking data. These thermodynamic data are basic and needed for an understanding of the equilibria, kinetics, and mechanisms of reactions involving Pu in various processes. They are also basic input needed to calculate thermodynamic parameters for establishing phase boundaries of Pu-alloy systems.

Our current objective is to measure the free energies and enthalpies of formation of the Pu silicides. There are currently no experimental data on this system, and estimates that have been made are believed to be seriously in error. This thermodynamic information is of particular importance to programmatic studies on pyrochemical recovery of Pu from residual Pu wastes; however, it is also of general interest for theoretical reasons and for future programmatic needs.

Our approach in this study is to first obtain approximate thermodynamic data on the Pu silicides, then to obtain accurate measurements. The approximate data will be obtained through the study of exchange reactions such as $3\ Mo_3Si + 5\ Pu(l) = Pu_5Si_3 + 9\ Mo$, which (from the known thermodynamic data for Mo_3Si and the direction of the reaction) allows us to set upper or lower limits on ΔG_f for Pu_5Si_3. Exchange reactions of Pu_5Si_3 with Cr, W, and U will be also studied. After the exchange-reaction studies, accurate thermodynamic values will be determined for the various Pu silicides (Pu_5Si_3, Pu_3Si_2, PuSi, Pu_3Si_5, and $PuSi_2$) by measuring Pu vapor pressures using the Knudsen cell-effusion technique.

This fiscal year, we have prepared pure single-phase Pu_3Si_2 by arc-melting; we have also characterized it by metallography. This is one of the samples that will be used for vapor-pressure determinations. In addition, we have used metallography and XRD to characterize a pure single-phase sample of Pu_5Si_3 that we prepared earlier, and we have prepared the following reaction mixes by arc-melting:

$$Pu_5Si_3 + Cr$$
$$Pu_5Si_3 + W$$
$$Pu_5Si_3 + Mo$$
$$Pu_5Si_3 + U$$

We are now analyzing these mixtures by metallography and XRD to determine the reaction products.

We have reviewed the thermodynamic data in the literature on the silicides of Cr, Mo, W, and U. These data will be used for evaluation of the exchange reactions.

For the remainder of the fiscal year, we plan to complete the analysis of the Pu_5Si_3-plus-metal exchange reactions. If necessary, the arc-melted specimens will be annealed and re-analyzed to ensure equilibration. We plan to submit a paper for journal publication on the exchange-reaction study. We will also include estimates for the thermodynamic properties of the higher Pu silicides.

Liquid-Actinide Containment

M Adamson
J. C. Farmer
J. S. Huang
M. Stratman
G. F. Gallegos
E. Sedillo

Objective

The overall objective of this focus area is to develop a general mechanistic understanding of the liquid-metal/solid-metal interactions that occur in candidate container materials for reactive-liquid metals. The current emphasis is on refractory-metal containment materials and their behavior in the presence of selected reactive-liquid metals (U, Pu, and certain rare earths) in both the presence and absence of applied stress. The focus area encompasses two activities: (1) a new activity, "Liquid-Metal/Solid Interface Interactions," and (2) an activity continuing from 1987, "Effects of Stress and Surface Alloying on Refractory Metals in Liquid Actinide Environments." These two activities are strongly synergistic in the sense that detailed interpretation of liquid-metal-induced embrittlement or stress-corrosion cracking of solids requires in-depth understanding of liquid-metal/solid interactions in the absence of stress.

FY89 Accomplishments

In the refractory metal in liquid-actinide activities, we have continued to study the tensile behavior of different metals and alloys in liquid U in order to develop a criterion to predict the susceptibility of Group VA and VIA refractory metals and alloys to

embrittlement by liquid actinides. Additional materials studied this year include W, V, Ta-2.5 wt% W alloy, and five Nb-xTa binary alloys (x =.2, .4, .6, .8, .9 wt%). Ta was further investigated by varying the strain rate of testing and by examining the fracture surfaces using scanning electron microscopy (SEM). What we found has led to the following criterion: LME (liquid-metal embrittlement) occurs only in systems in which solid/liquid couples have very low mutual solubility as represented by the U-Ta and U-W phase diagrams. For example, the ductility and fracture strength of Ta-2.5% W alloy and W at 1200 °C are severely reduced by liquid U and the samples fail in a brittle manner. The behavior of V in liquid U (solubility 0.33 at.%) is different. Although the maximum tensile strength and total elongation are also reduced severely, the inherent physical mechanism of failure is ductile since the sample failed by severe plastic deformation and necking. The reduction of strength and total elongation are attributed to dissolution of the metal surface during testing. This behavior is similar to that reported previously for Nb.

The results of the study on the Nb-xTa binary alloy are especially clear with respect to the applicability of the proposed prediction principle. As the content of Ta increases, the solubility of U atoms in the solid phase decreases and the susceptibility to LME increases. It was found that embrittlement commenced when the content of Ta exceeded ~80 wt%. Because some of the materials studied were not homogeneous, we plan to repeat this series of measurements to establish the exact concentration threshold.

Using SEM imaging and x-ray analysis, we also found that liquid-U embrittlement is always associated with the penetration of U along grain boundaries of the susceptible materials. This penetration was found to occur even without the application of stress. We also observed that the fracture surfaces of Ta specimens embrittled by small quantities of U liquid showed evidence of preferential dissolution on certain crystallographic planes (as in Fig. PA-3). This feature disappeared as the strain rate increased from 3×10^{-5} to 3×10^{-2} s^{-1} (see Fig. PA-4). The significance of this is being evaluated.

Fig. PA-3. Tantalum deformed in liquid U at low strain-rate shows preferential attack along certain crystallographic directions.

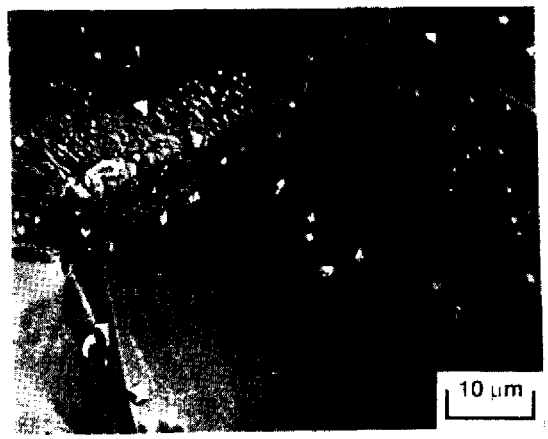

Fig. PA-4. Tantalum deformed at higher strain-rates does not show preferential attack; the features shown are indicative of embrittlement.

We have also shown that the fracture strengths of Ta-2.5% W and W are higher than is that of Ta. During FY89, we will complete the microstructural investigation of these alloys. The study on Nb-xTa binary alloys will be repeated to obtain a more reliable value for the Ta concentration threshold, even though the trend for the LME seems to be clear.

We have also been constructing an apparatus to perform tensile tests on refractory metals exposed to liquid actinides. Since this is of interest to both WSR and B-Program, we have depended heavily on B-Program funding to construct this apparatus, including a solid-state induction-heating supply. We anticipate having this apparatus installed and operational by the end of FY89 for testing in molten Pu and mixtures of Pu + U.

In this new activity, we have performed extensive searches of the classified and unclassified literature and, as a result, defined the important reactive-liquid metal (LM)/refractory-metal (RM) interaction (attack) mechanisms. Using these interaction mechanisms and key LM and RM properties as a basis, we established criteria for selecting several LM/RM systems for initial study, then designed a variety of experiments to elucidate key features of the two primary interaction mechanisms (intergranular penetration and uniform dissolution).

We have selected a matrix of solid refractory metals (V, Nb, Ta, Mo, W) and reactive-liquid metals (U, Ce, Gd, Sm, Yb) that covers sufficiently wide ranges of melting temperatures, atomic radii, electronic structures, and solubilities that the results may be used to predict the behavior of liquid Pu. Included in the liquid-metal candidates are eutectics with Fe, and ultimately it is intended to perform a few confirmatory experiments with liquid Pu and Pu-Fe eutectic. High-purity metals that will be used in the initial series of crucible-screening experiments have been ordered, as have the components of a hot-stage microscope that will be used to perform surface-wetting experiments to characterize the effect of grain-boundary carbides on grain-boundary wetting and penetration. On the theoretical front, we have found that a thermodynamic model developed and used by Pasternak to predict the solubilities of solid metals in liquid Pu works for W, Ta, and Nb but breaks down for V and Mo.

References

1. X.-G. Zhang and A. Gonis, *Phys. Rev. Lett.* **62**, 1161 (1989).

Publications and Presentations

H.F. Rizzo, T.B. Massalski, H. Baxi, and A.W. Echeverria, "Amorphous and Metastable Phase Formation in Systems with Positive Heats of Mixing using High Rate Sputter Deposition," presented at the Materials Research Society 1988 Fall Meeting, Boston, Mass., Nov. 30–Dec. 2, 1988; to be published in the *Proceedings*.

H.F. Rizzo, T.B. Massalski, and A.W. Echeverria, "Formation of Metastable Structures and Amorphous Phases in Pu-based Systems using the Sputtering Technique," *Trans. AIME* (1989), in press.

H. F. Rizzo ,T. Zocco, A. Echeverria, and Ed McClanahan, *Effects of Sputtering Parameters on Pu Coatings*, Lawrence Livermore National Laboratory, Livermore, Calif., UCRL-53888 (1988).

H. F. Rizzo, A. W. Echeverria, W. Wein, D. DelGiudice, and J. Furr, "Control of Texture of Metallic Coatings by Variations in Substrate Temperature and Deposition Environment," presented at SUBWOG 12 Coatings meeting, Livermore, Calif., Nov. 1988.

W. L. Morgan, H. F. Rizzo, and K. C. Kulander, "Enhanced Diffusion and Collisional Desorption On the Substrate Surface During Sputter Deposition," submitted to *J. Appl. Phys.*

T. G. Zocco, R. I. Sheldon , M. F. Stevens, and H. F. Rizzo, "Observations of Twinning in Alpha Pu by Transmission Electron Microscopy," accepted for publication in *J. Nucl. Mater.* (1989).

H. F. Rizzo, T. B. Massalski, and A. Echeverria, "Formation and Stability of Metastable Structures and Amorphous Phases Obtained by Sputtering in Cu-W System," presented at TMS meeting, Las Vegas, Nev., Mar. 1978.

J. S. Huang, R. Musket, and M. A. Wall, "Phases and Microstructures of Carbon-Ion Implanted Nb," presented at Materials Research Society meeting, Boston, Mass., Nov. 30–Dec. 2, 1988; to be published in the *Proceedings*.

J. S. Huang and G. F. Gallegos, "Tensile Behaviors of Group V and VI Refractory Metals and Alloys in Liquid U: Strain Rate Effects," presented at 118th Annual Metallurgical Society Meeting, Las Vegas, Nev., Feb. 27–Mar. 1, 1989.

J. S. Huang, G. F. Gallegos, M. P. Stratman, and E. M. Sedillo, "Deformation and Failure Mechanisms of Niobium and Tantalum During Tensile Testing in Uranium At 1473 K," *Scrip. Metall.* **23**, 103 (1989).

HIGH-EXPLOSIVES TECHNOLOGY

J. R. Humphrey *(Thrust Area Leader)*

Overview

Development and characterization of energetic materials require a detailed understanding of the hydrodynamics, thermodynamics, and kinetics governing the detonation and explosion regimes. Projects within the High-Explosives Technology thrust area focus on the following:

- Theoretical description of materials and reactions at high pressures and temperatures.
- Experimental characterization of detonation processes, intermediates, and products.
- Synthesis of new energetic materials.
- Application of synchrotron characterization techniques to determine defects in HE (high-explosive) crystals.

Structure and Dynamics of Molecular Fluids Under High-Density Conditions

D. F. Calef A. L. Nichols, III

The purpose of this project is to perform a theoretical investigation of chemical dynamics under high-pressure conditions. This requires study of both intra- and intermolecular structures of molecular fluids, the dynamics of their mixtures, and especially the role of the high-density dependence environment. Developing reliable, realistic models of mixtures is a prerequisite, as is developing efficient methods for using this information to model the dynamics.

The major areas of development during the last six months were:

- The molecular-fluid structure code
- Methods to incorporate the structural information into the dynamics
- Methods to study binary phase separations.

New features have been added to the integral equation code, MOLECULES. First, we can now calculate the excess Helmholtz free energy within the optimized reference hypernetted chain (ORHNC) approximation, which is needed for both the equilibrium aspects of detonation, as seen in the CHEQ code, and our approach to dynamics. It is also useful in determining the existence of fluid-phase changes and separations. Second, we can now calculate h_l, a set of constants that describe the extent of angular correlations between molecules in the fluid. These constants occur in expressions for macroscopic quantities such as the dielectric constant. They are useful in other ways. If, for example, any h_l goes to infinity, this indicates that a particular intermolecular angular correlation has

become very long-ranged. This, in turn, is an indication that the system is going into a new phase.

We have begun construction of the mixture code to permit looking at solvation processes in condensed media. In this first stage of dealing with mixtures, we are limiting our efforts to systems composed of a solvent fluid and a single solute particle, which is the "infinitely dilute mixture" limit. Much work is being done to keep the computer storage requirements for the correlation functions to the minimum required by symmetry. This has required developing several different algorithms to do the matrix multiplications. Also, the free-energy calculation is being modified to permit calculation of the chemical potential of the solute particle.

Before we can look at the mixture/solvation problem, we must construct the correlation functions for the appropriate solvent. In mid-December, we began a model solvent problem on the microVAX in T-3325; it was finished in mid-March. Fortunately, the results for this system proved to be very exciting in themselves. The system is a fluid composed of a linear triatomic molecule with a dipole moment and a length-to-width ratio of 1.4. The first exciting result was that the density obtained was the highest we have been able to examine with our methods. The second, as reported previously, was that the dielectric constant of the fluid at low densities was a monotonically increasing function of density. The new higher-density results show that the dielectric constant begins to decrease as a function of the density (Fig. HE-1). At very high densities, the packing forces overwhelm the electrostatic forces and the dielectric constant is forced to decrease.

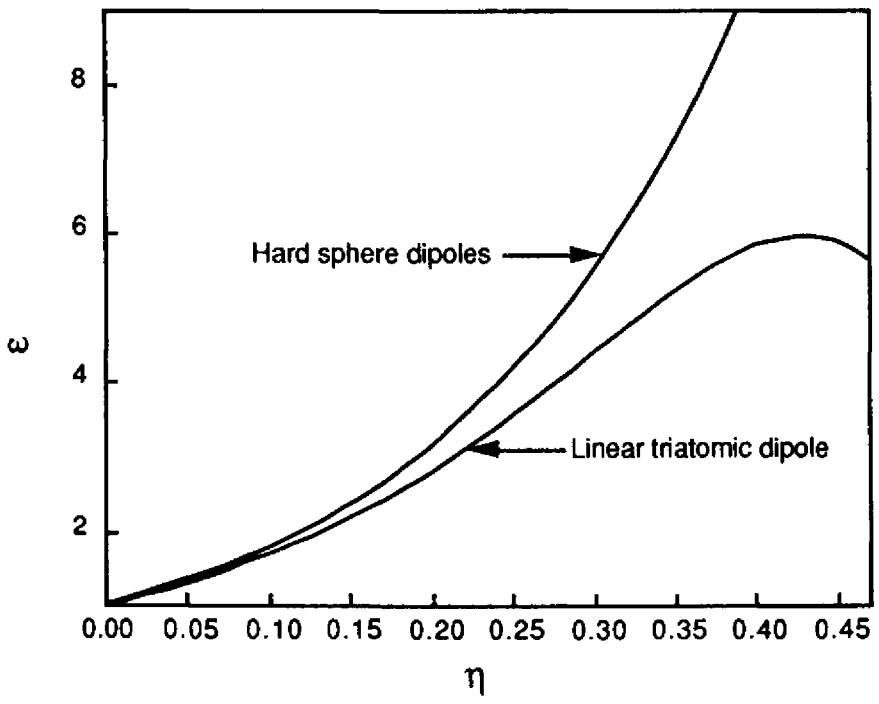

Fig. HE-1. Dielectric constant *vs.* density for two models (hard sphere dipoles and linear triatomic dipoles).

Such detailed structural output from MOLECULES allows us to continue investigating solvation dynamics. For example, we were able to use the h_l quantities to include molecular information into macroscopic relaxation times. Previous simplified models of the dynamics did not correctly treat anisotropic repulsive forces between molecules; the new results will include these effects. Work is under way to compare these results with the experimental work of J. Simon at UCSD. There has been considerable interest in the phase behavior of the product molecule mixture under detonation conditions. We have developed a new method, using molecular dynamics, to test whether the system is driven toward phase separation. The work is significant because traditional molecular dynamics encounters difficulties with finite size effects. We will also be able to compare solvation free energies with our mixture program. The basic idea is to allow the mixture to dynamically partition molecules between two "boxes." Standard molecular dynamics is performed in each box, and an additional variable with its own dynamics moves molecules between boxes. Stable mixtures will yield two equivalent boxes, whereas phase-separated systems will have one phase in each box. This also provides quantitative results on the composition of the two phases. We are currently comparing our model with the traditional thermodynamic calculations performed by F. H. Ree on H_2O and N_2 mixtures.

All-Arrhenius Reactive-Flow Model

C. M Tarver A. L. Nichols, III

The main objectives of this project are to:

- Link together our thermal, mechanical, and shock-reactive flow models in the various computer codes so that multiple stimuli and complex interactive phenomena produced by solid explosive reactions may be calculated
- Develop a shock initiation and detonation model for DYNA 2D that has a totally temperature and Arrhenius chemical kinetic basis.

The generalized TOPAZ chemical kinetics model was used on several heat-flow and heat-transfer problems for Mechanical Engineering and Sandia-Livermore. The link between TOPAZ (heat transfer) and NIKE (structural analysis) was essentially completed. Work progressed on the all-Arrhenius DYNA 2D model in the areas of shock compression of the unreacted explosive and the growth (or failure) of individual reaction sites.

High-Pressure-Reaction Chemistry

S. F. Rice

The research effort during FY89 has been directed into two areas:

- Study of the high-pressure deflagration rate of nitromethane within the diamond anvil cell.
- Study of carbon particle formation behind a shock front in benzene (in collaboration with N. C. Holmes in H Division).

The pulsed-laser-initiated deflagration rates of nitromethane and perdeuteronitromethane have been measured at pressures as high as 37 GPa. Deflagration rates of condensed energetic materials (usually propellants) are typically measured in "high-pressure strand burning" experiments that have upper limits of roughly 1.0 GPa. The new diamond anvil cell technique, developed over the past year solely by this research project, has completely redefined the pressure regime over which combustion propagation can be studied. This experiment fairly accurately models the phenomena of "hot spot" growth behind a shock front.

The results of the nearly completed work on nitromethane are shown in Fig. HE-2. Focusing first on the overall shape of the curve for nitromethane, we see that there are three general regions:

- 0–20 GPa: The rate of reaction-wavefront propagation (burn rate) varies relatively linearly with pressure. The products from the reaction are mostly gases and some carbonaceous solid.
- 20–30 GPa: The burn rate increases dramatically; the products are no longer gases but appear in the cell as a clear transparent fluid. The sample remains at high pressure after reaction.
- ≥30 GPa: The burn rate begins to decrease; however, the final products are the same as in the 20–30 GPa region.

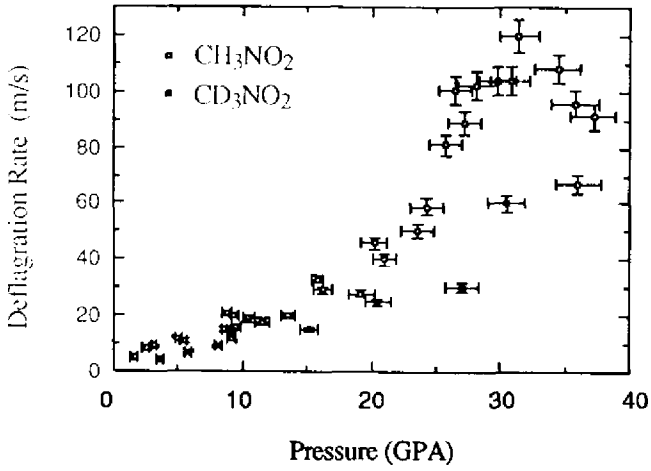

Fig. HE-2. Plot of the reaction-wavefront propagation rate as a function of pressure for nitromethane (open squares) and perdeuteronitromethane. Errors in the pressure measurement are from the slight inhomogeneities within the diamond anvil cell due to finite sample size. Errors in the propagation rate are due to the overall quality of the streak camera record.

The interpretation of these results is still speculative; however, several general statements can be made. At higher pressure, it appears as though a different reaction mechanism (with its own products) begins to dominate the chemistry. Although having a more severe pressure dependence than the low-pressure mechanism, this second mechanism appears to "stall out" at very high pressure. This may result from a slowing down of molecular diffusion and subsequent bimolecular reactions. It is very important to

carry out these experiments at pressures >40 GPa to determine whether the overall rate continues to drop or the first mechanism begins to participate again. Several modifications of the diamond anvil cell have been instituted to extend the working pressure range and experiments to 50 GPa.

Also presented in Fig. HE-2 are data for perdeuteronitromethane. Figure HE-3 shows an expansion of the results from 0–20 GPa. It is clear that the deuterated material exhibits a slower burn rate than does normal nitromethane. This may be a clue as to the nature of the rate-limiting step in the overall decomposition-reaction mechanism. An effort to model this experiment by including pressure-dependent reaction rates and mechanisms along with thermal and molecular diffusion will begin later in FY 89.

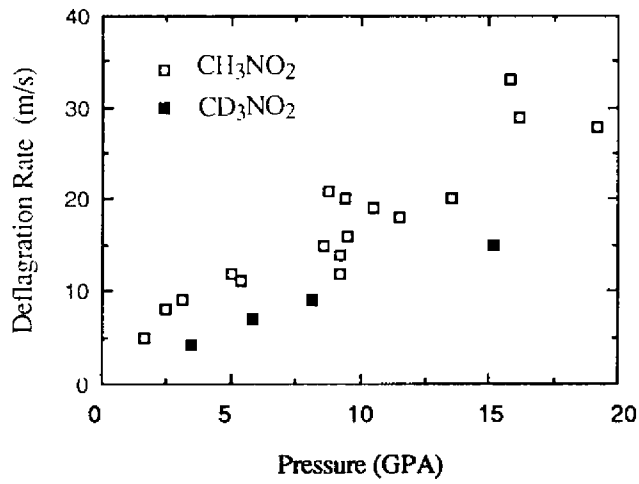

Fig. HE-3. Enlargement of the 0–20 GPa region of Fig. HE-2. The deuterated data are well outside the data obtained for normal nitromethane.

H Division's two-stage light-gas gun was used for a series of shots designed to examine carbon particle formation in shocked benzene using Mie scattering from small particles. The experiment simply measures the transmission spectrum of a 3.0-mm sample behind a planar shock front as a function of time. If the attenuation of the probe white light exhibits a λ^{-4} dependence, then scattering by conductive carbon particulate is likely to be the source of attenuation. Figure HE-4 shows the spectrum of a sample shocked to 12.6 GPa, plotted as the extinction coefficient *vs.* inverse wavelength (μm^{-1}). It appears that light scattering is the dominant effect at the longer wavelengths. These data can be precisely fit to λ^{-4}. At shorter wavelengths, indications are that the extinction is caused by electron absorption. Successful shots were obtained at 12.4, 12.6, 12.8, and 13.4 GPa.

Figure HE-5 shows the time dependence of the magnitude of the scattering at 13.4 GPa. Combining time resolution with spectral resolution as a function of shock pressure results in a detailed picture of the rate of growth of carbon precipitate in these reactive shocks. Carbon precipitation is a very important consideration for accurate modeling of C/H/N/O-based high explosives. This work will be extended to nitromethane and perhaps melt-cast TNT later in FY 89.

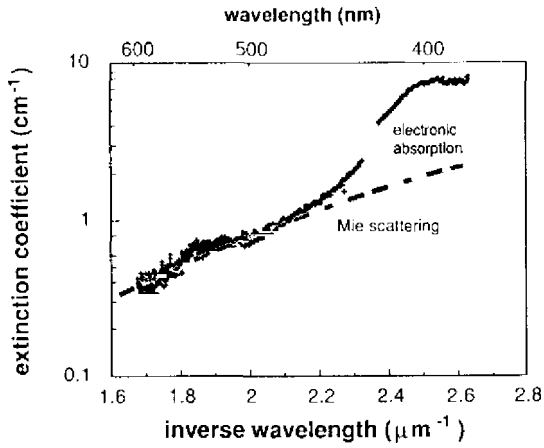

Fig. HE-4. Extinction coefficient *vs.* inverse wavelength as described in the text.

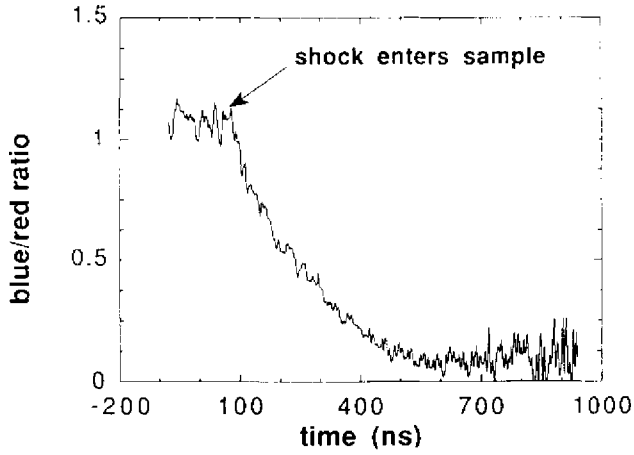

Fig. HE-5. The blue-to-red absorption ratio as a function of time, which is indicative of carbon formation.

Radiometric Observation of Detonation Products

R. L. Simpson

Thermodynamic codes for calculating the states of reactive systems are based on assumed product species and an equation-of-state to describe the physical properties of the system. When applied to explosives, verification of these models is hindered by the extreme environment of detonation. Currently, only pressure-volume behaviors have been determined experimentally. This work will attempt to thermodynamically define the equations-of-state of PETN and TNT by radiometric measurement of temperature at known pressure-volume states.

A secondary motive is to examine late-time reactions in TNT through observation of the temperature history behind the detonation front. Deviations from constant particle-velocity histories in sustained and overdriven detonations have been observed in carbon-rich explosives. Unfortunately, this information is insufficient to determine the extent of

reaction; reaction exothermicity tends to increase temperature, whereas decrease in number density of the product gas will reduce the particle velocity. Measurement of both particle velocity and temperature may enable these effects to be isolated.

This work is intended to consist of 10 experiments in which high-velocity flyer impactors shock-load the samples to precise states. The execution of the experiments will be carried out as one series. A collaboration with L. Green was established to attempt to attain the same shock states that were reached in his supracompressive work on PETN and TNT. Using this information, hydrodynamic calculations were carried out to design the experiments. A configuration was found that allowed sufficient time for the materials to transition to detonation when impacted by a flyer yet enabled attainment of the proper shock states. For TNT, three experiments will be conducted near the Chapman-Jouguet (CJ) state, one will be overdriven, and one will be taken to a state significantly below the CJ state. With PETN, three experiments will be performed just below CJ; two additional shots will be made using material with a low initial density to try to distinguish between the effects of compressive work and chemical reaction on the detonation temperature.

The explosive samples have all been fabricated and the targets are essentially completed. Modifications were also made to the four-channel radiometer to allow independent gain control over each channel. Some work is also being done on the calibration system.

The firing time is set to occur before July 1; the exact period is uncertain because of problems with facility scheduling. However, it can not extend past July 1 because the 100-mm-gun diagnostics will then be moved to the High-Explosives Applications Facility.

Synthesis of New Energetic Materials

C. L. Coon P. F. Pagoria

New HEs Derived from 4,5-Diaminofurazan

Initial efforts have been made at the synthesis of precursors to two new HEs derived from 4,5-diaminofurazan, (1) in the illustration below. The reaction of (1) with aqueous hexamine and conc. HCl to yield bicyclic compound (2) or the reaction of (1) with aqueous formaldehyde and urea to yield (3) has thus far yielded only a complex mixture of products (probably polymeric). Research is continuing to pursue the appropriate reaction conditions for the synthesis of (2) and (3).

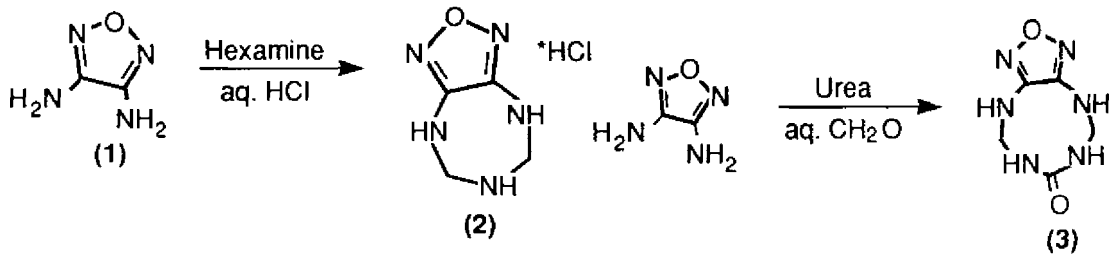

Synthesis and Hydrolysis of K-56

A new route for the synthesis of K-56 has been developed involving the hydrolysis of AcK-56 (4) which, upon subsequent nitration with N_2O_5, yields K-56 (6), Eq. HE-1 shown below. Initially, KH-56 was believed to be an interesting new HE, but x-ray crystallography of the material gave a crystal density of 1.84 g/cm^3, much too low for consideration for further applications.

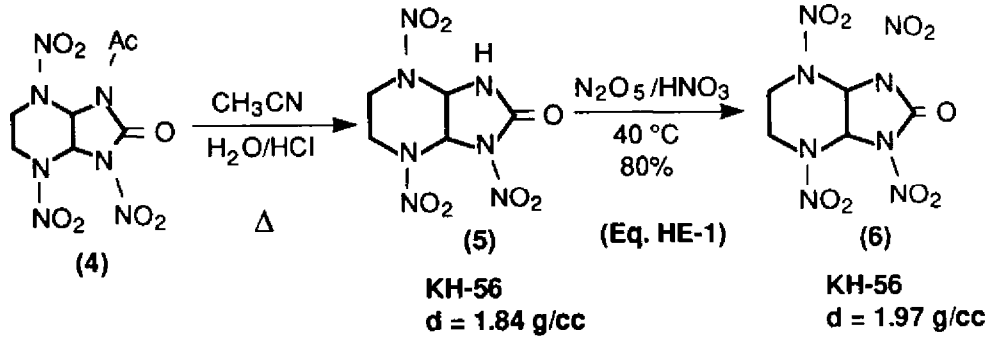

The methanolysis of K-56 to give 1,4-dinitro-2,3-dinitramino-1,4-diazacyclohexane (7) yielded some interesting results (Eq. HE-2 below). An x-ray crystallographic study of (7) revealed that the nitramino groups were in the *trans* configuration instead of *cis* as one would expect. This suggests that, under the reaction conditions, the piperazine ring underwent a ring-opening, followed by isomerization of the nitramino groups and subsequent ring-closure to give *trans* (7). The interest in *cis* (7) arose from the idea that the two nitramino groups could be reacted with formaldehyde to give the bicyclic L-56 (8), a target HE for some time now. The fact that only *trans* (7) is produced precludes ring closure with formaldehyde so that alternative methods for synthesizing L-56 must be investigated. Attempts have been made at hydrolyzing K-56 in the presence of formaldehyde (Eq. HE-3 below) in the hope that *cis* (7) can be trapped before it ring-opens. However, this has thus far been unsuccessful, yielding either ethylenedinitramine (EDNA) (10) or the ring-opened compound (9).

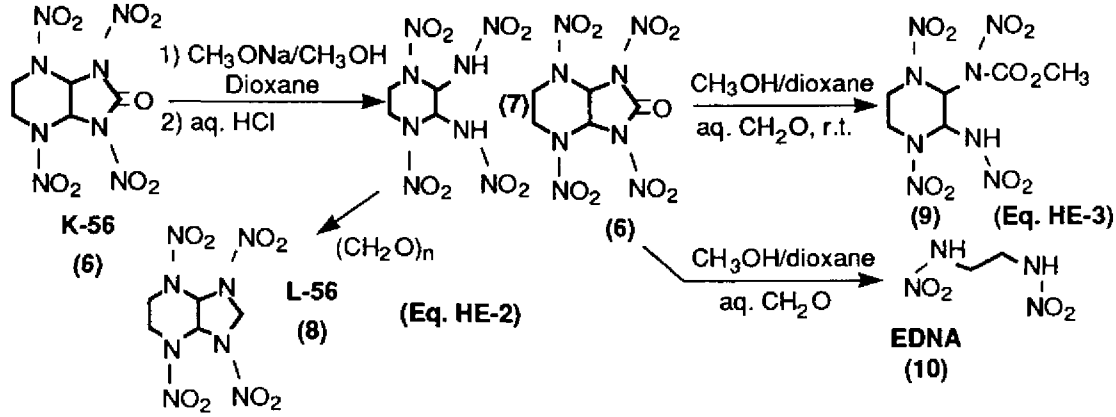

Reactions of K-6

As shown below, K-6 (11) has been hydrolyzed by two methods to yield 1,3,5-triaza-1,3,5-trinitropentane (TTP) (12). TTP is unstable and decomposes on heating to MEDINA (13) + N_2O + CH_2O. Attempts to crystallize TTP for x-ray crystallographic analysis have failed, either yielding a mixture of MEDINA and TTP or decomposing the TTP completely. Our interest in TTP lies in its possible use to synthesize new bicyclic HEs in the way that MEDINA and EDNA were used to synthesize bicyclo-HMX and K-56, respectively. Our initial attempt at the reaction of TTP with 4,5-dibromo-1,3-diacetyl-1,3-diazacyclopentane in the presence of triethylamine produced an unidentifiable mixture of products (Eq. HE-4).

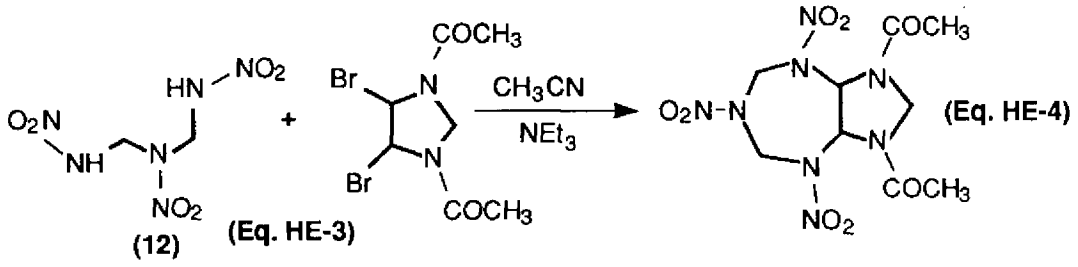

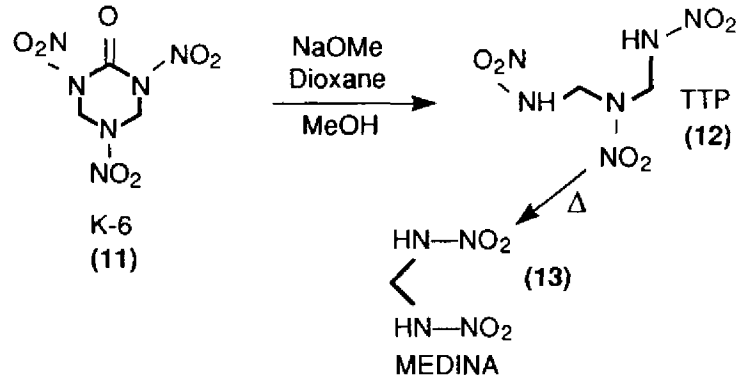

Progress on the Synthesis of L-57

Successful synthesis of bicyclo-HMX, L-55, encouraged research on synthesis of the homologous compound, L-57 (below). L-57 is of interest because its predicted density is ~2 g/cm^3. The conditions to nitrolyze the L-55 precursors were ineffective for L-57, and the starting materials could be recovered. Stronger reaction conditions indicated nitrolysis, but no identifiable products have been isolated. Work on synthesis of L-57 will continue.

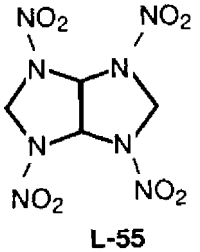

L-55

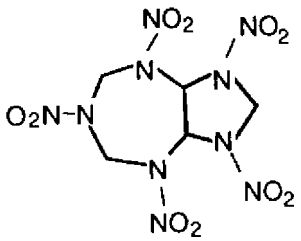

L-57

Amine-Metal Salt Complexes

As a spin-off from our work on the synthesis of CL-20, we discovered and briefly studied the reaction of amines with various transition-metal salts to form stable, crystalline complexes containing two amine molecules to one metal salt molecule. A listing of the complexes prepared and characterized is shown below.

Amine	Metal Salt
$R\text{-}NH_2$	$AgNO_3$
R = Et, n-Bu, $CH_3CH_2C(CH_3)_2$, C_5H_{11}, $(\text{-}CH_2CH_2OCH_2CH^{2-})_2CH$, $H_2NCH_2CH_2NH_2$	
$t\text{-}Bu\text{-}NH_2$	$AgNO_3$, $Cu(NO_3)_2$, $Hg(NO_3)_2$
$(n\text{-}Bu)_2NH$	$AgNO_3$

These complexes form immediately when the reactants are mixed in acetonitrile. X-ray crystal analysis of several of these products confirms their structure as the two-to-one complex. The structure of the product synthesized with ethylenediamine is especially interesting in that it is a linear polymer with the silver atoms packed closely together in the crystal lattice. Some properties of these new materials, such as electrical conductance, will be determined.

HE Defects Characterized by Synchrotron Radiation

W. C. Tao J. H. Kinney

Predictive models for analyzing hydrodynamic flow, shock propagation, and shock growth in granular explosives require understanding of the thermal and mechanical properties within the unreacted explosive. This is especially true of the rate of chemical energy release based on the nature of "hot-spot" generation and burning. The rate of release of chemical energy depends on the explosive's chemical compositions, the mechanical and thermal material properties of the explosive, and—most important—the heterogeneous microstructure within the unshocked material. The objectives of this research are to nondestructively characterize the type and distribution of defects in HE single crystals and to examine their respective influences on hot-spot generation and propagation. The formation of hot-spots originates from shock interactions with local density discontinuities within the HE. These disorders within the granular solid take on the form of intergranular defects such as twin and split planes, surface defects such as voids and reentrant cavities, and intragranular defects consisting of stacking faults, microcracks, and point dislocations.

We have successfully performed non-invasive, detailed characterization of defect structures within PETN and HMX single crystals by computerized tomographic and topographic (CT) methods using synchrotron x-radiation (SR). We have demonstrated the feasibility of using microtomography to study pore distributions with resolution of 2–3 μm

in materials similar in x-ray absorption to HE. Latex SEM calibration spheres ranging from ~0.1 to 1.5 μm give scattering curves predicted from theory. The problem of determining pore sizes in HE materials is simply the inverse problem of scattering from the latex spheres.

In addition to using the HASYLAB facility in West Germany, we have investigated the feasibility of using local x-ray radiation facilities for our experimental study. The Stanford Synchrotron Radiation Laboratory (SSRL) would be ideal, but a year of shutdown caused extensive setbacks in startup of facilities in the first quarter of 1989. We have also investigated the feasibility of optical 3-D tomography in Bio-Med for characterizing most of the translucent crystals. The setup in Bio-Med performed well, and the data can be directly transported to our computation system for analysis. We will be evaluating the use of the XRD facility in MD for our characterization in April.

After the HE crystal defects are initially mapped by CT with SR, the single crystals are suspended in an impedance-matching medium and subjected to shock-loading to determine their initiation sensitivity. Two experimental methods are employed in this phase of the study: microphotography and infrared emission. Coupled with streak and frame cameras, microphotography yields spatial and temporal resolutions of 1 μm and 1 ns, respectively. Measuring infrared emission *vs.* time yields information on the rate of release of chemical energy. To study the influence of defect microstructure on shock-wave propagation and energy coupling into the shock front, we have devised a simple barrel matrix attached to a single electric gun laminate to measure wave profile as a function of HE crystal thickness. The breakout time and position of the shock wave on the surface of the HE crystal are recorded by a streaking camera. We have obtained a series of HMX crystals from H. Cady of Los Alamos for our shock experiments.

Publications and Presentations

C. M. Tarver, "All-Arrhenius Reactive Flow Model," presented at the Joint Working Group on Explosives, LANL, Los Alamos, N.M., Dec. 1988.

A number of publications are in preparation and presentations are scheduled to be given in the near future:

D. F. Calef and A. L. Nichols, III, a paper describing the MOLECULES program, the resulting improved dynamics model, and the new molecular dynamics method.

C. M Tarver and A. L. Nichols, III, a paper on the growth (or failure) of shock induced hot spots in HMX- and TATB-based solid explosives.

S. F. Rice, a paper describing the high pressure deflagration rates of nitromethane and perdeuteronitromethane (Combustion and Flame); a presentation and paper describing the carbon particle formation (9th Detonation Symposium, Sep. 1989, Portland, Ore., and *Phys. Rev. Lett.*, respectively).

C. M. Coon and P. F. Pagoria, a paper describing the bicyclo-HMX synthesis.

W. C. Tao and J. H. Kinney, a presentation describing the synchrotron characterization of defects and initiation sensitivity at the 9th Detonation Symposium, Portland, Ore., Sep. 1989.

FUNDAMENTAL MECHANISMS OF METAL PROCESSING

M. E. Kassner *(Thrust Area Leader)*

Large-Strain Deformation of Metals and Alloys

M. E. Kassner

Ambient-Temperature and Near-Ambient-Temperature Deformation of Silver

Substantial progress was made during FY88 in the area of dislocation microstructure and rate-dependence of high-purity silver deformed to large strains between 0.16 and 0.30 T_m. This "bulk property" work was partly in support of the silver-interlayer diffusion-bonding task described below. Most experimental work was completed in FY88; the theoretical analysis of the rate processes was completed and documented in FY89. The results were documented, submitted, and recently accepted for publication (see publication list).

Large-Strain Deformation of Aluminum Single Crystals at Elevated Temperature

Large-strain torsional deformation of Al single crystals is one of the concluding sets of experiments on the dislocation microstructure and fracture of aluminum deformed to ultralarge strains at elevated temperature. Large-strain torsional tests on aluminum single crystals were intended to confirm the concepts for the microstructural evolution and basic deformation mechanism (of aluminum polycrystals deformed to large strains at elevated temperature) that were formulated in an earlier portion of this research project [1].

Microstructural observation by TEM of single crystals subjected to large-strain torsional deformation confirmed our new concept (geometric-dynamic-recrystallization) for the source of increased high-angle boundaries. The experiments were completed, analyzed, and documented in FY89. The results have been accepted for publication.

Ductility of Aluminum Polycrystals

During FY88, we determined the variation of the torsional ductility of aluminum with temperature and strain-rate. The trends of these "hot workability" tests are applicable to forming other high-stacking-fault-energy metals and alloys (e.g., Mo, Nb, Ta, V) at elevated temperature [2]. A detailed description of the motivation for these tests is included in the article by Kassner, Myshlyaev, and McQueen [1]. The FY88 work found that the torsional strain-to-failure for a fixed strain-rate initially increases with temperature until it reaches a "peak ductility" at a "peak temperature"; beyond that peak temperature, ductility decreases. Both peak ductility and peak temperature appear to increase with strain-rate.

These new trends were analyzed during FY89. Briefly, the behavior is rationalized at low temperatures by assuming that cracks initiate (or grow) by internal stresses that are a function of the applied (saturation) stress, which can be easily modeled as a function of T and ε. At higher temperatures, ductility trends can be described by changes in (coupled) cavity growth rate with T and ε. The cavities are presumably nucleated at relatively small strains by grain-boundary sliding. One additional set of ductility tests at a very low strain-rate may be performed this fiscal year.

The "baseline" aluminum results will be applied to more complicated alloys, such as Al-Mg. We expect to clarify fairly quickly the (at present, poorly understood) microstructural evolution process during elevated-temperature deformation in these alloys.

Delayed Failure in Silver-Aided Diffusion Welds

R. S. Rosen M. E. Kassner G. A. Henshall

As described in the thrust area proposal, at ambient and near-ambient temperatures these joints experience mechanical delayed or creep failure at stresses as low as one-fourth of the tensile strength. We determined (see Fig. MP-1) the stress-dependence and the activation energy for the fracture process (FY88 and 89). These measurements, plus FY89

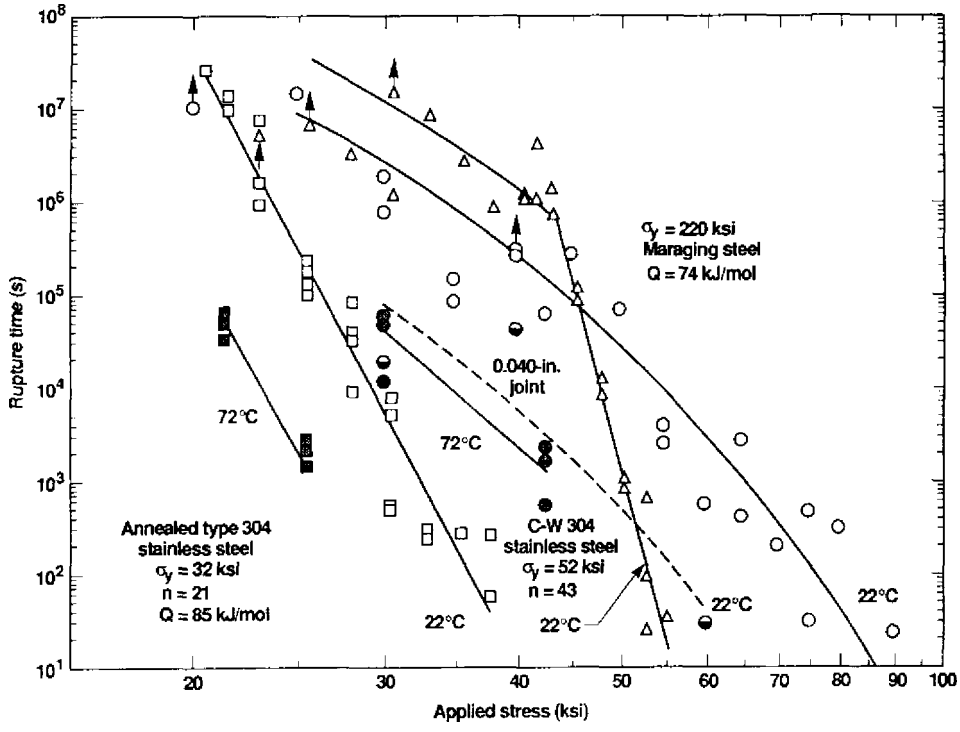

Fig. MP-1. Creep rupture time *vs.* applied tensile stress for silver-aided diffusion bonds between elastic and plastic base metals.

SEM, TEM, and finite-element-method (FEM) stress analysis of the stress state within the vicinity of the interlayers, indicated two distinct mechanisms for delayed failure in tension.

First, when essentially no plasticity is in the base metal during or after loading, voids nucleate at the silver-silver bond interface, and growth is controlled by the steady-state creep of silver and/or (perhaps depending on applied stress) a coupling [3] between cavity growth that is controlled by diffusion (surface or grain boundary) and steady-state creep of the silver. This category of failure has been termed "direct-void-growth" (DVG) failure.

Second, the delayed or creep failure of the interlayers may be accelerated if the applied stress is in the vicinity of the microyield stress of a rate-sensitive base metal or alloy, such as annealed and cold-worked austenitic stainless steel. Time-dependent plasticity or creep may then be observed in base metals, and concomitant shear occurs in the softer silver under a high triaxial stress-state. Fracture again occurs after relatively small strains in the silver, but activation-energy measurements, stress-sensitivity measurements, and FEM analysis confirm that these "premature" failures are controlled by the time-dependent plasticity (creep) of the base metal. This category of time-dependent tensile failure has been termed "base-metal-controlled" (BMC) failure. As the stress decreases to below about two-thirds the macroscopic (0.2% offset) yield stress, the DVG mechanism determines the rupture time. Recent fracture-morphology analysis by SEM is also very consistent with the above analysis (Fig. MP-2). FEM analysis using individual tests of the mechanical

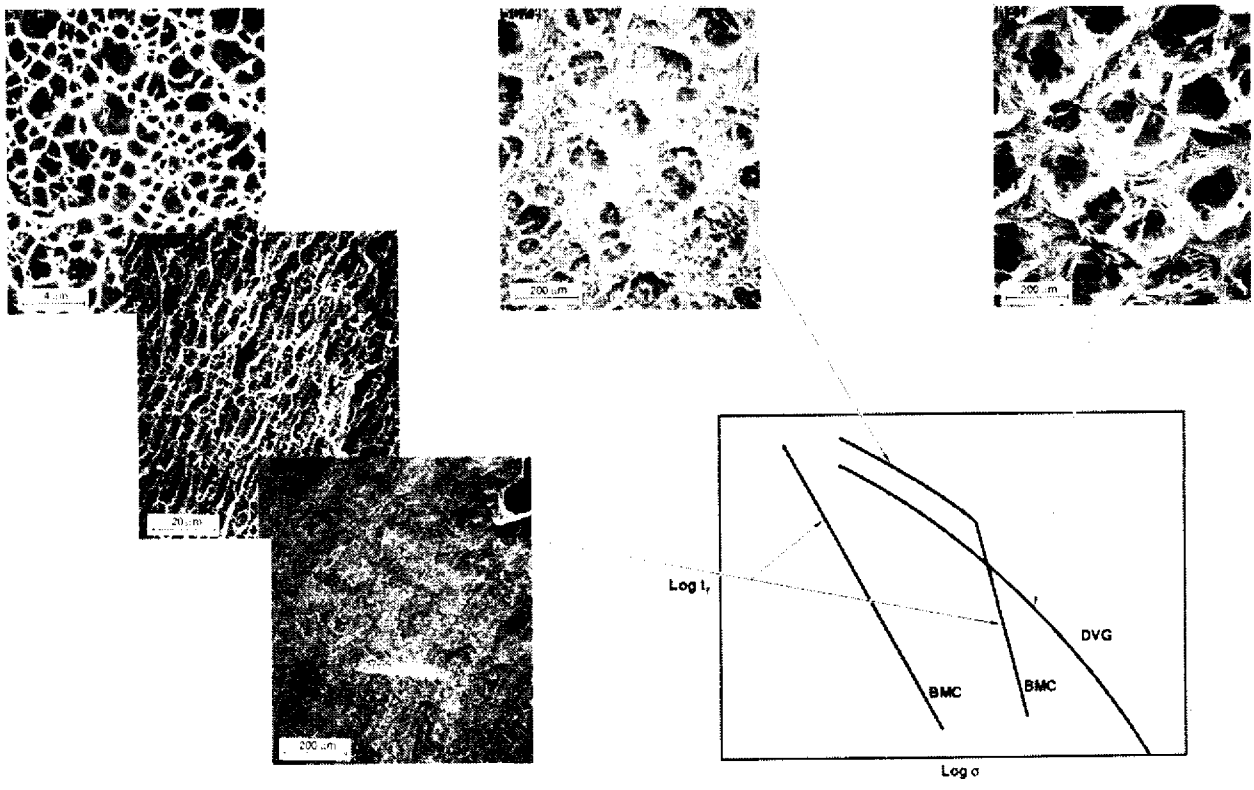

Fig. MP-2. SEM fracture morphology analysis.of silver-aided diffusion-weld bonds.

behavior of the bond materials shows that the detailed shape of the deforming bond is consistent with the above theory. This analysis required particularly careful mechanical and

microstructural characterization of the silver interlayer. The unusual mechanical results of the interlayer were understood by careful TEM measurements. The mechanisms described are valid for a variety of interlayer metals and may be independent of the fabrication process. The effects of processing parameters (temperature, pressure, alloying, base-metal surface preparation, etc.) on performance have been investigated during FY89 and will continue.

Separate analysis was performed on the vulnerability of the U-Ag bonded interface to stress-corrosion cracking in humid-air environments. These tests* confirmed substantial vulnerability. Further FY89 results confirmed the earlier FY88 tests [4].

Incorporation of Advanced Materials Models in FEM Codes

G. A. Henshall G. L. Goudreau**

The first subtask involves a joint project with the Methods Development Group in NEED of the Mechanical Engineering Department. This work concerns improving LLNL's FEM stress-analysis codes through implementation of advanced material-constitutive equations. Specifically, implementation of aspects of the MATMOD constitutive equations within NIKE 2D and DYNA 3D will be explored. This family of constitutive models has been developed over the past decade by a group (including Henshall) at Stanford. The goal for FY89 is, therefore, to implement aspects of the constitutive equations into the NIKE 2D and DYNA 3D codes and measure the resulting performance. Optimizing the balance between the capabilities of the constitutive equations and their complexity and cost will be a major concern.

The second subtask consists of applying the preceding to aspects of the solid-state bonding task described earlier. Although the first subtask is not yet complete, there has been sufficient progress to analyze both the stress state and strains as functions of time (see previous task). This was accomplished despite our relatively complex case in which (1) composite characteristics are evident near the silver interlayer and (2) complicated time-dependent plasticity of the base material is evident.

Recrystallization Kinetics

C. W. Price

Existing kinetic models used to predict recrystallization behavior are essentially empirical relations with substantial and often unrecognized limitations. This task supported development of a simplified computer simulation code that models grain impingement during the later stages of grain growth. Specifically, grains grow within specified or constrained volumes. From this, together with models of time-growth behavior, the

* Funded by Process Development.
** NEED.

fraction that transformed as a function of time could be predicted. These results show that classic Johnson-Mehl-Avrami (JMA) and Speich-Fisher (SF) relationships, contrary to some general thinking, reasonably compensate for grain impingement.

The computer model was used this fiscal year to investigate proposed limitations to the JMA and SF models based on real data. Basically, it was concluded that:

- JMA applies to those systems that have linear growth without competitive reactions.
- SF applies to systems having competitive reactions (e.g., recovery) that retard linear growth.

Rapid Solidification of Al-Be Alloys

J. Elmer L. Tanner M. Aziz*

A solidification model is being developed to explain the nm-sized particles that have been observed in rapidly-solidified Al-Be alloys at solidification-front velocities on the order of 0.1 m/s and faster. The Be particles have a random crystallographic orientation and a unique modulated appearance, forming in "waves" parallel to the advancing solidification front. These microstructural features indicate that the ultrafine Be particles periodically nucleate and grow from a liquid rather than from a solid phase during non-steady-state solidification conditions. This solidification mechanism has not been incorporated into present rapid-solidification theories; it may be responsible for the development of similar microstructures in other alloy systems.

Progress has been made in several modeling areas:

- First, the kinetic effects on phase equilibrium have been investigated with a continuous-growth model for interface motion during rapid solidification. This kinetic model, developed by M. J. Aziz of Harvard, will later be an integral part of the final computer model.
- Second, the variables that control the non-steady-state solidification problem have been isolated, and the equations and methods used to solve for these variables have been identified.
- Third, a review of the literature on the homogeneous nucleation of particles from the liquid phase has been completed. This review provides the basis for developing the liquid-phase nucleation criteria for the beryllium particles.

* Harvard University.

High-Strain-Rate Behavior and Failure of Metals

W. Gourdin

During this period, LLNL ring data for copper and tantalum were compared with constitutive models currently available in the literature. Thermally-activated models were emphasized because of their physical basis and the natural way in which they account for strain-rate and thermal effects. Although the ideas that underlie such descriptions are hardly new, the availability of more and better data, particularly for copper, has renewed interest in them. The parameters derived by Follansbee and Kocks [5] for 40-μm OFE copper provide a good description of both split Hopkinson pressure bar and ring data on OFE material that we (independently) processed to yield the same grain size. This demonstrates our ability to predict the constitutive behavior of a pure metal that has been carefully processed to a specified initial condition. Through adjustment of the athermal component of the flow stress in general accordance with the Hall-Petch relationship, excellent agreement was also found with the ring data for 10-μm OFE copper. Comparison with the data for material with grains sized 150–200 μm, however, indicates that hardening rate, saturation stress, or both decrease as grain size becomes large. The results of higher-temperature ring experiments are described qualitatively. The flow stresses predicted by the model are too large, suggesting that the activation energy used in the model is incorrect.

The tantalum data were compared to the model of Hoge and Mukherjee [6], which is similar in concept to, but different in detail from, that used for copper. Although the ring data are in general agreement with the test data used by Hoge and Mukherjee in deriving their model, the model itself provides only an overall estimate of observed flow stresses. One source of disagreement is the absence of any hardening in the model, with the result that the increase in temperature and the decrease in strain rate in the ring experiment imply that flow stress decreases with strain—an effect that is not observed. Interestingly, the hardening must be included in the athermal term, in contrast to copper for which the hardening ("structure evolution") is in the thermal component.

In response to a request from J. Dini (MFD), we undertook a study of electrolytically-deposited Udylite Bright Acid Copper (UBAC). Shaped-charge liners were fabricated from this material in anticipation that the extremely fine grain size (<10 μm) would lead to improved munition performance. In fact, the liners performed very poorly, breaking up early into many small fragments. The poor performance may be associated with impurities.

We have begun a study of the changes in mechanical behavior produced by the passage of a shock wave through OFE copper prior to high-strain-rate deformation. Several samples of 10-μm-grain material were shock-loaded to 11.5 GPa in our 63.5-mm light-gas gun. Ring specimens were prepared from these; to date, we have tested control specimens (unshocked material from the same billet) and two specimens each at 150 and 400 °C. Although the data are preliminary, those at the lower temperature show that the shock wave introduces 5–6% equivalent plastic strain, as compared with the unshocked material, and

that failure strains are reduced. Because of difficulties in measuring the specimen currents, analyses of the initial experiments at the higher temperature are not yet complete.

The exchange of data with Institut Saint Louis (ISL) on the properties of explosively-launched *vs.* electromagnetically-launched rings of ETP and OFE copper is complete. The ISL data for explosively-launched rings of our 10-μm and 150–200-μm OFE copper are too poor, because of extreme noise in the velocity records, to permit detailed analysis. The data, nevertheless, agree qualitatively with our observations on shock-loaded specimens.

Testing of tantalum during this period has been minimal because of the lack of material. New starting stock of electron-beam-melted, arc-melted, and powder metallurgy material has been received, however, and is now awaiting fabrication into specimens. Plans to characterize dislocation substructures as a function of deformation in copper and tantalum ring specimens have been abandoned because of funding cuts.

References

1. M. E. Kassner, M. M. Myshlyaev, and H. J. McQueen, *Mater. Sci. Eng.* **108**, 45 (1989).
2. H. J. McQueen and M. E. Kassner, in *Superplasticity in Aerospace*, H. C. Heikkenen and T. R. McNelley, Eds. (AIME, Warrendale, 1988), p. 77.
3. A. C. F. Cocks and M. F. Ashby, *Prog. Mater. Sci.* **27**, 189 (1982).
4. R. S. Rosen, S. Beitscher and M. E. Kassner, accepted for publication in *Environment Induced Cracking*, M. B. Ives, Ed. (National Association for Corrosion Engineers, Houston, 1989); UCRL-97917, May 9, 1988.
5. P. Follansbee and U. F. Kocks, *Acta Metall.* **36**, 81 (1988).
6. K. G. Hoge and A. K. Mukherjee, *J. Mater. Sci.* **12**, 1666 (1977).

Publications

M. E. Kassner, "The Rate-Dependence and Microstructure of High-Purity Silver Deformed to Large Strains Between 0.16 and 0.30 T_m," accepted by *Metall. Trans.*; UCRL-100162.

M. E. Kassner, "Large-Strain Deformation of Aluminum Single Crystals at Elevated Temperature as a Test of the Geometric-Dynamic-Recrystallization Concept," accepted by *Metall.*; UCRL-100551.

C. W. Price, "Comments on the Extent of Simultaneous Recovery During Recrystallization and Its Effect on Recrystallization Kinetics," submitted to *Scripta Metall.*; UCRL-100553.

C. W. Price, "Use of Johnson-Mehl-Avrami Kinetics in Recrystallization of Metals and Crystallization of Metallic Glasses," submitted to *Acta Metall.*; UCRL-99556.

W. H. Gourdin, "Constitutive Properties of Copper and Tantalum at High Rates of Tensile Strain: Expanding Ring Results," in: *Proceedings of the Fourth Inter-national Conference on the Behavior of Materials at High rates of Strain*, Oxford, U.K., Mar. 19–22, 1989; UCRL-98812.

Presentations

R. S. Rosen, S. Beitscher, and M. E. Kassner, "Stress Corrosion Cracking of Uranium-Silver Interfaces in Silver-Aided Diffusion Welds," presented at Environment-Induced Cracking of Metals, Kohler, Wisc., Oct. 2–7, 1988.

L. E. Tanner, R. E. Lewis, and J. W. Elmer, "Phase Transformations in Rapidly Solidified Al-Be and Al-Be-Li Alloys," presented at TMS-AIME, Chicago, Ill., Sep. 26–29, 1988.

R. S. Rosen, J. W. Elmer, and M. E. Kassner, "Silver-Aided Diffusion Welding of Actinides (Fabrication and Failure Modes)," presented at JOWOG 22D, Aldermasten, U.K., Oct. 4–7, 1988.

W. H. Gourdin, "Behavior of Tantalum at High Rates of Tensile Strain," presented at the Workshop on Aerostable EFPs, ARDEC, Picatinny Arsenal, N.J., Oct. 18, 1988.

W. H. Gourdin, "Constitutive Properties of Copper and Tantalum at High Rates of Tensile Strain: Expanding Ring Results," presented at the Fourth International Conference on the behavior of Materials at High Rates of Strain, Oxford, U.K., Mar. 19–22, 1989.

W. H. Gourdin, presentation on program progress to Technical Coordination Group I, Computational Mechanics and Material Modeling, Los Alamos, N.M., Nov. 9, 1989.

R. S. Rosen, M. E. Kassner, G. A. Henshall, "Delayed Failure of Silver-Interlayer Diffusion Welds," presented at Spring IMOG Joining Subgroup meeting, Livermore, Calif., Apr. 18–20, 1989.

SYNCHROTRON-RADIATION-BASED MATERIALS SCIENCE

J. Wong *(Thrust Area Leader)*

Overview

This new thrust area has the objective of understanding the role of atomic and electronic structures in determining the physicochemical properties of materials and their processing. The tasks defined in this area exploit the unique characteristics of synchrotron radiation (high intensity, high collimation, high polarization, broadband tunability from VUV to hard x-ray, etc.) to probe the structures of selected elements at different levels (Table SR-1). The research areas involve:

(1) Expansion of our existing capabilities in material characterization using these powerful photon sources

(2) Development of new capabilities:
- To probe dilute species in bulk materials
- To detect submonolayer coverages on surface and interfaces
- To unravel chemical dynamics of reaction systems by time-resolved study *in situ*

Table SR-1. Capabilities and Research Areas for Synchrotron Radiation Studies

Research Area	*Existing Capability*	*Capability to Develop*
Local atomic structure*	XANES, EXAFS	
Crystal Structure	High-resolution powder diffraction	Rietveld refinement
3-D microstructure	Microtomography	Topography, SAXS
Dynamic Structure		Time-resolved XRD, dispersive EXAFS
Surface, thin-film, and interface structure		Photoemission, evanescent standing wave, glancing-angle scattering

Kinetics of Material Synthesis

Objective

The objective of this task is to study the kinetics of materials synthesis, phase transformation, and structural evolution—*in situ* and in real time—in three subtasks:

* See also "Site-Specific Chemistry using Synchrotron Radiation," p. 91.

- Study the chemical dynamics and detect phase transformations in combustion-synthesis systems using time-resolved x-ray diffraction (TR-XRD)
- Follow the vapor deposition of atoms on a substrate, cluster growth, coalescence, thin-film formation, and interfacial development using standing-wave fluorescent EXAFS
- Develop and apply time-resolved x-ray imaging and small-angle x-ray scattering (SAXS) to characterize microstructural changes and defect growth kinetics in composite materials.

Solid Combustion Reaction

J. Wong E. M. Larson J. B. Holt

A simple binary Ti + C = TiC combustion system was selected for our TR-XRD study. The Bragg peaks of hexagonal Ti metal and the final product, TiC, are conveniently located in a common 2θ-space. Some preliminary tests at SSRL were performed on a solid-state, position-sensitive detector—a linear array of photodiodes, consisting of 1024 pixels and able to record 250 scans per second (4 ms per scan). With a combustion-front velocity of 10 mm/s, one scan will cover 0.4 mm of the combustion front. Unfortunately, the detector test at SSRL was far from complete because of the poor quality of the beam delivered by SPEAR.

Thin-Film Growth

T. Barbee J. Wong E. M. Larson

In November 1987, we performed a 9561-eV, glancing-angle, evanescent fluorescent EXAFS study of a 0.5-nm-thick Hf film in the vicinity of its L_3 absorption edge. This film was deposited on a Pt-C multilayer having a period of 3.17 nm. The results indicated that high-quality EXAFS spectra of species at a surface coverage of 0.01 ML can be easily obtained [1].

To test this result further, we measured the fluorescent EXAFS signal from Cu overlayers of various coverages, from 5 to <<1 ML, on 50 nm of tungsten deposited on optically-flat, fused-quartz plates 4×10 cm^2 using a glancing-angle geometry. The Cu layers were covered with a 1-nm layer of amorphous carbon for oxidation protection during handling.

This binary system was chosen because it exhibits unique properties attributable to an interfacial electronic-bonding state between tungsten and copper. It is well established that tungsten and copper are mutually insoluble in both solid and liquid states. However, it is also known that liquid copper wets tungsten, a fact consistent with field-emission microscopy studies, which indicate that the first ML of copper deposited on a tungsten (100) or (110) surface is more strongly bound to the tungsten than is expected for a copper substrate [2]. This is an interfacial effect that promotes layer-by-layer growth and ad-layer stability to unexpected temperatures. The effect appears to be limited to the first two

monolayers of the copper ad layer. The localized interfacial bonding is believed to result from an interfacial antibonding state between the copper and tungsten that has a strength of 0.4–0.6 eV per atom. It is possible that this localized state will be manifested in the XANES spectra. Indeed, recent calculations for the Pd-on-Nb and Ag-on-Nb systems [3] predicted such a state for these binaries. Furthermore, such an interfacial antibonding state has been observed by photoemission studies of the Cu-on-Ru binary [4].

In Fig. SR-1, the EXAFS signals for bulk fcc Cu metal and 5-ML-, 2-ML-, and 1-ML-thick Cu overlayers are shown. At coverage of 2 ML and more, the EXAFS spectra for the Cu overlayers bear close resemblance to the bulk metal, although there are quantitative

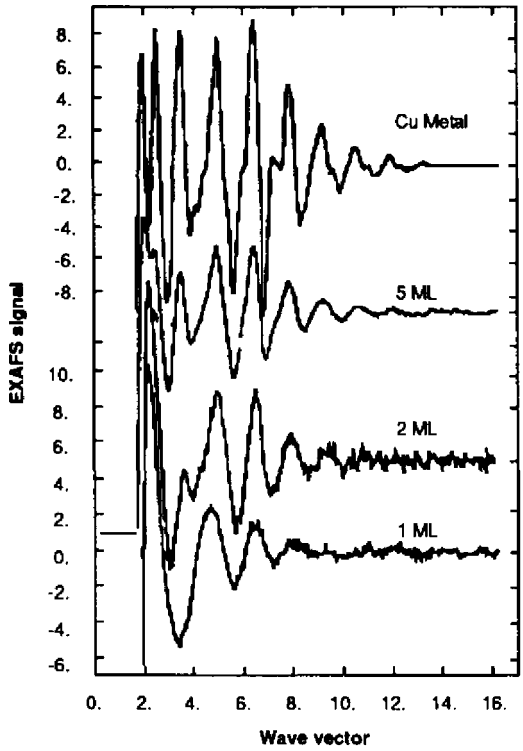

Fig. SR-1. Cu EXAFS signals (reading from the top) from Bulk Cu metal, 5-ML, 2-ML, and 1-ML Cu overlayers on 30-nm W on quartz. The Cu overlayers are covered with 1 nm of amorphous carbon.

differences in the low wave-vector region and in the signal amplitude. For 1-ML Cu film, the EXAFS signal is very different, with the signal envelope resembling that of a low-Z atom. Phase-corrected Fourier transforms of these Cu EXAFS are shown in Fig. SR-2.

At 2-ML coverage and above, the radial structure function about the Cu in these films shows a Cu-Cu distance of ~0.25 nm. A low-R shoulder is evident in the transform of the 2-ML film, which emerges as the dominant radial distance at 0.2 nm in the 1-ML film. This distance mostly likely corresponds to a Cu-C distance; it is also seen in the spectrum and corresponding Fourier transform for the 0.1-ML film in Fig. SR-3. Thus, we have demonstrated experimentally that high-quality EXAFS data for 0.1 ML can be obtained. This series of static experiments serves as a precursor to design our *in situ* thin-film deposition and interface-growth study.

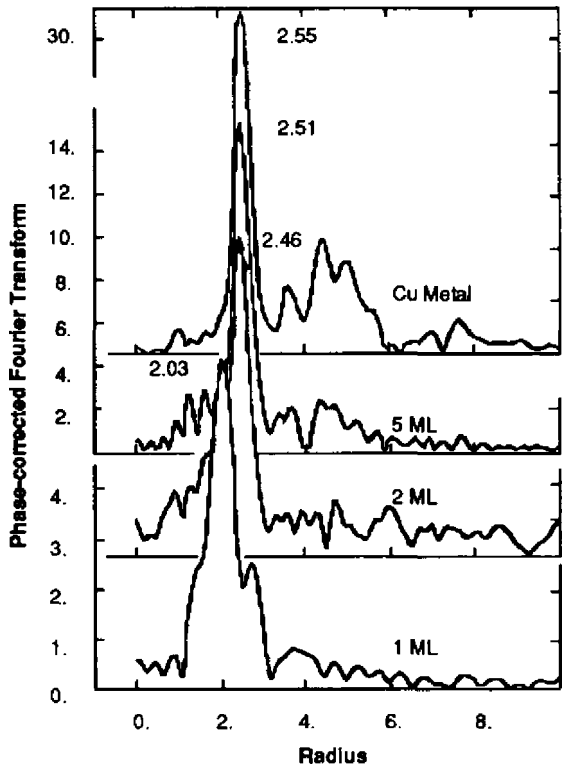

Fig. SR-2. Phase-corrected Fourier transforms of the EXAFS spectra of Fig. SR-1.

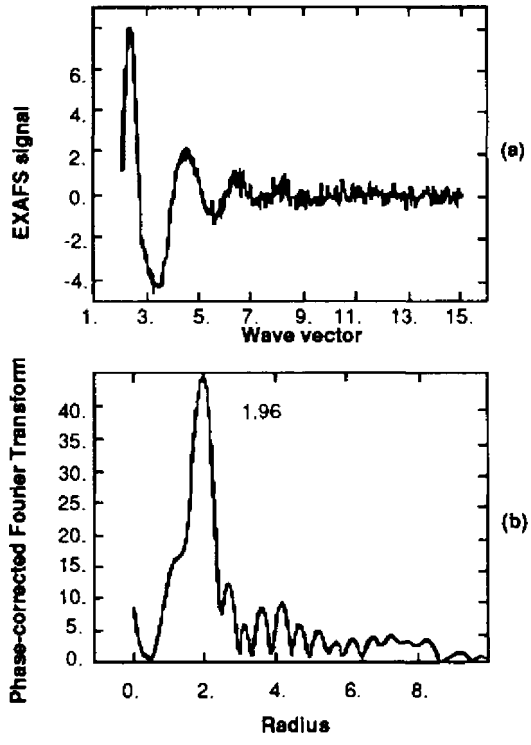

Fig. SR-3. (a) Cu EXAFS and (b) Fourier transform of 0.1 ML of Cu on tungsten.

Dynamic Microstructure

J. H. Kinney
S. R. Stock*
Q. Johnson
U. Bonse**
A. Saroyan

Using an improved optical system, we have successfully recorded tomographic images of SiC-Al composites with 5-μm resolution and have nondestructively identified cracks and grain-boundary segregation in these materials for the first time [5]. A 1.5×1.5×10 mm^3 specimen of an Al/SiC composite was examined with x-ray tomographic microscopy (XTM) on the 31-pole wiggler beamline at SSRL. An x-ray energy of 21 keV was selected for good sample transparency and x-ray contrast between SiC and Al. Figure SR-4 shows a single XTM slice of the composite from a set of 97 contiguous cross-sections obtained with the XTM. The slice thickness is 2.8 μm; spatial resolution is 5 μm. Data were collected at 1-degree intervals. This undersampling leads to some loss in image quality; nevertheless, the 33-μm-diameter graphite cores and surrounding 140-μm-diameter SiC sheaths are clearly visible. Cracks running longitudinally in the plane of the fiber layup are evident. These cracks, which do not penetrate the fiber, may be caused by the grips used to hold the sample during cutting. This would explain the greater crack density near the exterior surfaces, where grip marks are observed. Smaller cracks can be seen nucleating at the SiC/Al interfaces within the interior in response to these stresses.

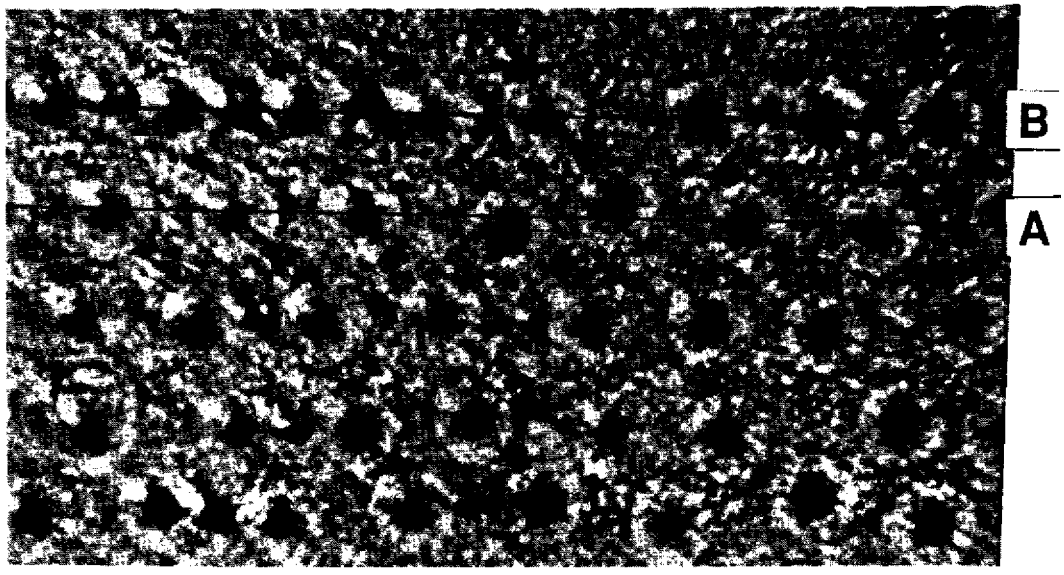

Fig. SR-4. A cross-section of the Al/SiC composite taken with the XTM on the 31-pole wiggler at SSRL. The 33-μm graphite cores are clearly resolved, as are the SiC sheaths surrounding them. Cracks running between the fibers can be seen, especially near the sample surfaces. The slice thickness is 2.8 μm, and the spatial resolution is approximately 5 μm.

* Georgia Institute of Technology.
** University of Dortmund, West Germany.

Figure SR-5a is a planar cut through the same sample parallel to the fibers. In this ply, the fibers are regularly arranged and a few cracks are present. Figure SR-5b is a similar plane taken through a ply that is heavily populated with cracks. This view demonstrates that the cracks tend to run along the fiber/matrix interface rather than across the composite.

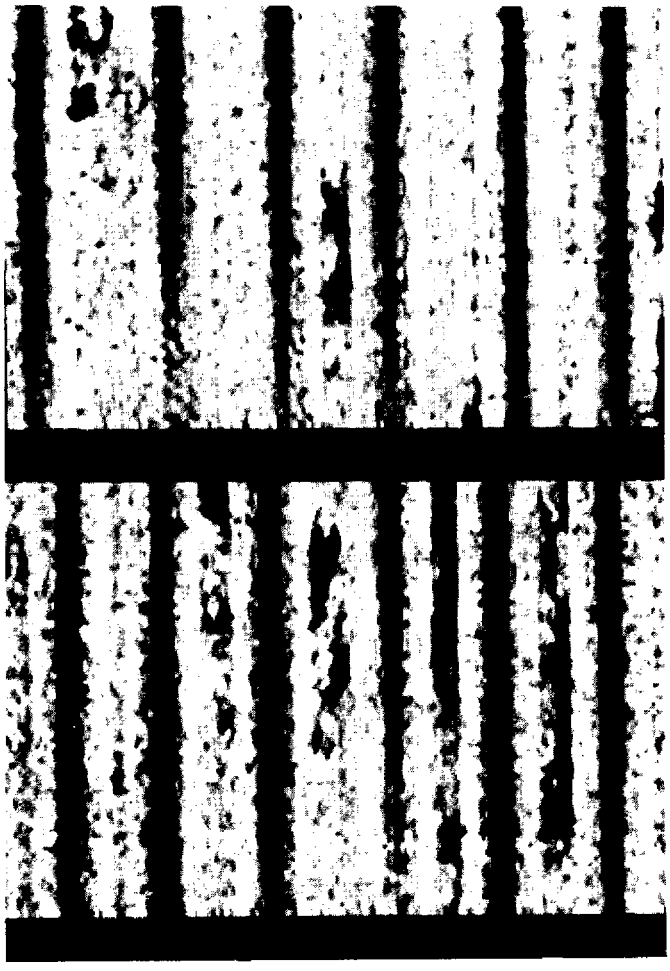

Fig. SR-5. XTM sections in the plane of the fibers are shown for the specimen in Fig. SR-4. (a) The section cutting the line "A" in Fig. SR-4 is in an interior containing a lower crack density. The fibers are clearly shown as well as cracks nucleating from the ceramic/metal interface. Even the interior regions are not free of cracks. The fact that not all fibers are in alignment to the plane creates the variations in the fiber contrast seen in the image. (b) The section from the line "B" in Fig. SR-4 demonstrates the extension of the cracks within the ply.

Figure SR-6 is a view of a single fiber showing the graphite core and the SiC sheath surrounding it. The change in columnar SiC subgrain size produced during the growth of the sheath is evident, as is the SCS-8 coating in the final few μm near the Al interface. The line trace of the XTM data in Fig. SR-7 graphically shows the variation in carbon content across the fiber and is consistent with reported variations.

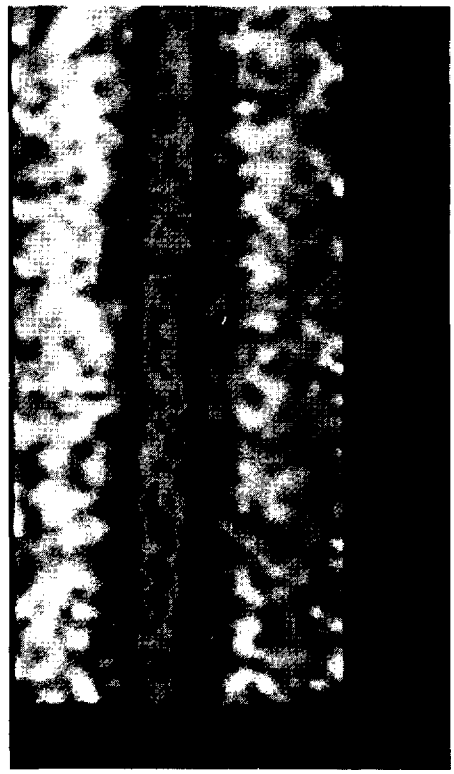

Fig. SR-6. XTM image of a single fiber within the composite. The image shows the graphite core, the SiC subgrain size variations, and the SCS-8 coating at the SiC/Al interface near the outer edge of the fiber.

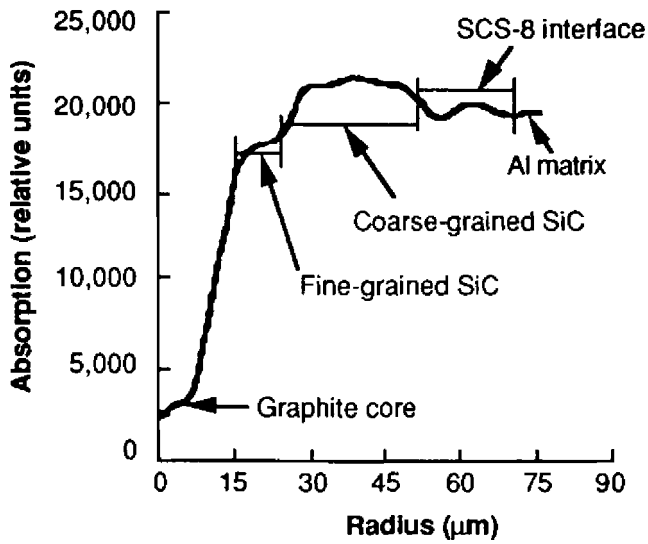

Fig. SR-7. A plot of the absorption data across the fiber shown in Fig. SR-6.

FY89 Goals

We plan to characterize our photodiode-array detector in more detail—at SSRL, if the beam situation is stable and reliable, or at Brookhaven National Synchrotron Light Source. Based on this finding, a reaction chamber has been designed to optimize the scattering geometry to measure the time-resolved diffraction patterns of solid combustion systems at high temperatures. We also plan to perform energy-dispersive EXAFS measurements on the Ti site in the Ti + C system. The EXAFS work will be collaborating with A. Fontaine of the LURE synchrotron facility in France.

The fluorescent EXAFS data will be analyzed to determine the levels of coverage at which Cu ceases to behave structurally as bulk copper and loses the fcc structure. A deposition chamber and vacuum-compatible detector will also be designed to accommodate the *in situ* deposition study of thin-film growth.

In the 3-D microstructural study, we plan to extend our tomographic capability to the soft x-ray region to look at low-Z materials. The USAXS (ultrasmall-angle x-ray scattering) setup will be used to observe real-time gelation in foam materials and other polymers.

YB_{66}

J. Wong
M. Eckart*
H. Tompkins
G. Shimkaveg*
L. Wilson*
T. Tanaka†
W. Goldstein*
Z. Rek**

The objective of this activity is to understand how to grow a large single crystal of YB_{66} that is perfect enough to serve as a dispersive element (monochromator) in the 1–2-keV range of the soft x-ray region. A systematic literature search, based on material requirements and x-ray properties, proves this material to be a candidate crystal. The 1–2-keV region is important to our laser diagnostics and test program; it also satisfies all of the material requirements for use in synchrotron radiation. It is a semiconductor similar to Ge and Si. The 2d value of the (400) reflection is 1.176 nm with a calculated Darwin width of 2.53×10^{-4} rad at 1100 eV.

Status

In collaboration with T. Tanaka, who has recently grown large single crystals of YB_{66} (5 cm long × 1 cm diameter), we have initiated a modest interdepartmental effort to characterize this material and evaluate its potential for use as an x-ray spectrometer and monochromator. Calculations using an existing BRAGG code indeed show that YB_{66} has superior soft x-ray dispersing properties—a narrower rocking curve and higher reflectivity

* L-Division.
** Stanford Synchrotron Radiation Laboratory.
† National Institute for Inorganic Materials Research, Japan.

than beryl. Five crystals of YB_{66} have been grown, at rates ranging from 6 to 100 mm/hr. Hard x-ray rocking-curve measurements showed a systematic variation of crystal quality with growth rate.

Metallographic examinations have been performed at LLNL, topographic images at SSRL. They were correlated with the mosaic subgrain microstructure and other grown-in defects in the crystals. The results are very encouraging in that, at a 25-mm/hr growth rate, we succeeded in getting a single-peak rocking curve.

FY89 Goal

We plan a systematic topographic study of the good crystal along the crystal boule axis from seed to the bottom end for evaluation of the defect concentration and microstructure in relationship to growth history. Topographic results will be correlated with the soft x-ray rocking-curve measurements to be performed on a synchrotron beamline. We will also study the solid/liquid interface during crystal growth as a function of pull rate, rotation rate, power input, etc. It is hoped that such advanced crystal characterization will provide the insight needed to optimize the crystal growth process to yield large and sufficiently perfect crystals to disperse x-rays in the 1–2-keV region.

Advanced Laser Crystals

J. Wong
L. Chase*
E. M. Larson
S. Payne*
M. Weber
R. Powell*

The objective of this activity is to determine the local coordination of the Cr ions in $LiCaAlF_6$, SrF_2, and Mg_2SiO_4 and to relate to their optical spectra. The resulting understanding should lead to a better predictive capability for new tunable-laser materials.

Status

High-resolution K-edge XANES and EXAFS spectra of Cr ions in $LiCaAlF_6$, SrF_2, CaF_2, and Mg_2SiO_4 have been recorded at SSRL. The spectra of CrF_3 and Cr_2O_3 (of known crystal structure) were also measured to model the local environment of Cr in the laser hosts.

FY89 Goals

We plan to analyze and reduce the XANES and EXAFS data to determine site symmetry, valence, bond distance, and coordination about the Cr site in these materials and to correlate with their optical spectra. The combined optical/structural studies will be extended to other fluoride- and oxide-crystal hosts based on these initial findings.

* Y-Division.

Photocatalysis on Doped Aerogels

C. Colmenares M. Connor C. Evans
R. Gaver*

The objective of this project is to demonstrate that SiO_2, Al_2O_3, or ThO_2 aerogels doped with photochemically-active ions can be used as heterogeneous catalysts for the production of hydrocarbons from simple gas mixtures ($CO + H_2$, $CO_2 + H_2$, etc.) using sunlight as the energy source. Also, the energy-transfer mechanisms effecting the chemical reactions will be investigated.

Status

Progress on this project, particularly manufacturing and testing the needed aerogels, has been affected by project Dayton. However, we have set up and made operational the equipment needed to explore the energy-transfer mechanisms, namely:

- A stainless steel autoclave to produce high-purity aerogels has been set up and tested. An operational safety procedure was written and approved.
- A fast-scan optical spectrometer (250–800 nm) and a solar-simulator source to obtain optical spectra of chemisorbed gas species on aerogels have been set up and tested.
- An ultrahigh-vacuum system equipped with ultraviolet, x-ray, and Auger electron spectroscopies has been made operational to carry out the investigations of the energy-transfer mechanisms on aerogels.

FY89 Goals

We plan to prepare thin films of aerogels doped with Ce, Eu, Fe, and UO_2^{++} and to perform detailed experiments to elucidate the energy-transfer mechanism on them when exposed to sunlight.

References

1. T. W. Barbee, Jr., and J. Wong, "EXAFS of Near Monolayer and Sub-monolayer Coverage Films," presentation at Materials Research Society Synchrotron Radiation Symposium, Boston, Mass., Nov. 1988.
2. A. J. Melnod, *J. Appl. Phys.* **36**, 3585 (1965).
3. M. Weinert, R. E. Watson, J. W. Davenport, and G. W. Fernando, private communication (1988).
4. J. E. Houston, C. H. F. Pader, P. J. Feibelman, and D. R. Hanann, *Phys. Rev. Lett.* **56**, 395 (1986).

* San Jose State University.

5. J. H. Kinney, S. R. Stock, M. C. Nichols, U. Bonse, T. Breunig, Q. C. Johnson, R. A. Saroyan, R. Nusshardt, F. Busch, and S. D. Antolovich, "Nondestructive Investigation of Damage in Composites using X-ray Tomographic Microscopy (XTM)," submitted to *Nature* (1989).

Invited Talks

J. H. Kinney, "Scientific Applications of 3-D Chemical Tomography," presented at 15th Annual SSRL Users Group meeting, Stanford, Calif., Oct. 1988; also presented at Materials Science Seminar, Argonne National Laboratory, Argonne, Ill., Jan. 1989.

WEAPONS-SUPPORTING RESEARCH

Individual Projects

ENZYME MIMICS FOR METHANE CONVERSION

M. Droege *(Principal Investigator)*

Introduction

Transportation fuels are a critical energy commodity that impact nearly every sector of this country and account for 27% of its total energy consumption. Since almost all transportation fuels are derived from crude oil, they also account for 63% of all U.S. oil needs. Transportation alone uses more oil than the nation produces, and it is projected to do so well into the next century. Consequently, strong emphasis is on the economical conversion of domestic, non-petroleum, fossil-energy resources to hydrocarbon liquids that can be used as transportation fuels.

Interest is currently intense in developing economical technologies that convert natural gas to liquid fuels. However, the future for methane conversion and natural-gas processing will depend on the development of catalyzed routes that directly convert methane to liquid hydrocarbons. The thermodynamically-allowed general reaction that transforms methane (CH_4) to higher hydrocarbons,

$$nCH_4 + (y/2)O_2 \longrightarrow C_nH_{4n-2y} + yH_2O$$

is an oxidative process that requires a catalyst to facilitate the reaction. Non-catalyzed, simple thermal reactions of methane and oxygen require very high operating temperatures (700–800 °C); as a result, the desired product yield of hydrocarbons is unacceptably low, in large part because of uncontrolled overoxidation of methane to CO and (CO_2. The key to upgrading methane to liquid fuels is *controlled* catalytic activation of the C–H bond, thus preventing overoxidation.

The major emphasis of this research is the development of new catalyst materials to facilitate the reactions that convert methane to liquid fuels. Our approach is to link traditional catalysis research with the emerging field of biotechnology. The advantage of this approach is that it derives knowledge from a biocatalytic system that is already transforming methane to useful products and applies the information to development of new "traditional" inorganic catalysts. We expect this approach to offer a shortcut in the development of novel catalysts for methane conversion.

Background

It is well-known that a select group of aerobic soil/water bacteria called methanotrophs can efficiently and selectively use methane as their sole source of energy and carbon for cellular growth. The first reaction in this metabolic pathway is catalyzed by the enzyme methane monooxygenase (MMO) forming methanol:

$$CH_4 + O_2 + NADH + H^+ \xrightarrow{25\text{–}50\ ^\circ C} CH_3OH + H_2O + NAD^+$$

Methanol is a technologically-important product from the partial oxidation of methane since it can be easily converted to liquid-hydrocarbon transportation fuels or used directly as a liquid fuel. In addition to studying naturally-occurring bacterial systems that consume methane and catalyze the methane-to-methanol conversion, this research will attempt to develop "bioinorganic" (non-biological) catalysts that might mimic MMO enzymatic action. The substrate NADH is nicotine adenine dinucleotide in its hydrogenated form.

The MMO enzyme is known (EXAFS studies) to contain two closely paired iron ions at the active site for catalysis. The iron site appears to be binuclear, containing either a μ-oxo- or a μ-hydroxo-bridge between the iron atoms. The remaining ligands (derived from adjacent amino acid residues) are either N- or O-containing, and the Fe-Fe distance is between 0.3 and 0.35 nm. Other information, such as tertiary protein structure or amino acid sequence, that would help determine the composition and structure of the active site is currently unknown.

Binuclear iron sites have been described for other protein systems. Hemerythrin, an oxygen-transport protein found in some marine worms, is the most studied and structurally well characterized of these binuclear iron-containing proteins. Although functionally similar to hemoglobin, it is structurally distinct and the mechanism of action is quite different. The deoxygenated form of hemerythrin contains two Fe(II) ions; the oxygenated form is best described as containing two Fe(III) ions. This reversible oxidation of iron on oxygenation does not occur in hemoglobin. The best structural picture has been obtained from both EXAFS and single-crystal XRD:

Deoxygenated Form

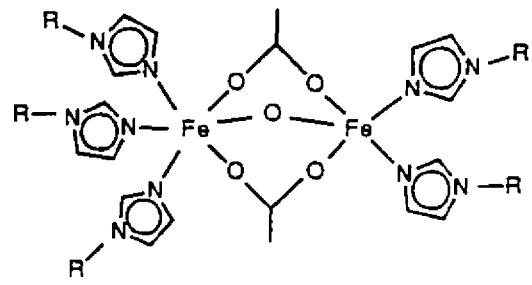

Approach

Proteins containing metallic elements are essentially highly-elaborated coordination complexes in which the metal-containing "active site" is usually the center of electron transfer, substrate binding, and catalysis. Our approach is to synthesize inorganic/organic chemical models of the biocatalyst(enzyme)-active site in order to probe its reactivity and to generate new catalyst materials. Using these complexes as a starting point, we can systematically modify the complexes and, by monitoring both their physical properties and chemical reactions as compared to the native enzyme, can obtain a good correspondence to

the action of the native enzyme. This allows for both a detailed study of the events of the catalytic reaction and the development of an active catalytic material that performs the desired transformation of methane to liquid products. The preliminary structural data on MMO suggest that incorporating many of the structural features of hemerythrin is an appropriate starting point in the development of synthetic chemical models.

Experimental Progress

Ligand Preparation

Currently, we are preparing low-molecular-weight complexes in which a metal of interest (Fe, Cu, etc.) is coordinated to atoms or molecules that may resemble components of the enzyme. We have prepared symmetrical chelating structures that bind two metal ions in a fashion thought to be similar to that found in the native enzyme. The chelating ligands were prepared using condensation reactions as shown here:

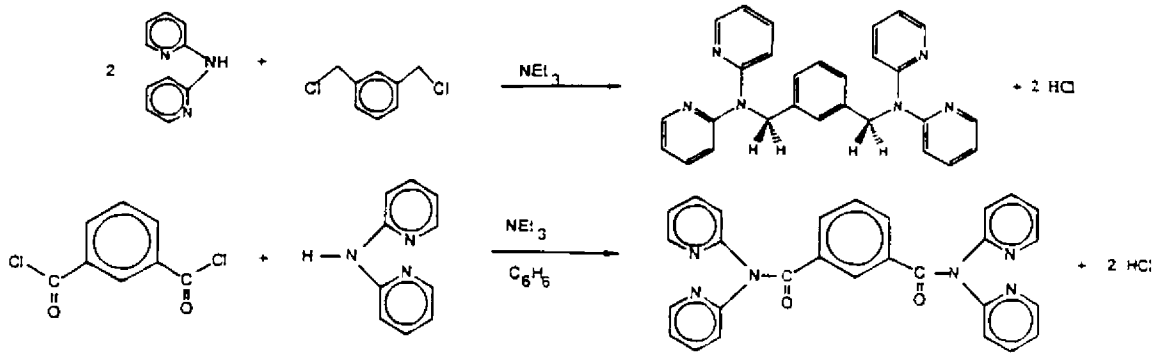

The organic structures have been characterized by ^{1}H and ^{13}C NMR spectroscopy, IR spectroscopy, and elemental analysis.

Metal Complex Synthesis

To date, complexes containing Co, Cu, and Fe have been synthesized and isolated as crystalline complexes through the use of chelating structures with either pyridine or benzimidazole coordinating groups. These complexes are synthesized by stoichiometric reactions in methanol using hydrated metal salts with either ClO^{4-} or BF^{4-} counterions. The colored metal-containing complexes are formed rapidly and are isolated by vapor diffusion using diethyl ether. A typical reaction using benzimidazole groups is shown at the top of the next page. The complexes have been characterized by IR spectroscopy and elemental analysis. Additional characterization studies including single-crystal x-ray studies are planned.

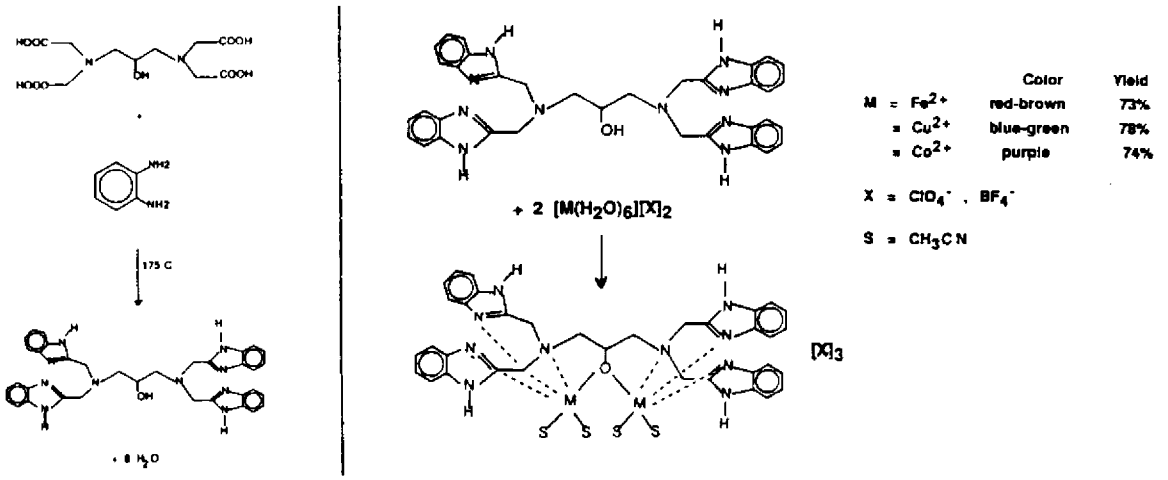

Future Work for FY89

For the remainder of the fiscal year, work on synthesizing more elaborate, unsymmetrical structures is in progress and will continue. These ligands are important since they force reaction at one metal site (as the enzyme does) as opposed to the symmetrical ligands described above. New ligand routes under investigation include:

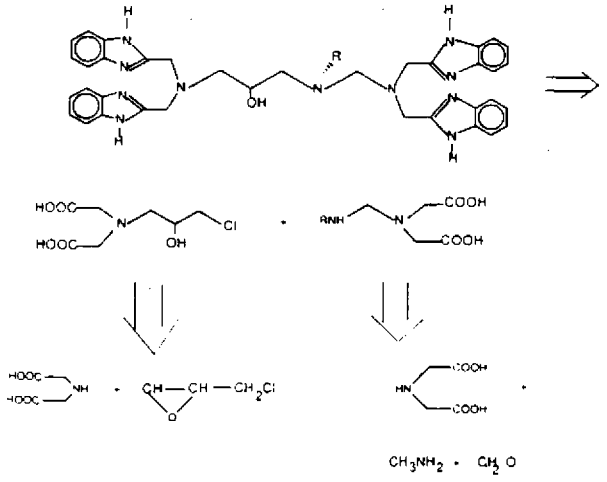

Future work includes full characterization on models including spectral (UV/VIS, ESR, IR/Raman), magnetic, and redox properties (electrochemistry). These properties will be compared with those generated by studying the native MMO enzyme. The comparison of the physical properties will be used to suggest modification to the ligand system in order to better model the active site of MMO. Binding studies of methane and oxygen with the isolated complexes and/or new complexes will begin. These studies will probe both structural requirements and reaction pathways important for catalysts that convert methane to methanol.

STRUCTURAL CHARACTERIZATION AND MODELING OF ORGANIC AEROGELS

R. W. Pekala *(Principal Investigator)*
S. A. Letts R. C. Cook

Overview

During the last four months, we have focused on characterization and modeling of organic aerogels made from resorcinol and formaldehyde. The polycondensation of resorcinol with formaldehyde under alkaline conditions follows a sol-gel pathway in which surface-functionalized polymer "beads" are formed. The covalent crosslinking of these beads produces gels that can be dried under supercritical conditions to obtain low-density organic aerogels ($\leq$0.30 g/cm^3). High-density organic xerogels ($\geq$0.60 g/cm^3) result if the solvent is slowly evaporated from the gel. Both materials have continuous porosity with cell/pore sizes less than 100 nm. Their microstructure is composed of interconnected colloidal-like particles with diameters of 3–15 nm. The particle size, cell size, surface area, and density of these materials are predominantly controlled by the catalyst concentration in the original mixture. Details of the gel synthesis have been previously described [1,2]. These aerogels/xerogels can be further processed into a glassy carbon state by pyrolysis in an inert atmosphere. To characterize a material composed of small particles, we have used light scattering, SAXS, and high-resolution TEM.

Light Scattering

We have set up a new laser light-scattering spectrometer to analyze bead formation and aggregation prior to gelation. The effects of catalyst concentration (R/C or resorcinol-to-catalyst ratio) and polymerization time on aggregation have been studied. After one hour of polymerization, low catalyst concentration (R/C = 300; produces large beads) results in more scattering intensity than does higher catalyst concentration (R/C = 200 or 50). After 11 hours of polymerization, all gels show approximately the same scattering intensity.

Small-Angle X-ray Scattering

Structural properties of resorcinol-formaldehyde (RF) foams were investigated using an ultrasmall-angle scattering camera at a synchrotron radiation source in West Germany. Because of the expected high correlation lengths, we used the USAXS camera developed by Bonse et al. [3]. This unique equipment can examine materials at the 100- to 1000-nm scattering-vector range.

Increasing the R/C ratio during fabrication of the foams coincides strongly with increased scattering power (Fig. SC-1). High catalyst concentration results in a decreased diameter of the polymer beads and interparticle distance as indicated by Guinier plots.

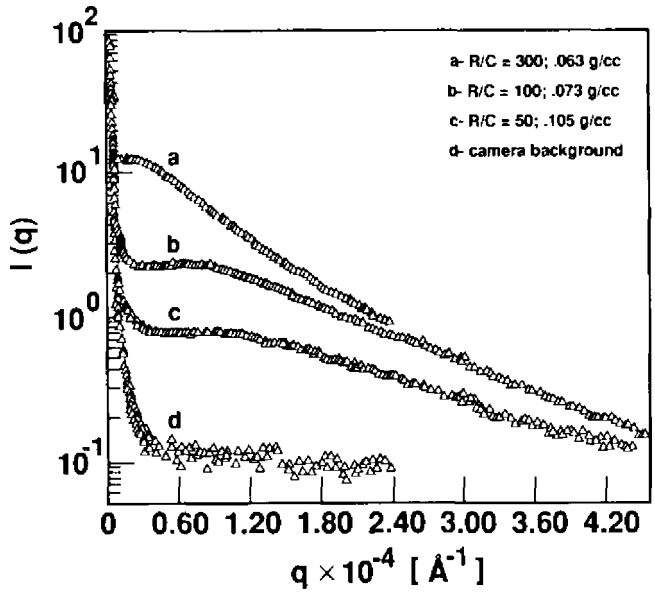

Fig. SC-1. USAXS curves of various RF foams made using different R/C ratios.

From least-square fits to the experimental data, Guinier radii (R_g) of 7 nm and 50 nm were calculated for beads; R_g values of 80 and 350 nm were assigned to the aggregated aerogel system. The x-ray scattering results showed that RF foams do have properties similar to those of silica aerogels, which should explain the differences in mechanical properties observed in compression experiments. We have also worked in collaboration with D. W. Schaefer of SNLA on SAXS. Here we have examined the 0.1- to 100-nm scattering-vector range. Fractal structure analysis of the aerogels is under way.

High-Resolution TEM

This aspect of organic aerogel characterization is being conducted through a contract with G. C. Ruben of Dartmouth. Ruben has a unique facility for high-resolution TEM that includes special replica-production capabilities and experience with silica aerogels [4]. In silica aerogels, Ruben has observed 0.5-nm structure showing individual beads and has shown the beads to be microporous. We are planning to interact closely with Ruben so that the capability can later be developed at LLNL.

Modeling

We have initiated computer simulation modeling studies of the gelation process in order to obtain a better understanding of the variables that govern gel structure. Our model system consists of a collection of spheres in a box with periodic boundary conditions. The dimensions of the box are based on the desired mass density in the system. In the results reported here, we chose to use 1000 particles of radius 5 nm and intrinsic density of 1.0 g/cm^3 at a system density of 0.10 g/cm^3. The particles are initially placed in the box

randomly in such a way that they do not overlap. We then proceed to solve the Brownian dynamics equations of motion for the system and to follow its time evolution.

The sphere surfaces are modeled to be reactive as follows. When the distance between two spheres becomes less than the sum of their radii, a Hookean spring (bond) is created between them with equilibrium length equal to the sum of the radii. When a particle encounters a particle that is already bonded to one or more other particles we can consider the existence of a "bond-angle"-like force. We have examined three ways to model this interaction. First, we can ignore it, letting all chain segments be freely jointed. Second, we can fix the angle made by the three atoms as they initially formed and create a Hookean potential centered at that value. The effect of this potential is to "freeze-in" the configuration of the particles upon contact. A third model for the angle potential uses a Hookean potential with its minimum centered at 180 degrees—*regardless* of the angle of initial contact. The motivation for this model is to simulate electrical double-layer effects. Because of these effects, addition of particles in more linear strings might be expected, as suggested by SEM analyses of our materials, which tend to show an extended "string-of-pearls" structure.

Simulations were run using all three of these angle potentials. In Fig. SC-2, we show the weight average molecular weight of the system as a function of time. Note that the

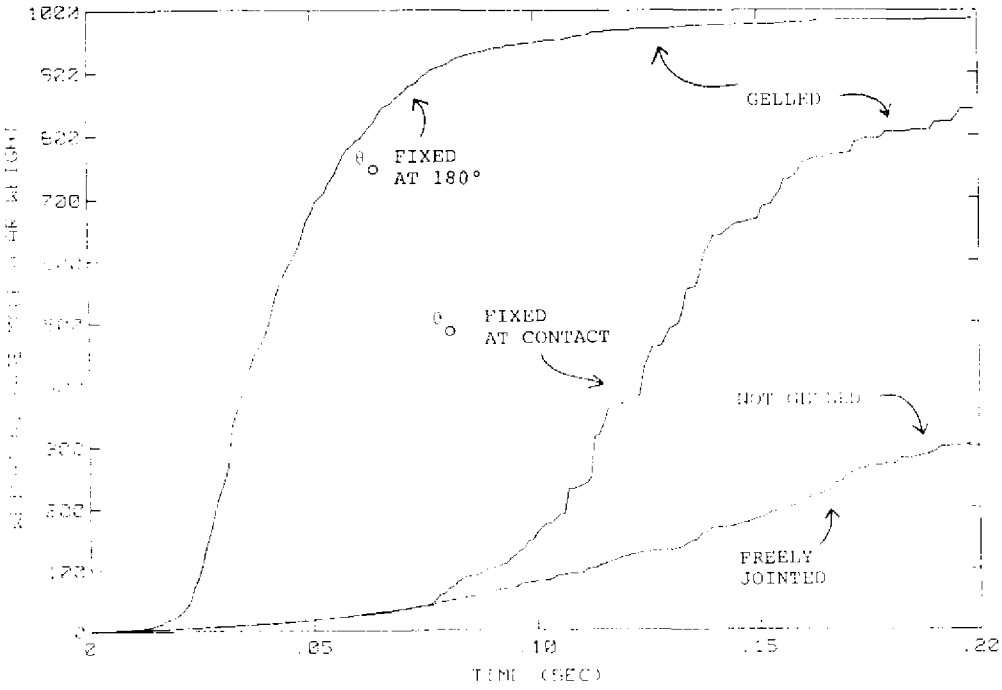

Fig. SC-2. Time evolution of the weight average molecule weight for a 1000-particle system for each of the bond-angle (θ) potentials used.

system without any angle potential (freely jointed) has not gelled but consists of ~3 clusters that are quite dense. The average coordination number (or number of bonds) that a particle has in these clusters is >4 and still climbing as the run ends, suggesting a continually

increasing crosslinked density and more densely packed clusters. By contrast, those runs with either of the other two angle potentials have an average coordination number that levels off between 2.0 and 2.5, consistent with a crosslinked system without significant compaction. In Fig. SC-2, we can see that both of these systems have gelled, which we define as a state in which the box contains one "large" cluster that spans all parts of the available space. The simulation runs that have the bond angle fixed at 180° clearly gel more rapidly due to the attempt of the potential to straighten the chain segments.

We can also calculate the appropriate scattering functions in order to compare with the experimental measurements of these quantities. Our objectives now are to further explore the differences in these potentials and to explore the effect of changes in the overall system density, temperature, and solvent viscosity on the gelation process and structures formed.

References

1. R. W. Pekala, submitted to *J. Mater. Sci.* (1989).
2. R. W. Pekala and R. W. Hopper, *J. Mater. Sci.* **22**, 1840 (1987).
3. U. Bonse, R. Pahl, and R. Nusshardt, *Acta Cryst.* **A43**, C 259 (1987).
4. G. C. Ruben and M. W. Shafer, *Mater. Res. Soc. Symp. Proc.* **73**, 207 (1986).

Publications

R. W. Pekala and F-M. Kong, "Resorcinol-Formaldehyde Aerogels and Their Carbonized Derivatives," *Am. Chem. Soc. Div. Polym. Prepr.* (1989).

R. W. Pekala, "Aerogels and Xerogels From Organic Precursors," submitted to *Mater. Res. Soc. Symp. Proc.* (1989).

R. W. Pekala, "Organic Aerogels from the Polycondensation of Resorcinol with Formaldehyde," *J. Mater. Sci.* (1989), in press.

Presentations

R. W. Pekala and F-M. Kong, "Resorcinol-Formaldehyde Aerogels and Their Carbonized Derivatives," presented at ACS National Convention, Dallas, Tex., Apr. 9–14, 1989.

R. W. Pekala, "Aerogels and Xerogels From Organic Precursors," presented at 4th International Conference on Ultrastructure Processing of Ceramics, Glasses and Composites, Tucson, Ariz., Feb. 20–24, 1989.

ULTRATRACE ANALYSIS OF EXPLOSIVE RESIDUES

B. D. Andresen *(Principal Investigator)*
E. Raber R. Eagle

Overview

Explosives analysis is an ongoing activity at LLNL. Not only are known explosives subjected to a variety of analytical techniques, new synthetic explosives must be analyzed, tested, and studied in great detail. In addition to dealing with the parent explosive agents, methods are needed to simultaneously analyze chemical binders, stabilizers, and impurities associated with explosives. A program has been designed to investigate new methods for explosive analysis.*

There is a need to analyze environmental samples and to identify explosives and detonation residues that may be present only in very low concentrations of complex mixtures. We have therefore initiated studies to detect trace levels of explosives. Computer-guided gas-chromatographic/mass-spectrometric (GC/MS) analysis has high sensitivity and specificity that would seem to make it a ideal tool for identifying explosives. However, GC/MS alone was initially determined to be an analytical technique that was not readily amenable to thermally unstable and highly polar compounds.

All published methods of explosive analysis appear to center on detection of the intact parent compound only. In addition, they almost always ignore the minor compounds or chemicals that are very dissimilar to the parent explosive. In contrast, our new approach to these problems utilizes unique derivatization schemes that render explosives and their residue products more amenable to GC/MS analysis. This approach allows very low levels of explosives, their detonation products, and other important compounds to be identified simultaneously in complex mixtures while using the high sensitivity and unique analytical specificity of GC/MS analysis.

Derivatization of TATB

Initial experiments with triaminotrinitrobenzene (TATB) have supported our preliminary hypothesis: This explosive cannot be identified easily by conventional chromatographic techniques. Preliminary experiments show that a new derivatization procedure can now allow analysis of TATB by GC/MS. The derivatization procedure uses excess dimethylsulfoxide/sodium-DMSO as a combined solvent and strong base to remove the protons from the amino groups on TATB. The strongly basic solution is treated with excess ethyliodide and quenched with water, and the derivatized products are extracted into

* Funded jointly by WSR and other DOE programs.

a suitable solvent. A microscale reaction, using as little as a few nanograms of material, appears to be complete in 15 minutes with mild heating.

The reaction appears to generate a nucleophilic, TATB intermediate that reacts easily with ethyliodide:

$$R\text{-}NH_2 + Na\text{-}DMSO \longrightarrow R\text{-}NH^-Na^+$$
$$R\text{-}NH^-Na^+ + Ethyl\text{-}I \longrightarrow R\text{-}NH\text{-}Ethyl$$
$$R\text{-}NH\text{-}Ethyl \longrightarrow R\text{-}N(Ethyl)_2$$

From our studies, it appears that the TATB molecule is fully derivatized (addition of six ethyl groups). This may be partly due to the strong electron-withdrawing effects of three nitro groups symmetrically placed on the aromatic ring. This unique configuration allows the amino moieties to behave as weak acids.

The analysis of a 10-ng sample of TATB is shown in Fig. UA-1. The GC/MS total ionization plot (lower trace) reveals impurities and other compounds associated with the sample. The upper trace is a single mass plot which highlights only the new molecular ion (m/z 426) of the ethyl-derivatized TATB sample. The mass spectrum of the new TATB derivative (Fig. UA-2) reveals a characteristic fragmentation pattern and a unique and abundant molecular ion (base peak), which aid in trace-level measurements of TATB in complex environmental mixtures.

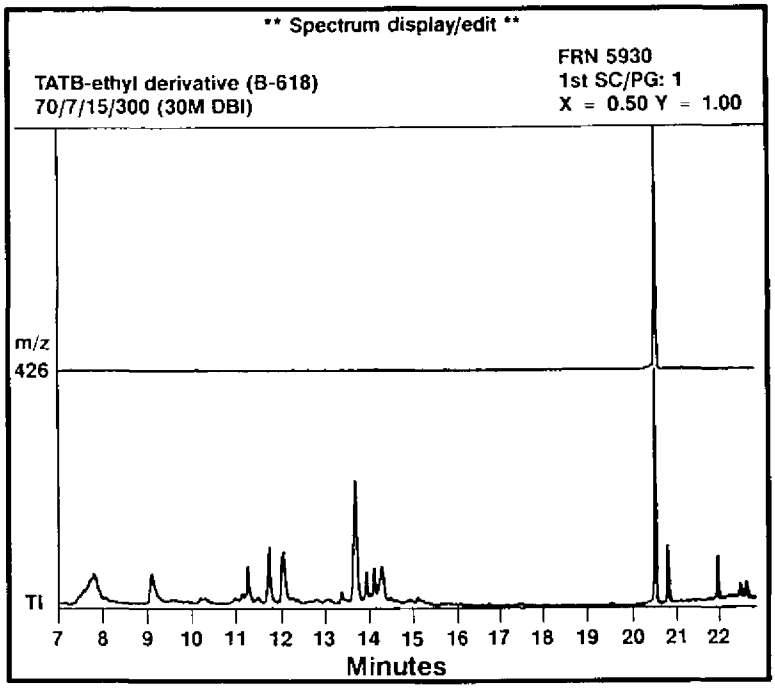

Fig. UA-1. Gas chromatographic/mass spectrometric total-ionization plot of derivatized TATB (bottom trace). Upper trace (m/z 426) is a plot of only the molecular ion of the newly derivatized TATB compound (observed at 20.5 minutes; chromatographic conditions: 30-meter capillary gas chromatographic column; isothermal: 70 °C for 7 minutes; programmed to 300 °C at 15 °C/minute).

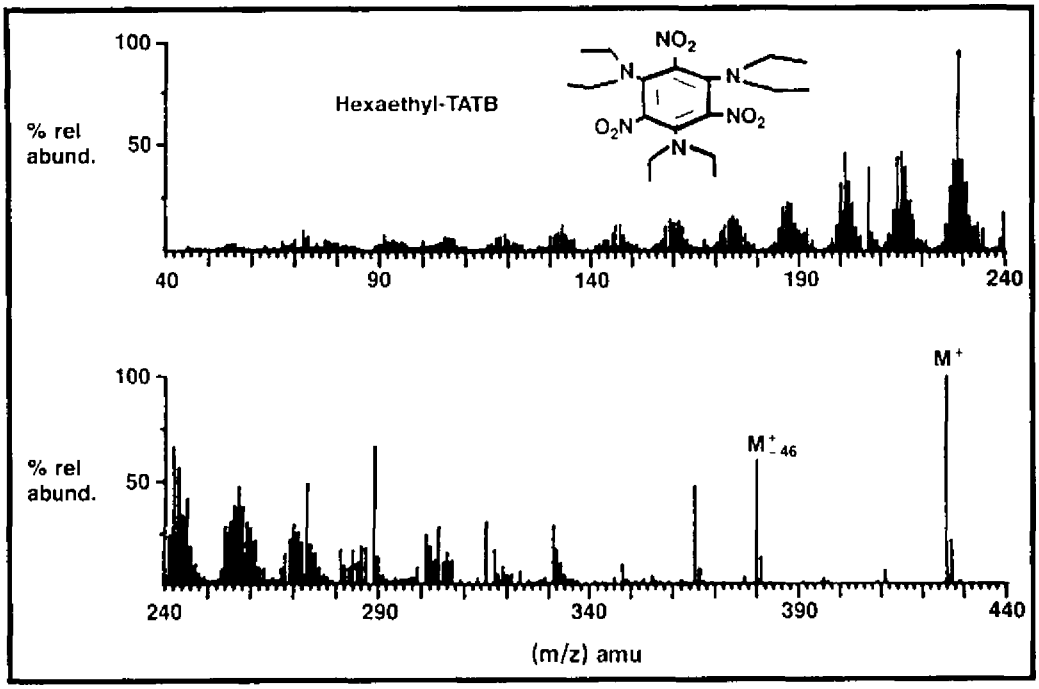

Fig. UA-2. Mass spectrum of the new derivative of TATB. A new molecular ion is seen at m/z 426 and a unique series of fragment ions is observed which appears to be characteristic of TATB. The fragment ion at m/z 380 appears to be the molecular ion minus one nitro group.

Fingerprinting Explosive Residues

Studies are in progress to isolate and fingerprint trace levels of many common explosive residues. The experiments have required detonation of 300-gram samples of pure explosives, collection of smoke and particles, isolation of trace levels of organic residues, derivatization, and GC/MS analyses. The first phase of the work successfully identified unique fingerprint patterns associated with individual explosives. Figure UA-3 shows several GC/MS total-ionization plots of explosives that will be useful for future work aimed at fingerprinting explosives in environmental samples.

Future Work

We plan to investigate a variety of derivatization schemes that appear to generate thermally-stable compounds amenable to GC/MS and other types of chromatographic analysis.

An important discovery made during the course of this work was that major amounts of nonspecific explosive residues and side-reaction products were *always* present in the isolated explosive residues. This made the identification of unique chemical fingerprint patterns difficult. It appeared that minor nitrogen-containing compounds associated with the explosive residues generated a more accurate fingerprint of the true parent explosive. However, these minor compounds are often completely obscured when major amounts of

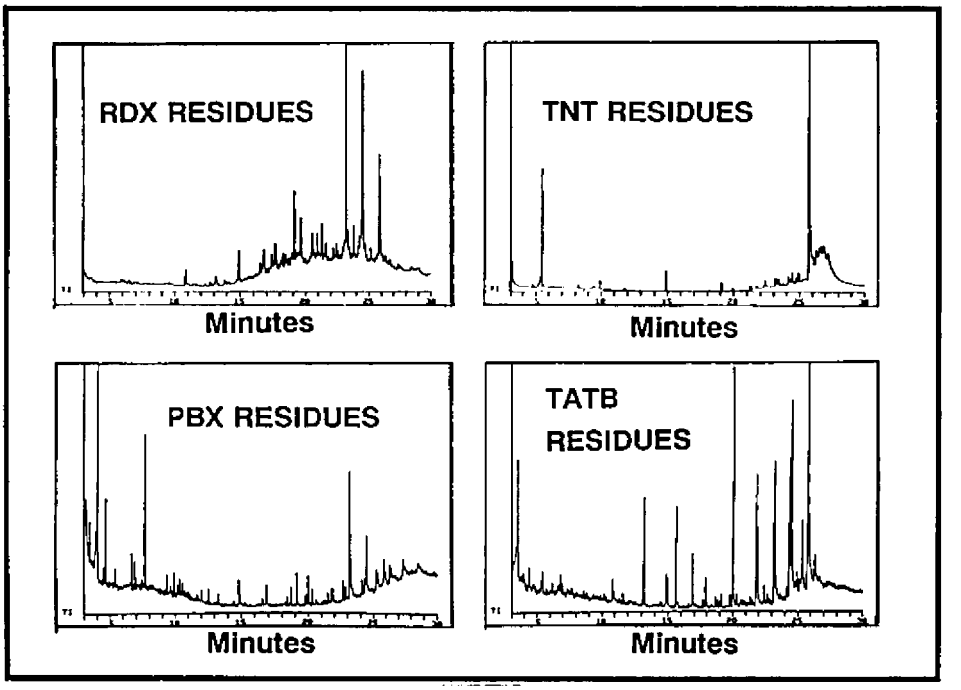

Fig. UA-3. Total-ionization plots generated from different explosive residues of smoke and particles. Each explosive chemical fingerprint has characteristics that may be used to identify the parent explosive.

products derived from common plasticizers, binders, and moderators are present. What is needed is a method that will give additional fingerprinting data to the GC/MS analyses.

A new thermal-energy analysis (TEA) technique that identifies only nitrogen-containing chromatographic peaks during GC/MS analysis is being investigated. The goal of this work will be to more clearly highlight the differences in the fingerprint patterns of nitrogen-containing compounds generated during the analysis of trace explosive residues. By combining TEA with GC/MS, we anticipate the availability of a very powerful new analytical tool that will clearly differentiate explosive-related residues from background contaminations.

Bibliography

L.P. Rigdon, F.B. Stephens, and J. E. Harrar, "Precise Analysis of TATB by the Determination of Total Amino and Nitro Functional Groups," *Propellants, Explos., Pyrotechnics* **8**, 206 (1983).

C.L. Schaffer and W.T. Quinlin, *HPLC Assay Methods for TATB*, Mason and Hanger-Silas Mason Co. Pantex Plant, Inc., Amarillo, Tex., MHSMP-85 Technical Process Development Report 101 (1985).

N. Crow, R. Elwood, and P. Webster-Scholten, *Distribution of High Explosives Compounds in Soil and Water at the 806/807 Lagoons, HE Process Area, LLNL Site 300*, Lawrence Livermore National Laboratory, Livermore, Calif., UCAR-10169 (1986).

A. L. Lafleur and K. M. Mills, "Trace Level Determination of Selected Nitroaromatic Compounds By Gas Chromatography With Pyrolysis/Chemiluminescent Detection," *Anal. Chem.* **53**, 1202 (1983).

H. R. Messler, "On-Line Computer Search System Applied to Explosives," in the Proceedings of the International Symposium on the Analysis and Detection of Explosives held at Quantico, Va., 1983.

DEPARTMENTAL
INSTITUTIONAL RESEARCH & DEVELOPMENT

Individual Projects

SITE-SPECIFIC CHEMISTRY USING SYNCHROTRON RADIATION

Joe Wong *(Principal Investigator)*
E. M. Larson M. J. Weber

Overview

In this period, we completed (1) a systematic study of the valence and site occupancy of 3d metals Ti, V, Cu, and Zn ions substituted in $YBa_2Cu_3O_7$ and correlated with the effect of T_c suppression by such dopant and (2) a detailed investigation of the local coordination of Nd^{3+} ion in a series of binary alkali BeF_2 glasses and correlated with known optical properties and molecular dynamics structure simulations.

Results

3d Metal Substitution in $YBa_2Cu_3O_7$

The experimental findings are summarized in Fig. SS-1, which shows (a) the Fourier transform of the K-edge EXAFS of Cr, Mn, Fe, Co, Ni, and Zn incorporated into the 1,2,3 compound; (b) the XANES spectra of the corresponding 3d ions including Ti and V; and (c) a series of XANES spectra of Cr compounds of known structure to model the environment of Cr in the superconductor. The analysis of the XANES and EXAFS shows

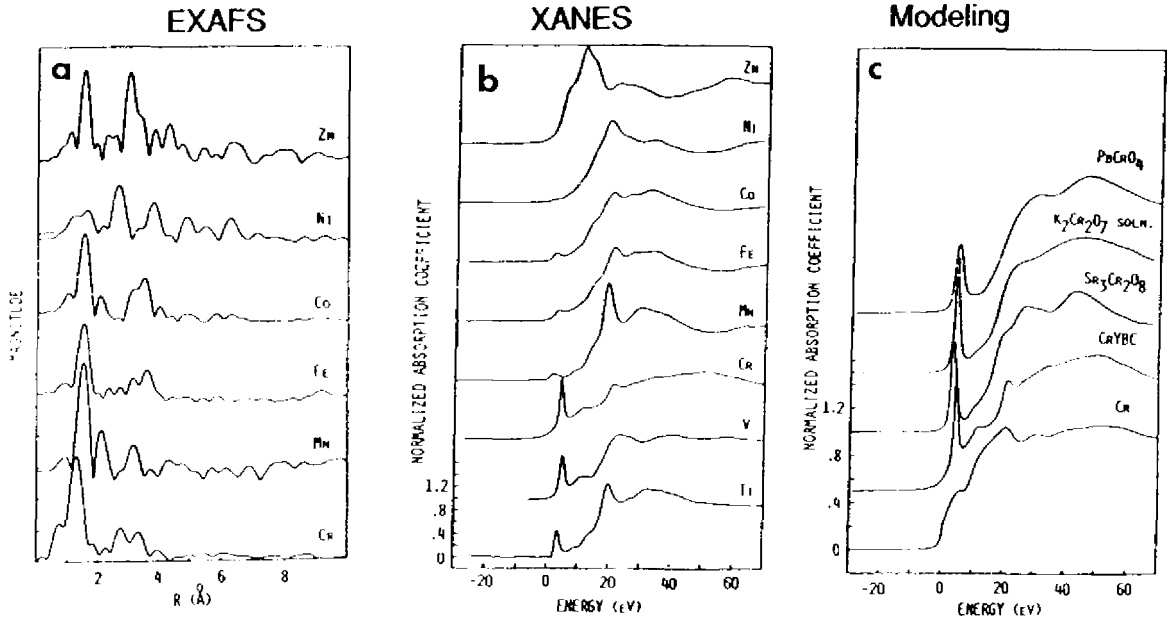

Fig. SS-1. (a) EXAFS spectra, (b) XANES spectra, and (c) model spectra of 3d metal ions substituted in $YBa_2Cu_3O_7$.

that Ti, Mn, Fe, and Co substitute primarily into the Cu(1) site, V and Zn into the Cu(2) site; Cr is present as a chromate phase, and Ni is in a very mixed environment. Ni could be substituting into both Cu sites, but the majority phase is like NiO. All elements appear to be present at some level as segregated oxides but with a grain size below that detectable by XRD. The valence of the elements as determined from the XANES is Ti^{4+}, $V^{4\text{ or }5+}$, Cr^{6+}, $Mn^{2\text{ or }3+}$, Fe^{3+}, Co^{3+}, Ni^{2+}, and Zn^{2+}.

Nd^{3+} Coordination in Alkali BeF_2 Laser Glasses

To substantiate our previous white-line studies of Nd^{3+} L_3 XANES in these binary alkali BeF_2 glasses, we performed a systematic study to determine the Nd coordination of fluoride ions in the series of 45MF-55 BeF_2 glasses, where M = Li, K, and Rb. We use the experimental fluoride envelope function from the L_3 edge of BaF_2 to model the amplitude of the EXAFS signal from the glasses using a three-shell model derived initially to simulate the spectrum of crystalline NdF_3. A typical simulation is shown in Fig. SS-2 for Nd in LiF-BeF_2 glass. The average coordination of Nd^{3+} by F ions is the summation of the three sub-shells. The results are summarized in Table SS-1. The increase in F neighbors about the Nd^{3+} ion is in accordance with earlier molecular dynamic structure simulation and correlates with narrowing of the optical spectra of these glasses.

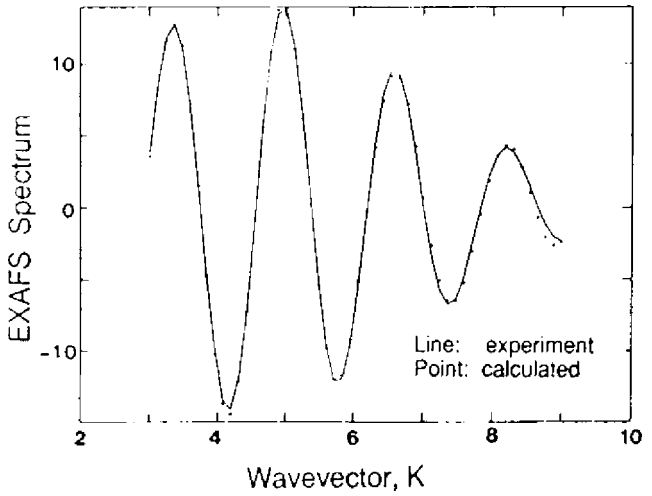

Fig. SS-2. Experimental (line) and calculated (points) Nd EXAFS signal from nearest-neighbor fluoride ions in LiF-BeF_2 glass.

Table SS-1. Nd^{3+} Coordination in Alkali BeF_2 Glasses Derived from EXAFS Analysis

Glass	No. of fluoride ions
BeF_2	7.8
45 LiF - 55 BeF_2	8.5
45 KF - 55 BeF_2	8.6
45 RbF - 55 BeF_2	9.6

Work in Progress

In November, we had a 4-day run at Brookhaven. Experiments were performed to investigate:

- The valence of Bi and the K environment in $(Ba,K)BiO_3$ superconductor
- Nd^{3+} in silica sol gels and glasses
- Ti catalysts in sol gel intermediates and products
- The Sn environment in special low-temperature fluorophosphate glasses.

Data analyses of these systems are now under way. We are currently performing detailed analyses of our EXAFS data to determine if we can quantify the Cu/Y anti-site substitution (disorder) in $YBa_2Cu_3O_7$. We also plan to perform a detailed HREM (high-resolution electron microscope) image simulation for Cu/Y substitution in $YBa_2Cu_3O_7$ to determine if the simulated images can enable us to systematically distinguish such anti-site disorder at 10, 20, 30% levels. If the simulation proves positive, we shall attempt direct HREM observation with carefully designed Cu-rich and Cu-poor materials.

Synthesis of substituted perovskites is being carried out to produce new materials and to learn physical properties of compounds such as $(Ba,Ca)(K,Gd,La)(Ti,Sn)O_3$. Ti and Sn may behave in a manner similar to Bi. Compounds known are $(Ca,La)TiO_3$, which is like a tungsten bronze with metallic conductivity, and $BaTiO_3$, which has an extremely high dielectric constant and is used in capacitors and PTCRs (positive-temperature-coefficient resistors). It is now known that $(Ba,K)BiO_3$ superconducts around 30 K, whereas $BaBiO_3$ does not. This should be a very interesting experiment.

A preliminary effort has recently been devoted to evaluation of the feasibility of studying, and a possible experimental design to study, local atomic configurational changes of optical centers in excited electronic states.

Publications

R. B. Greggor, F. W. Lytle, J. Wong, and E. M. Larson, "X-ray absorption spectroscopic investigation of 3d metals substituted in $YBa_2Cu_3O_7$," SSRL Activity Report (1988); *Phys. Rev. B* (1989), in preparation.

F. W. Lytle, R. B. Greggor, J. Wong, and E. M. Larson, "Investigation of the valence of Pr in $YBa_2Cu_3O_7$," SSRL Activity Report, (1988); *Phys. Rev. B* (1989), in preparation.

B. G. Rao, K. J. Rao, and J. Wong, "L-edge EXAFS Study of the Coordination of Lead in $PbO\text{-}PbF_2$ glasses," *J. Chem. Soc. Fl* **84**, 1773 (1988).

K. J. Rao, B. G. Rao, and J. Wong, "Investigation of the Coordination of Lead in $PbO\text{-}PbF_2$ glasses using EXAFS," *J. Chem. Soc. Fl* **84**, 1779 (1988).

Presentations

Invited

J. Wong, "Materials Studies with X-ray Absorption Spectroscopy," presented at Joint AAAS-APS Symposium on Synchrotron Radiation, San Francisco, Calif., Jan. 1989.

Contributed

J. Wong, D. A. Jefferson, T. G. Sparrow, and J. M. Thomas, "HREM, EELS and STEM Characterization of SIPOS and Is Interface with Si," presented at Materials Research Society HREM Symposium, Boston, Mass., Nov. 1988.

J. Wong and G. A. Slack, "Metals in Beta Boron," presented at Materials Research Society Synchrotron Radiation Symposium, Boston, Mass., Nov. 1988.

J. Wong and I. Wachs, "Coordination and Bonding of Ti and V in Model Compounds and Supported Catalysts," presented at Materials Research Society Interface Characterization Symposium, Boston, Mass., Nov. 1988.

ELECTRONIC STRUCTURE OF SYSTEMS WITH REDUCED SYMMETRY

A. Gonis *(Principal Investigator)*

Overview

Motivation

Existing methods to calculate the electronic structure of matter are usually characterized by a number of approximation schemes, either to the shape of the one-particle potential entering the Schrödinger equation for a material or to the underlying structure. Quite often, the potential is considered as vanishing outside a sphere inscribed inside the Wigner-Seitz cell, the muffin-tin (MT) approximation; in nearly all applications, it is assumed to be spherically symmetric. Approximations to the underlying crystal structure include the use of supercells to treat the problem of isolated impurities or the use of slabs or repeating slabs, to investigate surfaces or interfaces, respectively. Many such approximations are adequate in a number of physically important problems and have contributed both to our understanding of physical properties and to the development of fairly accurate computer codes.

At the same time, it is well appreciated that use of these approximations can present conceptual as well as computational problems. For example, the MT approximation cannot be expected to properly describe the potential in highly undirectional cells (e.g., diamond) or near regions of severely reduced symmetry (e.g., surfaces and grain boundaries). Thus, it is desirable to construct methods for the calculation of electronic structure that are not encumbered by approximations to either the shape of the one-particle potential or the structure of the material.

Currently, LLNL is involved in a number of activities in which the physics of surfaces and interfaces plays a significant role. These activities include a thrust area on the study of adhesion and bonding at internal interfaces, work in scanning tunneling microscopy, and studies of Pu and its alloys. This work is expected to impact all of those areas.

Objective

The objective of this work is determination of the electronic structure and energetics of systems with reduced symmetry, such as surfaces and internal interfaces. This requires solving the Schrödinger equation for semi-infinite periodic systems (surfaces) or doubly semi-infinite periodic materials (interfaces, grain boundaries) by properly taking into account the boundary conditions of the problem. Thus, no approximations to a material's underlying structure are made, and no extraneous conditions (repeating slabs, supercells, etc.) are used in the calculation.

Methodology

The formalism used in this study is based on a new RSMST and was developed by the principal investigator of this project and a Ph.D. thesis graduate student. It is based on the general principle that the physical properties of a system such as a surface do not change when an integral number of planes is removed from the free end.

In addition to the first-principles formalism, we use EAM, an atomistic simulation technique, to determine the equilibrium positions of atoms on and near a surface or interface. Thus, the EAM plays the same role in establishing the structure of a semi-infinite material (surface) that x-ray crystallography plays in establishing that of three-dimensional periodic solids.

Progress

We have been able to calculate the electronic DOSs for ideal surfaces, as well as unrelaxed and structurally relaxed twist and tilt grain boundaries in Cu. The atomic coordinates of the relaxed grain boundaries were obtained from applications of the EAM. Thus, these calculations mark the first time that atomistic simulations, the EAM, and first-principles electronic structure methods, the RSMST, have been combined in the study of electronic properties of solid materials.

Although originally developed exclusively for the treatment of systems with reduced periodicity, such as surfaces and interfaces, the method can also be used to treat complicated structures with polyatomic unit cells, such as α-Pu. We are currently laboring to complete development of the code so that such applications can be made.

Publications

X.-G. Zhang and A. Gonis, "New Real-Space Method for the Determination of Electronic Structure," *Phys. Rev. Let.* **62**, 1161 (1989).

X.-G. Zhang, E. C. Sowa, and A. Gonis, "A First-Principles Method for the Determination of the Electronic Structure of Grain Boundaries," presented at the Acta/Scripta Conference on Metal/Ceramic Interfaces, Santa Barbara, Calif., Jan. 19–24, 1989; accepted for the *Proceedings*.

A. Gonis, X.-G. Zhang, J. M. MacLaren, R. C. Albers, S. Crampin, and D. D. Vveddensky, "An Alternative Layer Korringa-Kohn-Rostoker (LKKR) Approach to Surface and Interface Electronic Structure," *Bull. Am. Phys. Soc.* **34**, 825 (1989).

E. C. Sowa, A. Gonis, X.-G. Zhang, and S. M. Foiles, "The Electronic Structure of Unrelaxed and Relaxed Grain Boundaries," *Bull. Am. Phys. Soc.* **34**, 825 (1989).

STUDIES OF THIN MOLECULAR PLASMAS

C. Stevens *(Principal Investigator)*
A. Droege G. Haugen
W. Conaway S. Steward

Overview

Our objective in this project* is to obtain an understanding of the thermodynamic properties (equation-of-state) of materials heated to temperatures between 3,000 K (hot vapors) and 15,000 K (fully atomized plasmas). This "molecular-plasma" regime is important to many of LLNL's technical areas of interest, including materials production and analysis by plasma techniques. A fundamental understanding of materials heated to these temperatures is also central to confident prediction of the performance of materials in nuclear-weapons research and development.

Study of dense, complex plasmas in this low-temperature range is a relatively unexplored area of chemical physics and materials science. They are not classical atomic plasmas, nor are they simple molecular systems. Predictive uncertainties about temperature and pressure in the early stages of weapons ignition result from lack of information about the integrated heat capacities of these materials in this temperature range. The degree of fragmentation and atomization can only be approximated at present. The pressure uncertainties and the possible presence of large molecular fragments will directly impact the performance (e.g., material interface shocks and scattering centers).

Laboratory study of materials heated to these temperatures and these plasma densities is hampered by difficulties in two areas:

- Heating bulk materials uniformly
- Diagnosing the resulting plasma

We are circumventing the difficulties by investigating the uniform heating of thin free-standing polymeric films ranging in thickness from 100 nm to 1 μm. By restricting the thickness of the film, the laser fluence requirements to uniformly heat the materials can be held below nonlinear-absorption thresholds. The absorptivity and other properties can be tailored by selection of specific polymers and mixtures. The free-standing films are optically thin, which allows use of optical absorption and emission to diagnose the species development in the evolving plasma. Temperature measurements are made by viewing the light emission along the optically thick dimension.

An 8-ns, frequency-quadrupled Nd:YAG laser (266 nm) is used to heat the films with the objective of establishing local thermodynamic equilibrium. We then measure energy absorbed, temperature, pressure, and molecular and atomic speciation under these conditions. The speciation information provides an experimental check on thermodynamics

* Jointly supported by the IR&D and Nuclear Design Programs.

codes that compute speciation fractions and that are used to predict the properties of materials at these extreme conditions. These codes are based on extrapolated thermodynamic properties and have not been subjected to experimental verification.

Technical Activities and Results

A major part of the effort this year has been activating and calibrating our optical spectrometer and gated photodiode-array detector system. A calibrated light source was used to establish the diode response and spectrometer throughput. Data acquisition programs have been written and debugged. A generalized nonlinear least-squares routine for fitting blackbody spectral profiles was written for our system and is now operational. The standard source spectral profile was used to measure its temperature to within 5%.

We can now measure spectral-emission and blackbody temperatures of plasmas created by the 266-nm laser. The first concern is whether energy is being uniformly deposited into our thin films, creating a thermally homogeneous plasma in the temperature range of interest.

The films we are investigating are 120 nm thick and designed by polymer blending of polystyrene and polypropylene oxide to absorb 10% of the incident 266-nm laser light. Preliminary studies, using time-of-flight mass-spectral analysis of ionized species ejected from both front and back of the film, had suggested uniform heating. We have obtained more direct evidence for uniform heating by photographing the film on edge, using self-luminosity to image the plasma. The results (one of which is shown in Fig. TMP-1) are very encouraging, if not confirmatory.

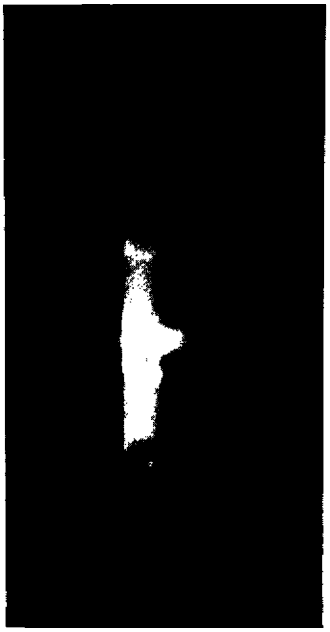

Fig. TMP-1. Thin-film luminescent image following laser heating. Laser incident on film located along right side of holder where light tick marks are evident.

In this photograph, a thin film, adhered to the right side of a comb-like holder, is viewed on-edge as the 8-ns laser pulse strikes it from the left. A plasma is created that then expands into the surrounding vacuum; its spatial extent on either side of the film depends on the plasma energy. Symmetry in the expansion indicates success in uniform deposition of the laser energy throughout the film thickness. From the photograph, it is evident that the extent of the plasma in line with the laser beam on either side is symmetrical. Expansion of the plasma in directions not parallel to the laser beam on the left side is restricted because of the finite thickness of the film holder. Temperature measurements depend the ability to make short-time, broadband spectral measurements of the hot plasma. We have demonstrated the ability to collect 5-ns exposures of the plasma. Currently, we are working on reducing the time jitter from the laser pretrigger (to better define our time discrimination) and on implementing a small-field-of-view, long-distance microscope (to better define our spatial discrimination).

Initial emission studies of thin films heated with ~5×10^4 J/cm^3 of laser energy density showed a spectrum dominated by a violet emission band located near 400 nm. This band is the result of emission by molecular species, possibly C_3; higher-resolution spectral measurements are needed for positive identification. We plan to restrict the field-of-view of the emission to approximately 6° and to increase the laser energy and spot size in order to view an optically thick column emission, a prerequisite for obtaining blackbody spectral profiles.

Measuring pressure inside these microplasmas is a major challenge. We have identified an approach that can yield internal pressures accurate to within 10%: measure the velocity of a shock wave launched into a surrounding rare gas, such as argon. A quantitative relationship has been developed between measured shock velocity in the gas and the initial material driving pressure—the desired plasma pressure. Preliminary experiments have been conducted; we have measured shock velocities using laser backlight and a streak camera to record movements of a shock front through thin films. A Schlieren-like image is created by passage of a density gradient caused by the shock wave. One such image is shown in Fig. TMP-2. The shock velocity is given by the slope of the horizontally-traveling shock *vs.* the vertical streak image. This technique is being adapted to measure shock velocities in surrounding argon gas, providing a determination of plasma pressure.

Finally, preparations are being made to measure plasma species concentration as a function of energy deposition and temperature. We have experimented with creation of an absorption backlight by laser spark generation in high-pressure gases. This will provide a point source of light that will pass through the optically thin plasma dimension and into the spectrometer diode-array system. A high-pressure cell has been constructed, and a continuum white-light source has been demonstrated. Problems with laser scattering are being addressed.

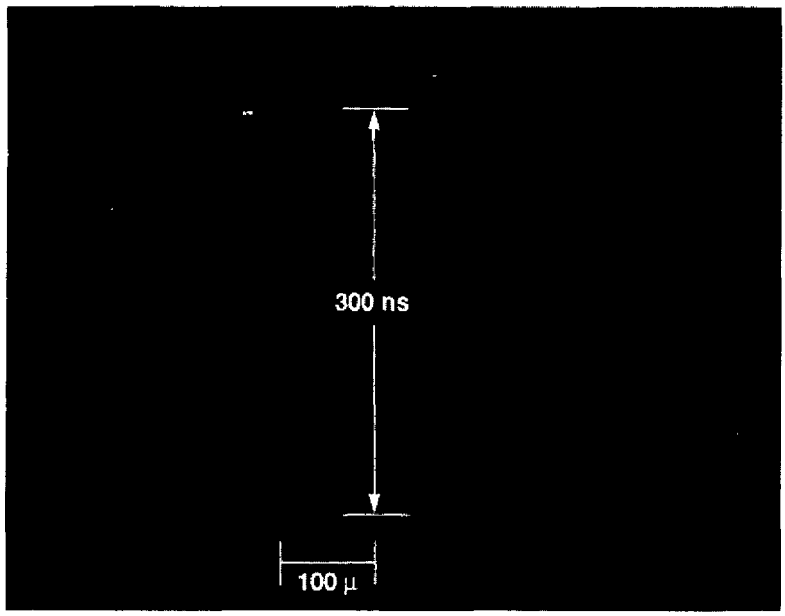

Fig. TMP-2. Streak photograph of laser-induced shock traveling through thin, free-standing film.

THE STRUCTURE-PROPERTY LINK IN SUBNANOMETER MATERIALS

A. F. Jankowski *(Principal Investigator)*

Overview

The emphasis of this project is on the structure-property relationship of interface-dominated, artificially-ordered materials. A fundamental understanding is sought of physical property effects that occur via atomistic rearrangements in superlattice structures, with repeat periodicities less than 3 nm. The fabrication and characterization of sub-nm multilayers has proceeded as outlined in the following section.

Activities and Results

Synthesis

The planar-magnetron sputter-deposition process is being used to synthesize metallic-based thin (<1 μm thick) films, with individual layers ranging from 0.3 to 1.5 nm. Several deposition runs of Au/Ni multilayers have been produced. In addition, pure elemental coatings have been made for calibration purposes with respect to composition, structure, and mechanical behavior.

Structural characterization

The "strain wave" profile [1] of Au/Ni multilayers is being measured and modelled using a kinematical x-ray approach. Initial results [2] indicate maximum elastic strain at, with relaxation away from, the interfaces. Cross-section TEM provides an excellent means of imaging the multilayer microstructure (Fig. SP-1). The single/multiple phase nature of Au/Ni "superlattices" has been revealed primarily with electron diffraction [3]. The interface-dominated, short-period structures (layers thinner than 1 nm) are a single phase, whereas the longer-period structures have additional bulk components.

Physical Properties

Mechanical microindentation techniques provide possible quantification of elastic moduli and hardness without the tedious removal and subsequent handling of the multilayer films from their substrates. Elastic moduli measurements have thus far been difficult to analytically extract from load-displacement curves using this technique. Hardness data (unpublished) presented below, however, do correspond with more historically elaborate, moduli measurement techniques. A maximum enhancement in hardness, H_c, is found near a 2-nm repeat period, D, as shown by:

D (nm)	0.82	1.24	1.77	2.51	4.41
H_c (GPa)	6.75	6.25	8.50	6.30	5.90

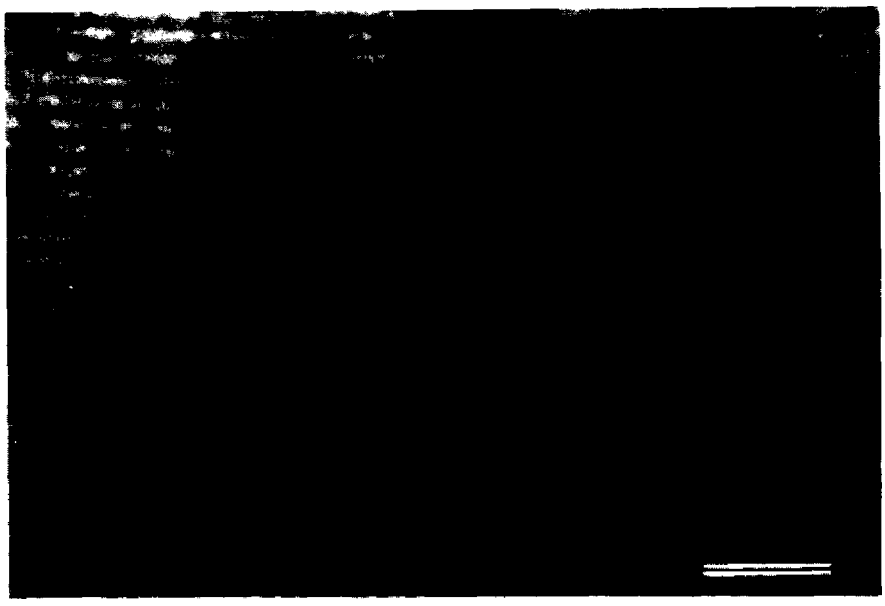

Fig. SP-1. A TEM bright-field image, in cross-section, of a 4.4-nm repeat-period Au/Ni multilayer. Bar = 25 nm.

A qualitative theoretical treatment of elastic/plastic property phenomena has taken form using a strain-wave approach within the coherency strain model [1,4]. The model has been successfully extended to systems such as Cu/Nb [5], in which modulus softening is observed.

In sum, metallic superlattices that emphasize the role of interface, both in structure and property, have been synthesized. Structural characterizations correlate well with a postulated distorted lattice. Subsequent mechanical property evaluation, using a microindenter, shows promising use and correspondence with modelled mechanical behavior. The microstructure (on a nanometric scale) is being linked to macroscopic mechanical properties (elastic moduli).

References

1. A.F. Jankowski, "The Strain Wave Approach to Modulus Enhancement and Stability of Metallic Multilayers," *J. Phys. Chem. Solids* (1989), in press.
2. J. Chaudhuri, S. Shah, and A. Jankowski, "X-Ray Diffraction Analysis of Au/Ni Multilayers," *Mater. Res. Soc. Symp. Proc.* **132** (1989), in press*.
3. S.R. Nutt, K.A. Green, S.P. Baker, W.D. Nix, and A. Jankowski, "Gold-Nickel Multilayer Films: Structure-Property Correlations," *Mater. Res. Soc. Symp. Proc.* **130** (1989), in press*.
4. T. Tsakalakos and A. Jankowski, "Critical Phenomena in Nanoscale Multilayer Materials," *Mater. Res. Soc. Symp. Proc.* **132** (1989) in press*.
5. A.F. Jankowski, "Coherency Strain Modeling of Elastic Moduli in Cu/Nb Multilayers," *Mater. Res. Soc. Symp. Proc.* **141** (1989), in press*.

* Also presented at the Materials Research Society Fall Meeting, Boston, Mass., Nov. 28–Dec. 3, 1988.